



UNIVERSIDAD DE CHILE
FACULTAD DE CIENCIAS FÍSICAS Y MATEMÁTICAS
DEPARTAMENTO DE INGENIERÍA ELÉCTRICA

DESIGN OF A RECEIVER AT 31–45 GHz BASED ON HEMT AMPLIFIERS AND
SCHOTTKY MIXERS

TESIS PARA OPTAR AL GRADO DE DOCTOR EN INGENIERÍA ELÉCTRICA

NICOLÁS ANDRÉS REYES GUZMÁN

PROFESOR GUÍA:
FAUSTO PATRICIO MENA MENA

MIEMBROS DE LA COMISIÓN:
WALTER GROTE HAHN
ERNEST MICHAEL
DAVID RABANUS
LEONARDO BRONFMAN AGUILÓ

Este trabajo ha sido parcialmente financiado por :
CONICYT, a través de sus programas Fondo Basal, proyecto PBF06, fondos ALMA para el
desarrollo de la astronomía, proyectos 31060002, 31080003, 31080004, Becas Chile,
FONDEQUIP, proyecto AIC-27.
MECESUP a través de proyecto FSM 0601.
Sociedad Chilena de Astronomía.

SANTIAGO DE CHILE
JANUARY 2013

Abstract

The Atacama Large Millimeter Array (ALMA) is an international partnership of Europe, North America and East Asia in cooperation with the Republic of Chile. It consists of an array of 66 antennas designed to work as an interferometer in the millimetric and sub-millimetric range (from 30 to 950 GHz). It is located at 5000 meters altitude in the Chajnantor Plateau, north of Chile. It will start full scientific operations by 2014 being the most important instrument for radio-astronomy in the world. Presently with 36 antennas, it is already delivering transformational science data, providing astronomers with unprecedented sensitivity and quality images of the “radio-universe” with a resolution comparable with the Hubble telescope.

The lowest spectroscopic band envisioned for ALMA, the so-called Band 1, covers the frequency range from 31 to 45 GHz. This band was not implemented during the first construction phase of the telescope, but has been recently (2012) included for the second development phase of the project, including the indication of extending the frequency coverage up to 50 GHz. In the context of this thesis we have developed technological solutions to cover this band, especially focused on the development of low-noise amplifiers using High Electron Mobility transistors (HEMT). Among the most burdensome challenges of ALMA Band 1 are the stringent specifications on noise temperature, the large required bandwidth, and the limited space available for this receiver within the ALMA cryostat. In this work we present an overview of the scientific importance of Band 1, along with the technological solutions we have developed, including the design of key components, like the horn, lens, ortho-mode transducer, and low noise amplifiers. We also present an evaluation of third-party components which can be used in the receiver. The work is used to present a preliminary layout of the Band-1 receiver which was implemented and tested in order to be used as technological demonstrator for a fully operational receiver.

Resumen

El Atacama Large Millimeter Array (ALMA por sus siglas en inglés) es una asociación internacional entre Europa, América del Norte y Asia del Este en cooperación con la República de Chile. Consiste de un conjunto de 66 antenas diseñadas para funcionar como un interferómetro en el rango milimétrico y sub-milimétrico (de 30 a 950 GHz). Se encuentra ubicado a 5000 metros de altura sobre el nivel del mar en el Llano de Chajnantor, norte de Chile. Iniciará su completa operación científica en 2014 siendo el instrumento más importante para la radio-astronomía en el mundo. Actualmente, con 36 antenas, se encuentra en operación científica preliminar y a la fecha ha entregado importantes datos a la comunidad astronómica mundial.

La banda espectroscópica más baja prevista para ALMA, conocida como Banda 1, cubre el rango de frecuencias desde 31 a 45 GHz. Esta banda no se construyó durante la primera fase de construcción del telescopio, pero ha sido recientemente (2012) incluida para la segunda etapa de desarrollo de ALMA, incluyendo la indicación de extender la cobertura de frecuencia hasta los 50 GHz. En el contexto de esta tesis se han desarrollado soluciones tecnológicas para esta banda de frecuencia, con especial énfasis en el desarrollo de amplificadores de bajo ruido. Entre los mayores desafíos de la Banda 1 de ALMA están las estrictas especificaciones de ruido, el ancho de banda requerido y el limitado espacio disponible para este receptor en el criostato ALMA. En este trabajo se presenta una visión general de la importancia científica de banda 1, junto con las soluciones tecnológicas que hemos desarrollado, incluyendo el diseño de los componentes clave, como la bocina, la lente, el transductor de polarización y los amplificadores de bajo ruido. También se presenta una evaluación de componentes comerciales que pueden ser utilizados en el receptor. El trabajo se utiliza para presentar un diseño preliminar de la banda1, receptor que fue construido y probado en nuestro laboratorio para ser utilizado como demostrador tecnológico.

We remember J. May (R.I.P) for his unconditional support and interest to this project. I also thank the complete team at the Millimeter Wave Laboratory for their invaluable support and help. Finally to my family Pau, Mariana and Margarita.

Contents

1	Introduction	1
1.1	Scope of this thesis	3
2	Scientific case for ALMA Band 1	4
2.1	Protoplanetary disks	4
2.2	Molecular lines observations	5
2.3	Maser observations	6
2.4	High redshift CO emission	6
2.5	Sunyaev Zel'dovich (SZ) effect	8
2.6	Other instruments in the same band	8
2.7	Atmospheric conditions for ALMA Band 1	10
3	Low Noise Amplifiers	11
3.1	Heterodyne receivers for radio astronomy	11
3.1.1	Noise considerations	12
3.2	Low Noise Amplifiers	14
3.2.1	Design of LNAs	14
3.2.2	Design of a single stage amplifier	15
3.2.3	Stability	16
3.2.4	Noise	17
3.2.5	Gain stability	19
3.3	High Electron Mobility Transistors (HEMT)	19
3.3.1	Semiconductor structure of a GaAs HEMT	20
3.3.2	Materials	20
3.3.3	Transistor Layout	22
3.3.4	HEMT modelling	22
3.3.5	Fabrication of LNA	24
4	LNAs for Band 1	26
4.1	Band 1 LNAs problematic	26
4.1.1	Hybrid technology	28
4.1.2	MMIC Technology	29
4.2	LNAs development at Universidad de Chile	30
4.2.1	LNA characterization test setup	30
4.2.2	LNA based on commercial chips	33
4.2.3	LNA amplifier using UMS transistors	39

4.3	Conclusion	49
5	Band 1 development	50
5.1	Band 1 specifications and interfaces	50
5.2	Band 1 proposed design	51
5.2.1	Noise and power budget	52
5.3	Optics	54
5.3.1	Horn	54
5.3.2	Lens	57
5.3.3	Infra-red filters	57
5.4	Ortho Mode Transducer	58
5.5	Isolator	63
5.6	High pass filter	65
5.7	Mixer	67
5.8	IF Amplifiers	68
5.9	Band-1 prototype receiver	68
5.10	Preliminary results	70
5.10.1	Noise measurements	70
5.10.2	Beam Pattern	72
5.11	Conclusions	75
6	Conclusions and perspectives	76
	Appendix A Acronism index	78
	Appendix B List of publications	80
	Bibliography	98

Chapter 1

Introduction

Radio astronomy is the area of astronomy dedicated to the study of celestial objects using the electromagnetic radiation they emit in the radio band. As the technology has advanced from the 30's, when this branch of science was born, the concept of radio waves has been extended from few megahertz up to the sub millimeter band (around 1 THz). The importance of this observations is to allow astronomers to study several phenomena that are only visible at these frequencies ranges. As examples we can mention the synchrotron radiation from pulsars, the observation of dust obscured regions and the measurements of the cosmic microwave background. Observations at this frequency ranges are technologically challenging since the signal that must be detected is extremely weak and hidden by the noise produced by the atmosphere, contamination from other sources, and instrumental noise.

In the case of observations in the millimeter and sub-millimeter band excellent quality atmospheric conditions are required. This is because the electromagnetic radiation at this frequencies is severely attenuated by the water vapor present in the atmosphere. All around the world there are few sites that allows ground based observations in these frequencies, being the most notorious the sites located in the plateau of the northern Chilean Andes. They have altitudes above 5000 meters and an extremely dry atmosphere. During the 90's the project of building an international array of millimeter and sub-millimeter telescopes which could take advantage of this unique conditions started to take form. The project crystallized by the end of the 90's on the Atacama Large Millimeter/sub-millimeter Array (ALMA) [1] which is now under construction and providing limited scientific operations. When completed by 2014, it will be the largest millimeter and sub-millimeter array telescope in the world.

ALMA is located at 5000 meters altitude in the Chajnantor Plateau, north of Chile. It consists of an array of 54 antennas with a diameter of 12 m. When in extended configuration, it provide baselines up to 16 km. The array is completed with the Atacama Compact Array (ACA), which consist of 12 antennas with a diameter of 7 m allowing to map low angular resolution features. Finally, four 12-meters antennas complete the spectral coverage with total power data. All of these antennas have a surface accuracy of 25 μm allowing observations in several atmospheric windows, up to 950 GHz. The array will have baselines ranging from few meters to 16 km, obtaining a complete coverage of the u-v plane, with a maximum angular resolution of 6 miliarcsecond. Each antenna will house 10 low-noise receivers, allowing the



Figure 1.1: Seven ALMA Antennas working at Llano de Chajnantor, Chile.

instrument to have an excellent sensitivity in 10 bands between 31 and 950 GHz. The signals measured from the receivers are sent, via optical fibers, to the central computer which correlates all the signals and generates the final astronomical images.

ALMA is an international partnership of Europe, North America and East Asia in cooperation with the Republic of Chile. The receivers are state of the art electronics, showing the best possible performance. Special emphasis is done on minimizing the noise figure of each receiver, as it will affect directly the complete array efficiency. The receivers are designed and fabricated at different laboratories around the world. Bands 3 (84-116 GHz), 6 (211-275 GHz), 7 (275-373 GHz) and 9 (602-720 GHz) were planned as initial capacities of the observatory. Bands 4 (125-163 GHz), 8 (385-500 GHz) and 10 (787-950 GHz) were later incorporated and nowadays are at different levels of production. Six receivers for Band 5 (162-211 GHz) are built at Chalmers, Sweden, as a pre-production for the full band (66 receivers) to be incorporated to ALMA during the next years.

The presence of a lower band, named Band 1, covering the 31.3-45 GHz range, was declared as a high scientific priority by the ALMA Scientific Advisory Committee (ASAC-2001). The importance of the ALMA Band 1 is that it will allow the studies of several phenomena with an unprecedented sensitivity and angular resolution. Between this phenomena we have to mention:

- Detection of high red-shifted CO emission.
- High-resolution measurements of the Sunyaev Zel'dovich(SZ) effect.
- Micro-Kelvin Cosmic Microwave Background (CMB) anisotropies on very small angular scales.
- Study the molecular complexity using low frequency spectroscopy.
- Looking deep into proto-stellar disks, disentangling dust, f-f and synchrotron emission.

Band 1 will also provide a powerful tool for conventional radio astronomy in the southern

hemisphere, when most of the Milky Way and Magellanic clouds can be observed at the zenith.

1.1 Scope of this thesis

Universidad de Chile, through its Electrical Engineering and Astronomy Departments, is interested in developing the technology for a Band 1 receiver. As part of this effort, supported by the Center of Excellence in Astrophysics and Associated Technologies (PBF 06), the Millimeter Wave Laboratory was updated and new equipment was purchased to accomplish this task. The final goal of this effort was to build a Band-1 prototype receiver and, in the long term, participate in the design and construction of the final Band 1 hardware. This thesis project has been carried out under such long term program. Its main objective is to develop technology for astronomy, specially focused to investigate low noise techniques for this particular instrument. Different projects were accomplished towards this goal, being the main one the development of low noise amplifiers (LNAs) based on high electron mobility transistors (HEMT). This technology shows the lowest noise figure at the Q-band (30–50 GHz).

This thesis is structured as follows. In the second chapter a review of the scientific cases that motivated the construction of Band-1 receivers for ALMA is presented. In chapter 3 a complete review of the concepts, theory and previous work in the field of cryogenically cooled receivers is presented. Special emphasis is given to low noise technologies and theory as it is one of the key aspects of receivers and of this thesis. Since the LNAs are the most complex component, a separate chapter (Chapter 4) was devoted to present our work on developing such technology. Chapter 5 presents an overview of the Band 1 work at Universidad de Chile. The receiver specifications and architecture are presented and discussed, followed by a description of the work on the different receiver components. Finally, on Chapter 6 the current status of the project is reviewed and the future development plans are presented.

Chapter 2

Scientific case for ALMA Band 1

Band 1 is the lowest frequency range of observations that will be installed at ALMA according to the initial design of the instrument. The original frequency range proposed for Band 1 is from 31.3 to 45 GHz. In this frequency range several science goals can be achieved using the high angular resolution and excellent sensitivity of ALMA. A complete revision of the science case for ALMA Band 1 is presented in [2].

2.1 Protoplanetary disks

When ALMA was envisioned several science cases were considered to write the low level system specifications. One of this key science enabling features was ALMA to have:

“The ability to image the gas kinematics in protostars and in protoplanetary disks around young Sun-like stars at a distance of 150 pc (roughly the distance of the star-forming clouds in Ophiuchus or Corona Australis), enabling the study of their physical, chemical and magnetic field structures and to detect the tidal gaps created by planets undergoing formation in the disks”¹.

Planet formation takes place in disks of dust and gas surrounding young stars. It is known that within this protoplanetary disk the material has to agglomerate to form dust, pebbles, rocks and finally terrestrial planets, but the details of the process are mostly unknown. In the case of giant planets (as Jupiter) the process is, in its major extent, unknown. ALMA will be capable to resolve the protoplanetary disks and detect the tidal gaps where planets are formed. By using ALMA the composition of the disk can be studied, determining the amount of gas, dust and particles that constitute it. In this scenario Band 1 will be a fundamental tool to detect continuous emission from centimeter size particles, which tends to emit more in the millimeter-wave range than in the sub-millimeter.

¹Taken from NRAO web site at: <http://www.mma.nrao.edu/science/>

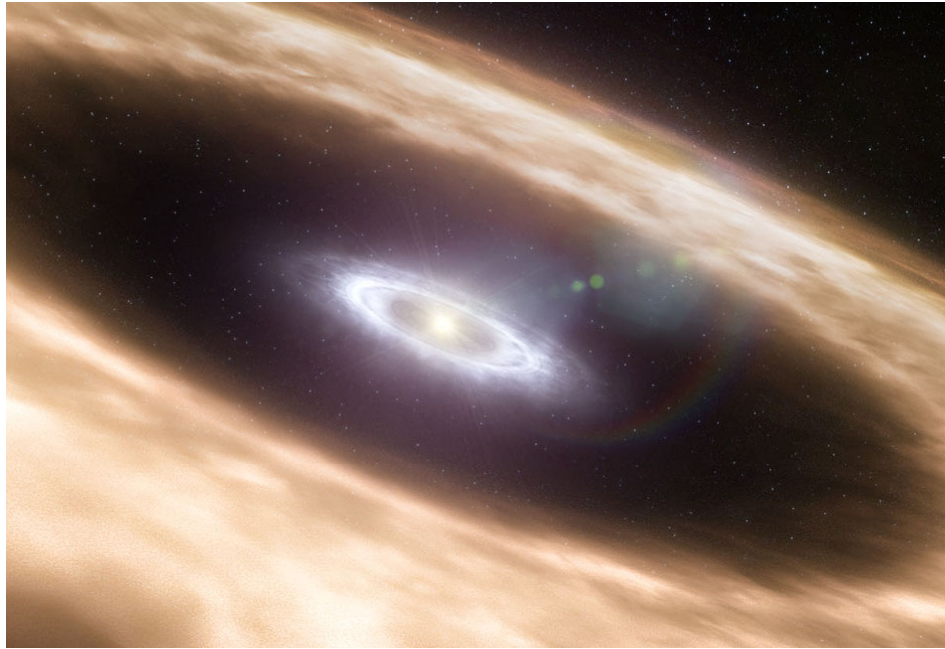


Figure 2.1: Artist impression of a protoplanetary disk around a young star. The gap in the disk is known as tidal gap and is caused by a planet that is under formation in this area. Credit: ESO

2.2 Molecular lines observations

Stars form out in dense gas pockets inside molecular clouds, called “cores”. Tracing molecular line emission from cores within our Galaxy gives us direct insight into the dynamics and chemistry associated with star formation. Of special interest are the characteristics of gas early in the development of cores, i.e., when cores themselves condense out of ambient molecular material. Such locations are now being identified in abundance through continuum observations from the Herschel Space Observatory but little kinematic data exist to characterize their dynamics. Lower-density gas can be traced well in general by lower-frequency lines, as the lines found in Band 1. The primary lines for tracing “early core material” come from CS (1-0), at 48.99 GHz.

Other important lines that trace early core material within this frequency range include those from the “carbon-chain” molecules, e.g., HC₅N and HC₃N which have numerous transitions between 30 and 50 GHz (see Table 2.1). In addition the 45.38 GHz transition of CCS has a relatively large Zeeman splitting factor, enabling to probe directly the strength of the line-of-sight component of magnetic fields associated with early cores. Finally, the Band-1 frequency range includes many CH₃OH transitions which traces shocks associated with molecular outflows and “hot” molecular cores associated with higher-mass star formation.

As seen in Table 2.1 most of the interesting molecular transitions for star forming research lay between 34 and 50 GHz. Attending this scientific driver it has been proposed to shift the Band-1 frequency range from the actual 31 to 45 GHz to the 35 to 50 GHz band. This change has been indicated by 2012 and therefore was not considered during the development of this thesis work.

Molecule	Frequency
HC ₅ N	7 transitions all over the frequency range
CH ₃ OH	14 transitions all over the frequency range
CCS	Transitions at 33.7, 38.8, 43.9 and 45.3 GHz
CCCS	Transitions at 34.6, 40.4 and 46.2 GHz
CH ₃ CCH	34.183 GHz
SO	36.202 GHz
HC ₃ N	36.392 GHz
HCS+	42.674 GHz
SiO	42.820 GHz
SiO	43.122 GHz
HC ₃ N	45.490 GHz
C ₃ H ₂	46.755 GHz
CS	48.991 GHz

Table 2.1: Molecular transitions between 31 and 50 GHz. As originally proposed, Band 1 covers 31 to 45 GHz. Data taken from [3]

2.3 Maser observations

Band 1 is suitable to carry out maser observations of SiO₁₀ and CH₃OH. Masers are formed under specific conditions, such as high molecular abundance, population inversion, large column density and velocity coherence of the molecules. By studying maser emission it is possible to determine the physical conditions of the region where masers are formed.

Maser observations are a tool to study magnetic properties of star forming regions using polarization analysis of the emission [4]. The high phase stability of ALMA allows the calculation of the four Stokes parameters with high accuracy, allowing the study of circular polarization of the emission that is correlated with the magnetic field in the line of sight.

Masers are also used to determine accurately the distances from star-forming regions in our galaxy. To perform this task a good angular resolution is needed to use parallax techniques. Some work has already been done using Very Long Baseline Interferometry (VLBI) observations [5]. Band 1 will allow the enhancement of ALMA by adding the capabilities of carrying out VLBI observations with other telescopes in the world that operate at the same frequency, specially with the Extended Very Large Array (EVLA) and Green Bank Telescope.

2.4 High redshift CO emission

Molecular Hydrogen (H₂) is the most abundant molecular gas in the universe but its transition lines are weak and therefore is difficult to be detected in areas of cold gas. Carbon Monoxide (CO) is tracer of H₂ and is the second most abundant molecule in space. It has rotational lines that emit with a frequency equal to $n \times 115$ GHz, with $n = 1, 2, \dots$ being the rotational energy levels. By studying the CO emission it is possible to characterize the H₂ gas. Lower

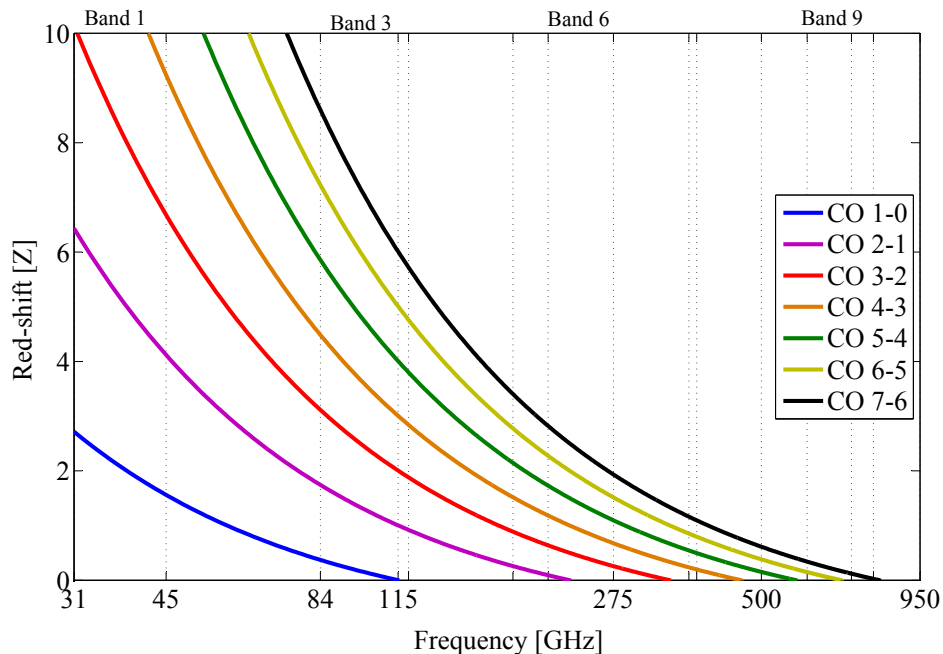


Figure 2.2: CO molecular line frequencies as a function of the redshift. It is clear that Band 1, Band 3, and Band 4 are key tools to observe CO from high-redshifted galaxies. While Band 3 and 4 observe high J-transitions (cores), Band 1 is fundamental for study low J-transitions (extended emissions).

transitions of CO are presents even on cold gas, while superior transitions traces warmer areas within the molecular cloud. These features made CO a powerful tool for observing star forming regions.

Due to the expansion of the universe the electromagnetic radiation from distant objects is redshifted to lower frequencies according with

$$Z = \frac{f_{emitted} - f_{observed}}{f_{observed}} \quad (2.1)$$

This is also the case of molecular lines detected from distant galaxies. The study of molecular gas, mainly through CO detection, in high redshifted galaxies is a key to understand the physical conditions and star formation process of early galaxies. In 2003, emission of the CO line was detected from a galaxy with $Z= 6.4$ [6]. In this work the CO_{3-2} , CO_{6-5} , CO_{7-6} lines where observed at 46.6, 93.2 and 108.7 GHz, respectively. After this initial detection there have been more detections of CO lines from other high-redshifted objects. All this detections have been in brighter high- Z galaxies. Therefore, statistical data of star forming rates at high- Z are biased to these brighter galaxies. Equipped with Band-1 receivers, the high angular resolution and excellent sensitivity of ALMA will allow to trace low J transitions from many standard galaxies at high redshift. Band 1 at ALMA allows observations of CO_{10} at $Z=1.3$ to 2.5, and CO_{21} at $Z=3.6$ to 6.0, as shown in Figure 2.2. These observations can be correlated with higher J transitions of CO using Bands 3 or 4.

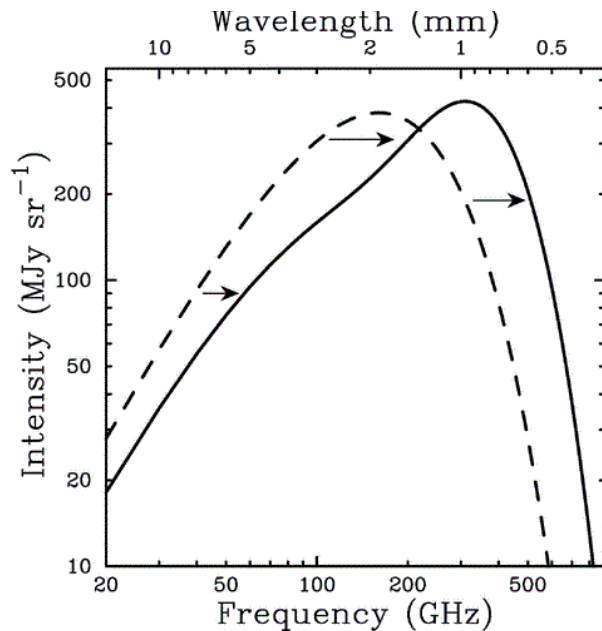


Figure 2.3: Sunyaev Zel'dovich (SZ) effect, hot electrons interact with low energy photons from CMB. As a result, the energy of these photons is increased and the blackbody spectra of CMB is modified. Dashed line is the original spectrum of CMB. The continuous line is the modified spectrum. Figure taken from [7]

2.5 Sunyaev Zel'dovich (SZ) effect

The SZ effect arises from inverse Thompson scattering produced by hot electrons in galaxy clusters over the cosmic microwave background (CMB) radiation. As a result the spectrum of the CMB is shifted up in frequency as we see in Figure 2.3. The net effect is an apparent decrease in the CMB for frequencies lower than 200 GHz. To study this effect CMB maps are correlated with X-ray data since the hot electrons that are involved in the process have temperatures around 10^7K and emit in the X ray range. Combining these data it is possible to estimate distances without more assumptions and, therefore, to estimate the Hubble constant [8]. This effect has been studied over the last twenty years using multiple frequency studies, to separate the SZ effect from other phenomena. Using the high angular resolution and sensitivity of ALMA it will be possible to perform studies about the micro-structure of galaxy cluster, looking for substructure, cold fronts, turbulence, active galaxy nuclei interactions and halos of groups and individual galaxies.

2.6 Other instruments in the same band

At the moment there are several radio-telescopes working in a frequency range similar to the frequency range of Band 1. Table 2.2 summarizes the features of these instruments and gives the references to the instrumentation developed for them. Some of this telescopes, as QUIET or CBI, were special purpose instrumentation devoted to cosmologic research. They are consequently different from ALMA Band 1 as Band 1 is a multi-purpose receiver. Other

Telescope	Location	Frequency range	$T_{receiver}$	T_{system}
Extended Very Large Array [9]	USA	26.5-40 GHz	40K	53K
Extended Very Large Array [9]	USA	40-50 GHz	20-40K	74-116K
Green Bank Telescope [10]	USA	30.5-37 GHz	20K	
Green Bank Telescope [10]	USA	38.2-49.8 GHz	40-70K	
Cosmic Background Imager [11]	Chile	26-36 GHz	15K	
QUIET [12]	Chile	26-40GHz	20K	
Effelsberg [13]	Germany	27-36.7GHz	20K	
Effelsberg [13]	Germany	41.6-44.4GHz	73K	
Kashima [14]	Japan	31.7-33.7 GHz	85K	150K
Kashima [14]	Japan	42.3-44.9 GHz	180K	350K
Mopra [15]	Australia	30-50GHz	35K	80K
Narrabri [16]	Australia	30-50GHz	35K	90K
Onsala 20m[17]	Sweden	26-50GHz	50K	

Table 2.2: Other instruments in the same frequency band that ALMA Band 1.

instruments in the 7 mm band are installed on single dishes big telescope, as Effelsberg in Germany, or Green Bank at USA. Both telescope are around 100 m diameter, designed for high point source sensitivity, but with limitations when mapping extended regions.

The most interesting case, because of similarities with the Band-1 receiver at ALMA, is the Extended Very Large Array (EVLA). It is located at a latitude of 34 degrees north at an altitude of 2124 m. It consists of 27 antennas with 25 m diameter. Presently it has the capability to cover, almost continuously, the frequencies between 1 and 50 GHz. Specifically the Band-1 frequency range is covered by two separate receivers, one at Ka-band (26.5-40 GHz) and the other at Q-band (40-50 GHz). At the low end of the range we consider (35 GHz), both instruments will have comparable point source sensitivities, being ALMA much faster (10 times) than E-VLA when mapping extended sources. This is because of its larger primary beam using 12 and 7 meters antennas. Moreover the high quality ALMA site will increase its efficiency at 50 GHz when compared to EVLA. Other advantages of ALMA will be its almost complete coverage of the u-v plane using the 4 total power antennas, the short baselines of the ACA, and the 54 antennas in extended configuration. In contrast, EVLA has maximum baselines of 36 km instead of the 16 km for ALMA, giving to EVLA a better angular resolution. As a conclusion we can say that they are complementary facilities, being ALMA better suited for extended sources mapping, while EVLA is superior to detect point sources. Finally, we can add that they present synergies on the sources they can observe, being EVLA is located in the northern hemisphere, having access to the part of the sky which is not accessible from ALMA.

The presence of Band 1 at ALMA will allow the interferometer to participate in the worldwide Very Long Base line Interferometer (VLBI). Under this mode of observation ALMA will work with other telescopes in the 7 mm range (41-45 GHz), such as Effelsberg, EVLA and Green Bank Telescope to obtain unprecedented high-resolution images with baselines up to 12.000 Km. It is important to remark that Band 1 will also be a useful engineering tool before starting programs which aim to use high frequency (100 GHz or 230 GHz) VLBI with ALMA working together with other millimeter and sub-millimeter telescopes in the world.

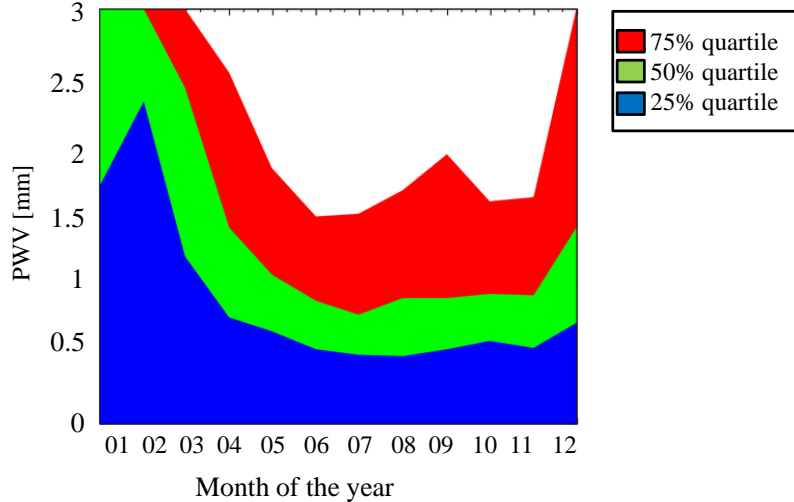


Figure 2.4: Annual variation of the Precipitable Water Vapor (PWV) content at Chajnantor, Data based over 10 years of site testing[18][19]. Figure adapted from [20]

2.7 Atmospheric conditions for ALMA Band 1

The atmospheric conditions at Chajnantor Plateau have been studied for over than ten years [18][19]. Figure 2.4 summarizes these observations and shows the expected precipitable water vapor (PWV) as a function of the month. It has been found that except from the altiplanic winter, which last from December to March, the PWV is around 1 mm (50 % quartile). According to this data the PWV can be even as low as 0.1 mm on some specific events, allowing observations up to 1.3 Thz. In the period from December to March worst conditions are expected wich would prevent observations with the higher frequency bands installed currently at ALMA. Band-1 observations can be done even during high PWV events as the transmission at Band 1 is almost unchanged when the PWV level is as high as 5 mm [21]. This singular feature would allow ALMA to increase the efficiency of the interferometer up to 100%, as Band-1 observation can always be performed.

Chapter 3

Low Noise Amplifiers

3.1 Heterodyne receivers for radio astronomy

Receivers used in radioastronomy are similar to those used in telecommunication. They are called heterodyne or coherent receivers. The main feature of these receivers is that they convert the incoming signal to a signal in a lower frequency range conserving the phase and amplitude information of the original one. This low frequency signal, known as Intermediate Frequency (IF), can be easily processed by the back-end electronics to extract the information needed for the particular application. In the case of an interferometer, such as ALMA, the IF frequency is digitized and send to a correlator for the extraction of scientific data. Figure 3.1 shows the classical configuration of an heterodyne receiver.

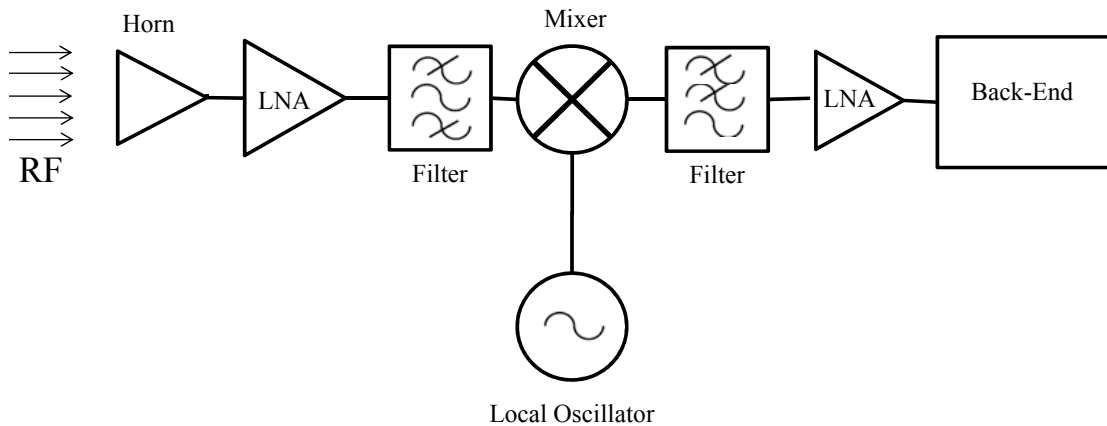


Figure 3.1: Classical diagram for an heterodyne receiver. The incoming signal (RF) is collected by the horn and sent to a LNA. After the amplification stage, the signal is filtered to suppress the image signal and down converted by the mixer. The down converted signal is filtered and amplified by the IF amplifier to reach the signal level required by the back-end

The incoming signal from the radio source is collected by the antenna and concentrated

at the focus. A horn confines the incoming radiation inside a waveguide. The signal is conducted by the waveguide to a Low Noise Amplifier (LNA) which amplifies the signal with a minimum added noise. After the amplification stage the signal is filtered and down-converted by a mixer. This is a nonlinear component that mixes the incoming signal with a reference signal known as Local Oscillator (LO). As a result of the nonlinear operation over this two signal, harmonics and inter-modulations are produced. A low pass filter selects the signal that has a frequency equal to the difference in frequency between LO and RF.

The most used technology for down-conversion are Schottky diodes. For high frequency receivers, more than 100 GHz, super conductive mixers are also used. The output of of a nonlinear device is

$$I_{out} = a(V_{in}) + b(V_{in})^2 + \vartheta(3) \quad (3.1)$$

where a Taylor expansion is used to represent the nonlinear features of the device. Third order terms are neglected. Considering that the input voltage is the composition of LO and the RF,

$$V_{in} = V_{RF} \cos(\omega_{RF}t) + V_{LO} \cos(\omega_{LO}t) \quad (3.2)$$

we can expand equation (3.1) using (3.2), getting

$$I_{out} = a_1 \cos(\omega_{RF}t) + a_2 \cos(\omega_{LO}t) + a_3 \cos((\omega_{RF} - \omega_{LO})t) + a_4 \cos(2\omega_{RF}t) + a_5 \cos(2\omega_{LO}t) \quad (3.3)$$

In this equation we can identify different inter-modulations and harmonic terms. We are interested on the component with a frequency

$$\Delta = \omega_{LO} - \omega_{RF} \quad (3.4)$$

whose amplitude, a_3 , is proportional to the amplitude of th RF signal we are measuring.

The main problem of this strategy is that the RF signal and the image signal are down-converted to the same IF range. To avoid this situation a filter can be used to allow only the RF signal to be processed by the mixer. If the RF signal is below the LO, the mixing scheme is called Lower Side Band (LSB), the opposite case is called Upper Side Band (USB). This situation is presented in Figure 3.2. Other solution to this problem are the sideband separating mixers. In any case the IF output has to be amplified to reach the power levels needed by the back-end system.

3.1.1 Noise considerations

The minimum amount of signal that a system could detect is determined by the noise level. There are two sources of noise, the atmosphere and the receiver itself. The atmospheric contribution can only be diminished by choosing an appropriate site for the telescope, such as the Chajnantor Plateau. The noise of the receiver has to be minimized by the use of the lowest-noise detectors available and by cooling them down to avoid thermal noise.

Every electronic device generates some amount of noise that is added to the signal that is received. The main source of noise is thermal noise which is produced by the thermal excitations of electrons inside the device. The amount of thermal noise produced only depends

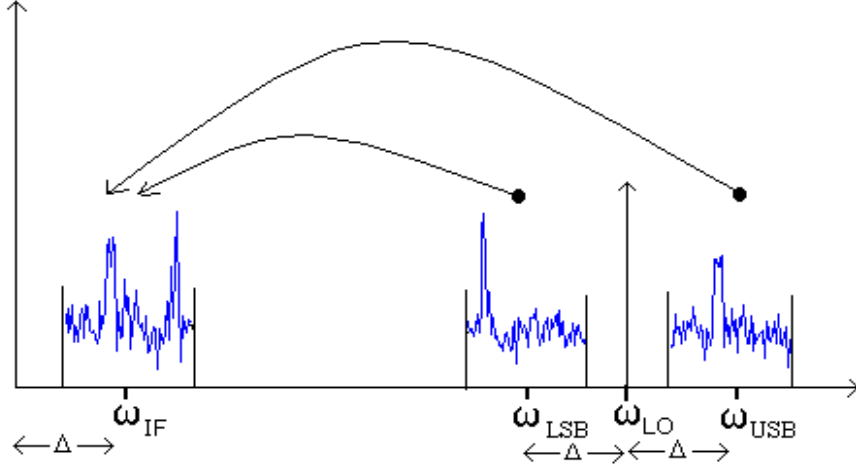


Figure 3.2: When the signal is down converted by the mixer, the LSB and USB signal are converted to the same frequency (Δ). This fact generates confusion due the information in both channels converted to the same location in the frequency spectrum. Also the noise of the system is increased by a factor two by the noise coming from the undesired channel.

on the temperature and its power per frequency unit is $P = kT\Delta\nu$, where k is the Boltzman constant, T is the temperature and $\Delta\nu$ is the bandwidth. There are also other sources of noise present in semiconductor devices which adds to the basic thermal contribution. Examples are the shot noise, the flicker noise and the Josephson noise [22]. As a consequence, if we put no signal at the input of the receiver there will be a power output that corresponds to the noise level of the electronic of the receiver, named P_{noise} .

To characterize the noise generated by a receiver the concept of noise temperature, T_{noise} , is used. To introduce this concept we consider the receiver to be an ideal one (no noise added) and that the noise power that is measured at the output (P_{noise}) is generated by a resistance at a physical temperature T_{noise} in front of the receiver. This temperature, T_{noise} , is called the noise temperature of the receiver. A conventional way to detect weak signals that are embedded in noise is to integrate the output for some time. In this case the lowest signal, ΔT_{min}^1 , that can be detected is

$$\Delta T_{min} = \frac{T_{system}}{\sqrt{\Delta\nu t}} \quad (3.5)$$

where t is the integration time, $\Delta\nu$ is the bandwidth and T_{system} is the noise of the system. In the case of an astronomic receiver T_{system} includes contributions from the receiver noise, T_{noise} , and from the atmosphere.

¹ Astronomers use the concept of Temperature as equivalent for power, both are related by $P = KT$, where K is the Boltzman constant. [23]

The overall noise temperature for a cascade of electronic components [22] is given by

$$T_{receiver} = T_1 + \frac{T_2}{G_1} + \frac{T_2}{G_1 G_2} + \dots + \frac{T_n}{\prod G_i} \quad (3.6)$$

where T_i and G_i are the noise temperature and gain of each element in the cascade. We can see that if the gain of the first amplifier is high enough to overcome the following terms of equation 3.6, the noise temperature of a receiver is completely dominated by the noise contribution of this first amplifier.

3.2 Low Noise Amplifiers

From Equation 3.6 it is clear that the noise of a receiver is dominated by the noise of the first amplifier, which should be carefully designed in order to minimize its noise contribution. This kind of amplifiers are generally referred as Low Noise Amplifiers (LNAs). There are two important factors that determine the noise of an amplifier. The first is the use of appropriate technology for the active devices (generally transistors), the second factor is the design of the amplifier which should be focus to get the minimum noise out from the active devices.

3.2.1 Design of LNAs

One amplifier consist of several stages of amplification, each one consisting on a transistor with its bias, input, and output matching networks. In a basic configuration the different amplification stages are connected in series. This topology, known as single-ended amplifiers, allow to achieve the lowest noise, having at the same time a low power consumption. These features have converted single-ended amplifiers in the obvious choice for LNAs that work in cryogenic environments.

The drawback of this topology is that the input stage is generally mismatched to 50 Ω . When this issue is critical, balanced configuration can be used at expense of doubling the power consumption and increasing the complexity in the manufacture of the LNA. Other limitation of single-ended amplifier is the limited power that can be managed by each transistors. In applications such as power amplifiers, where the output power is the main issue, parallel configuration is preferred.

The design of each stage of amplification consists on design the input and output matching network to achieve the desired gain, noise and input output matching with the adjacent stages. According with Equation 3.6, the first stage of a LNA has to be designed for low noise, while the final stages are designed to achieve the target gain and gain flatness. For this process is necessary to determine the transistor scattering and noise parameters. In the following sections a review of the concepts that have to be considered in the design of LNAs is presented. A more detailed treatment of this subjects can be found in [24], [25], [26], and [27].

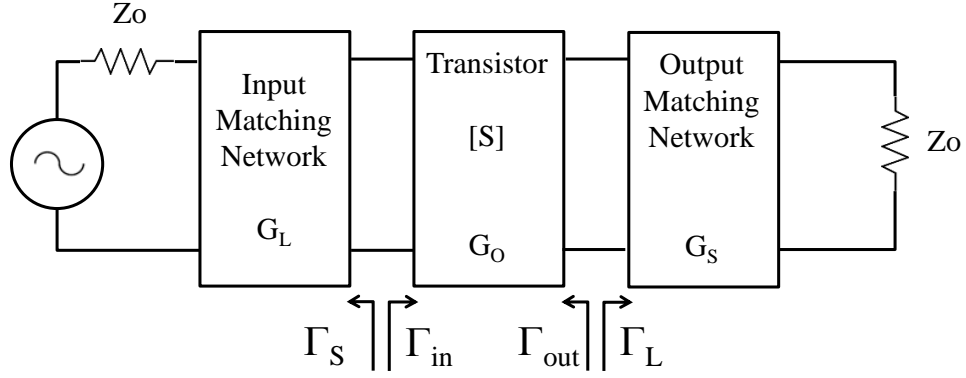


Figure 3.3: General schematic of a single stage amplifier.

3.2.2 Design of a single stage amplifier

A schematic of a single-stage amplifier is presented in Figure 3.3. The input and output matching networks transform the source and load impedance Z_0 into the source and load impedances, Z_S and Z_L at the port of the transistor. It can be demonstrated that the transducer gain of the single stage amplifier is $G = G_S G_O G_L$ where:

$$G_S = \frac{1 - |\Gamma_S|^2}{|1 - \Gamma_{in}\Gamma_S|} \quad (3.7)$$

$$G_O = |S_{21}|^2 \quad (3.8)$$

$$G_L = \frac{1 - |\Gamma_L|^2}{|1 - S_{22}\Gamma_L|} \quad (3.9)$$

We know that the maximum power transfer occurs when $\Gamma_{in} = \Gamma_S^*$ and $\Gamma_{out} = \Gamma_L^*$. Under this condition the amplifier will have the maximum achievable Gain, G_{max} .

$$G_{max} = \frac{1}{1 - |\Gamma_S|^2} |S_{21}|^2 \frac{1 - |\Gamma_L|^2}{|1 - S_{22}\Gamma_L|^2} \quad (3.10)$$

It is important to consider that if the transistor is bilateral, $|S_{12}| \neq 0$, Γ_{in} is affected by changes in Γ_{out} , and both matching network become dependent, having to be tuned simultaneously. The assumption of unilaterally for the transistor, $|S_{12}| = 0$ is only possible for low frequency applications (below few GHz).

In most applications achieving the maximum gain is not necessary because of the need of a nominal gain or for a compromise solution between bandwidth or noise. In these cases the input and output networks are designed using Equations 3.7 and 3.9 to achieve the desired

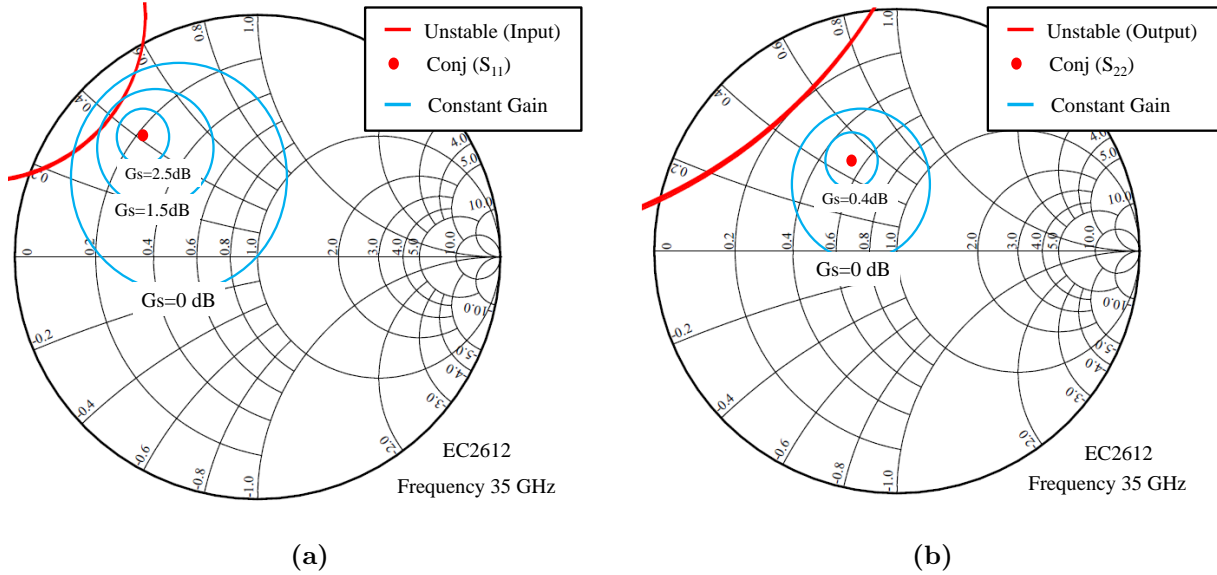


Figure 3.4: Example of constant gain circles for GaAs P-HEMT from UMS (EC2612). Constant gain circles for source (left) and load (right).

value of gain. A useful tool in this process are the constant-gain circles over a Smith Chart. It consists on drawing the locus of input and output reflection coefficients that are associated with a specific gain over the Smith chart. An example of this tool is presented in Figure 3.4 where constant gain circles are presented for a commercial HEMT.

3.2.3 Stability

One issue when dealing with amplifier design is the stability. An amplifier is considered to be unstable if $|\Gamma_{in}|$ or $|\Gamma_{out}|$ are greater than one. In this situation the amplifier becomes unstable and can oscillate. There are two definitions of Stability:

- Unconditionally stable when $|\Gamma_{in}| < 1$ and $|\Gamma_{out}| < 1$ for all passive source and load impedances.
- Conditionally stable when $|\Gamma_{in}| < 1$ and $|\Gamma_{out}| < 1$ for only some load and sources impedances.

Most of transistors are conditionally stable, and the values of $|\Gamma_S|$ and $|\Gamma_L|$ that causes the transistor to oscillate can be visualized over the Smith Chart as stability circles. An example of stability circles for a commercial HEMT is also presented in Figure 3.4. When designing the input and output network, stability criteria has to be considered in order to avoid $|\Gamma_S|$ and $|\Gamma_L|$ to fall in the unstable region.

If the matching network are properly designed the LNA have to be unconditionally stable. This condition has to be verified over a frequency range much broader than the design bandwidth. For example, for Q band LNAs we checked the stability from 1 to 80 GHz. The easiest way to check for stability is to use the Rollet condition:

$$K = \frac{1 - |S_{11}|^2 - |S_{22}|^2 + |\Delta|^2}{2|S_{12}S_{21}|} > 1 \quad (3.11)$$

where:

$$|\Delta| = |S_{11}S_{22} - S_{12}S_{21}| < 1 \quad (3.12)$$

If both conditions are met, then the amplifier is unconditionally stable.

To control the features that causes amplifiers to be unstable, it is important to understand the origin of this phenomena. Transistors presents gain, and if a feedback loop is present the device could start to oscillate. The more obvious feedback is the reverse transmission of the transistor, S_{21} but other source are the bias coupling, waveguide modes in the cavity where the transistor is located or ground coupling, phenomenas that are always present and have to be considered.

3.2.4 Noise

A basic asumption when designing LNA is that the signal is small enough to assure that the transistor operates in the linear regime. In this case it can be characterized by its scattering Parameters (S-Parameters). S-Parameters can be easiliy measured using a Vector Network Analyzer (VNA) and an appropriate test facility. The problem is that S-Parameters give not information about the noise features of the device. A set of aditional parameters must be known. These noise parameters are:

1. T_{min} is minimun noise that can be delivered by the transistor.
2. $Z_{opt} = R_{opt} + jX_{opt}$ is the generator impedance for which T_{min} is delivered.
3. g_n is the rate of change in noise when the transistor is not in the optimun noise point.

When these parameters are known the noise delivered by the transistor can be calculated as

$$T_{noise} = T_{min} + T_0 \frac{g_n}{R_n} |Z_G - Z_{opt}|^2 \quad (3.13)$$

where the generator impedance, Z_G , is the impedance of the input network. We notice that in the literature several versions of this formula can be found, but all of them have the same structure. We have followed the notation of [28], as it works with noise temperatures, which is the usual unit of noise in the field of radioastronomical instrumentation.

An important implication of equation 3.13 is that the minimum amount of noise that can be delivered by a transistor is T_{min} , being unpossible to have a LNA with a noise lower than T_{min} . This fact points to the importance of using the appropriate transistor for each application. At this moment the lowest T_{min} are achieved by High Electron Mobiity Transistors (HEMT), and particullary by InP HEMTS. A complete review on HEMT technology is presented in section 3.3

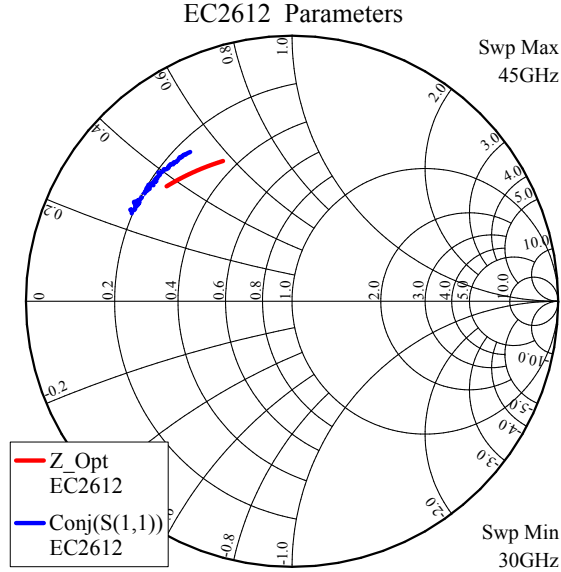


Figure 3.5: Z_{Opt} (red line) and S_{11} (blue line) for a GaAs P-HEMT from UMS (EC2612). Both traces are from 35 to 40 GHz. It is clear that is impossible to design a matching network that achieve good input matching and lowest noise at the same time.

A second implication of equation 3.13 is that the minimum noise is achieved when the generator impedance, Z_G is equal to Z_{opt} ². This source impedance is in principle different from the impedance needed for high gain and for good matching with 50Ω systems. This fact prohibits achieving simultaneously low noise and a high gain matching. There are some technics to get Γ_{opt} closer to S_{11}^* being the most used the series inductive feedback. This technique consists in adding a small inductance between the source of the transistor and ground increasing the real part of S_{11}^* . The drawback is a decrease in gain of the transistor.

A third implication comes from the fact that all this numbers are frequency dependant, being impossible to design a matching network that achieve the lowest noise over a determined bandwidth. This limitation follows the Bode-Fano criteria. Figure 3.5 shows the values of S_{11}^* and Γ_{opt} as function of frequency in a Smith Chart.

The problem is that measuring noise parameters is not an easy task, as it involve measure the output noise for different input impedances. To avoid that, models can be used to simulate the behaviour of the device. In the case of LNAs a lineal model is preferred since it shows a very good agreement between measured and simulated scattering and noise parameters. The limitation of this model is due the fact that it is strongly dependent on bias point, and can not predict any nonlinear phenomena as saturation or intermodulation. For applications, as power amplifiers, in which the nonlinear behaviour is important, more complex nonlinear model are used as presented in [29]. The lineal model for HEMT is presented in section 3.2.5.

² Remember that Γ_S is related to Z_S as: $\Gamma_S = \frac{Z_S - Z_0}{Z_S + Z_0}$, where $Z_0 = 50 \Omega$ is the standard impedance

3.2.5 Gain stability

A limitation to the receiver sensitivity arises from the instability of the gain. In this case Equation (3.5) becomes

$$\Delta T_{min} = T_{sistema} \sqrt{\frac{1}{\Delta\nu t} + \left(\frac{\Delta G}{G}\right)^2} \quad (3.14)$$

where G is the gain of the system and ΔG is the variance of the gain [23]. This gain fluctuations are generated by the amplifiers present in the receiver. It has been shown that the gain of HEMT amplifiers fluctuates as a function of time [30] [31]. Reference [32] summarizes the known facts about these fluctuations as:

1. The fluctuations vary as the inverse square root of the transistor gate width.
2. The fluctuations are larger at cryogenic temperatures.
3. The fluctuations do not depend upon the bias point.
4. Fluctuations are uncorrelated with drain current variations.
5. The fluctuation has a $1/f$ spectrum, but there are not variations in the time scale of days or months.

This instability is believed to be caused by carriers trapped in crystalline defects. This causes some random variation in carrier concentration and finally in the gain of the device. ALMA had proposed a maximum fluctuation of $\delta G/G = 1E^{-4}$ for the receivers [33].

3.3 High Electron Mobility Transistors (HEMT)

In the RF and millimeter wave range, amplifiers based on High Electron Mobility Transistor (HEMT) show the lowest noise figures. HEMT were invented in Japan in the early eighties [34]. They belong to the Field Effect Transistor (FET) family, being the main difference between a FET and a HEMT is the fact that the conduction channel is formed in a thin layer that is not doped. Electrons are confined to move in this layer, and due to the lack of impurities, do not suffer Coulomb scattering with the donors, improving the mobility coefficient, μ .

The maximum frequency at which the transistor could work, f_t is defined by the transit time of carriers through the active area, which is determined by the saturation velocity of the material and the length of the channel,

$$f_t = \frac{v_s}{2\pi L_g} \quad (3.15)$$

where the saturation velocity is defined as $v_s = E\mu$, being E the electric field applied between drain and source and μ is the mobility of the electrons in the channel. As seen from

equation 3.15, an improvement in the carrier mobility allows the transistor to work at higher frequencies.

3.3.1 Semiconductor structure of a GaAs HEMT

The first HEMT [34] was fabricated using an AlGaAs/GaAs junction. This structure use the fact that AlGaAs has a wider band-gap than GaAs. When a n-doped AlGaAs is placed in contact with a GaAs layer, electrons will diffuse from AlGaAs to GaAs. Electrons accumulate in a thin layer in the GaAs which is not doped, see Figure 3.6(a).

To improve the mobility of the electrons confined in the heterostructure a spacer layer is added between the doped n^+ AlGaAs and GaAs. This layer reduces the interactions of carriers with the donors in the n-type material. This structure is grown epitaxially over a GaAs substrate. To prevent impurities present in the substrate to diffuse to the active zone a buffer layer of GaAs is grown between the substrate and the active region. Figure 3.6(b) shows a conventional structure for AlGaAs/GaAs HEMT.

This first kind of HEMT was soon replaced by more complex structures that uses quantum wells. In this configuration a thin layer (few Å) of a narrow-band material is placed between two wider-band materials. Electrons are trapped in this thin layer, less than the Broglie wavelength for an electron, and are confined to move in this 2D structure. This regime is known as 2D electron gas.

3.3.2 Materials

Nowadays quantum well HEMTs have been implemented with different combinations of III-V semiconductors. Each material has its own advantages, therefore, are used for diferent

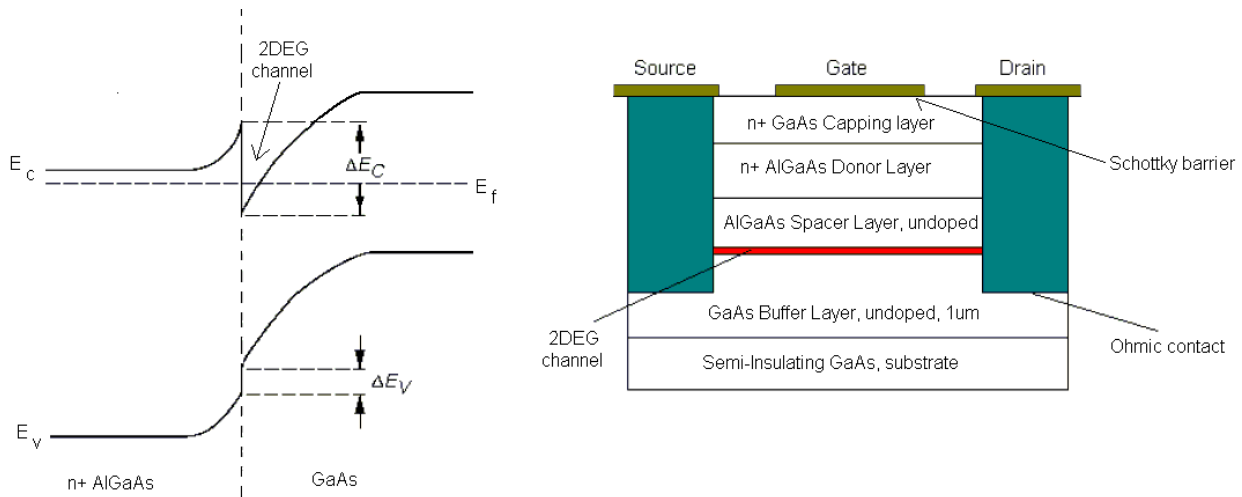


Figure 3.6: (a) Band diagrams for an AlGaAs/GaAS junction. (b) Conventional structure for an AlGaAs/GaAs HEMT

purposes. A good review of InP and GaAs HEMT technologies is presented in [35].

GaAs was the first material used in HEMT amplifiers. GaAs is cheaper and more reliable than other microwave materials, being the most common material for microwave transistors. As stated previously the first HEMT were based in a AlGaAs/GaAs junction over a GaAs substrate. This first structure was improved by adding ternary compounds including Indium in the channel, improving the mobility and confinement of carriers. Unfortunately, In compounds have a lattice constant that is not matched with GaAs and AlGaAs, then only low content of Indium can be used. As the channel layer is thinner than the critical thickness, the mismatch can be elastically absorbed by the crystalline network and dislocation will not occur. This kind of structures are known as pseudomorphic HEMT (p-HEMT).

InP HEMT are devices that use InP as substrate and a heterostructure based on InAlAs/InGaAs/InAlAs. InP is well matched with InAlAs and allows to use high In content in the channel. This allows InP p-HEMT to have lower noise and high f_{max} than GaAs p-HEMTs. The problems with indium phosphide are its fragility and high cost of substrates, which had prevented InP to be the most used devices in commercial applications.

During the last years InAlAs/InGaAs/InAlAs has been grown over GaAs substrates. To adapt the lattice constant of the GaAs substrate to InAlAs or InGaAs a buffer layer is used. This buffer layer is grown with a variable combination of quaternary or ternary compounds that change the lattice constant of the substrate. These kind of structure are called metamorphic HEMT (M-HEMT). By using this technology noise figures and f_{max} comparables with InP P-HEMTs have been obtained [36] [37] [38]. This technology is also well suited for industrial applications and is offered by several companies [39] [40]. At this moment this technology is being evaluated for cryogenic applications in radioastronomy.

To fabricate these complex structures Molecular Beam Epitaxial (MBE) or Metal Organic Vapor Deposition (MOCVD) processes are used. The best results are obtained with MBE which allow a better control on the uniformity of the structure and on the dimensions of each layer. MOCVD is used in industrial ambients as it allows the production of lower cost wafers.

Other HEMT technologies

GaN devices have been developed over the last years for high power applications. These materials have a Wurtzite crystalline structure (Instead of Zinblende for GAAs or InP) and are grown over Silicon Carbide or Silicon. In the last few years a lot of effort has been done to produce MMICS based on this technology [41][42] mainly for military applications.

Antimonium-based semiconductors such as AlSb/InAs [43] are under development. This kind of devices consume much less power than GaAs or InP being suitable for low power applications, such as space and remote operation.

3.3.3 Transistor Layout

Once the active layer has been grown the transistors have to be configured. There are several parameters that determines the transistor performance, being the most relevants the gate length and width. From equation 3.15 it is clear that f_{max} is affected by the mobility of carriers in the channel and by the length of the channel (equal to the gate length). With current electron beam techniques it is possible to achieve gate lengths of 35 nm [44]. To achieve this submicron structure without paying too much cost in the contact resistance and mechanical reliability of the structure, the gate is configured in a T or mushroom configuration.

The gate width refers to the width of the channel. By increasing it the transistor can manage more current and the effect of parasitic contact resistance is diminished. In order to achieve an increased gate width multifinger configuration is used. In this configuration several channels are configured in a parallel configuration. The draw back of increasing the gate width is the addition of extra capacitances between the ports of the device.

The process of building a transistor from an epitaxial structure, as described in the previous sections require several steps:

1. Mesa etching. The devices are isolated to define the area where conduction channel is present. The unused areas can be removed by etching, or on some processes ion bombarded to eliminate the conduction band on certain areas.
2. Ohmic contact. Drain and source transistor contacts have to be ohmic to minimize the existence of parasitic contact resistances. Ohmic contacts need a highly doped semiconductor under the metalization, layer that is know as cap layer. After depositing the suitable metal alloys, generally Titanium Palladium and Gold the contacts are annealed.
3. Gate configuration. The cap layer that is used for the ohmic contact has to be removed in order to deposit the gate contact near the conduction channel. The gate metalization is a Schotky contact. Different topologies can be used when submicrons gate lengths are need , as T-shape or mushrooms- shape.
4. Air bridges. If multiple finger configuration is used, air bridges are necessary to connect the source metallizations of different fingers.
5. Passivation. To protect the device from humidity, contamination or oxides, a thin layer of a dielectric material is deposited all over the device (except contacts).
6. Back side processing: The wafer is thinned to 3-4 mils to improve thermal disipation of the device and the backside of the transistor is metallized. In some applications vias are added to connect the source to ground.

3.3.4 HEMT modelling

Instead of using measured data an equivalent circuit approach can be used to model the transistor. The lineal model for HEMT devices is presented in Figure 3.7. In this model the active part of the transistor is represented by a current source controlled by the gate voltage, where g_n is the transconductance of the device and τ is the delay time. Capacitances C_{gd}

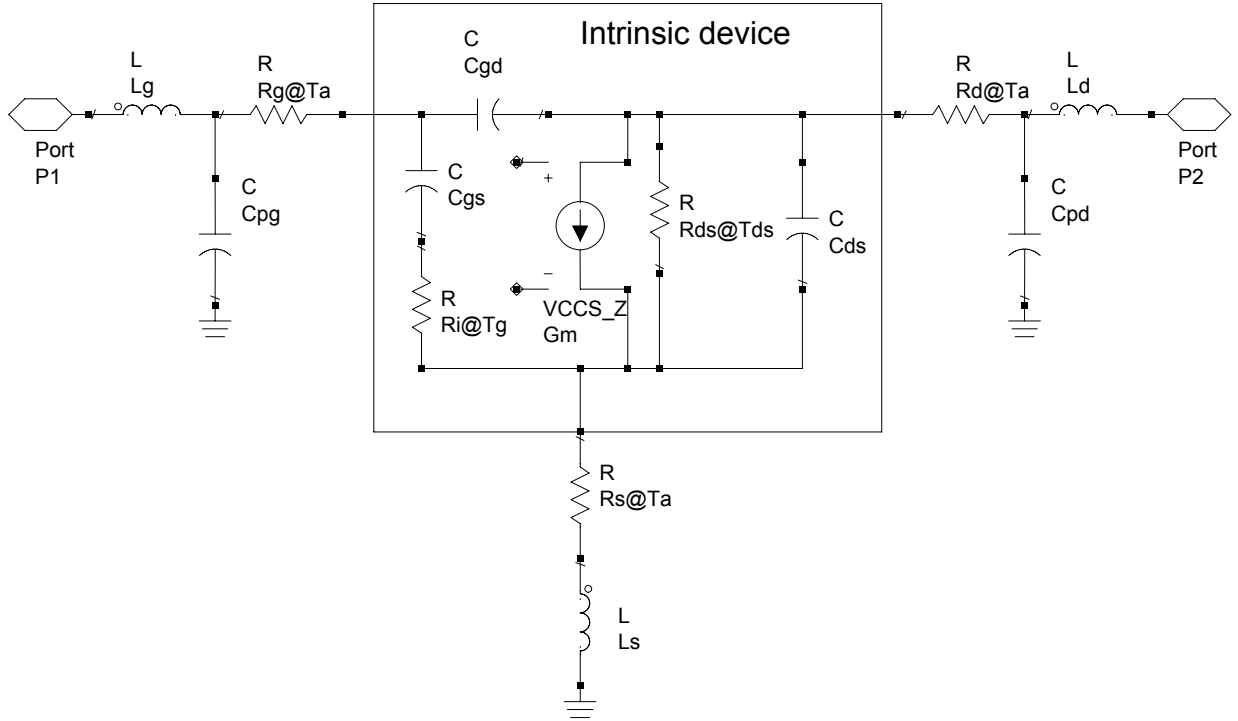


Figure 3.7: Lineal model for a HEMT. L_g , L_d and L_s represent the parasitic inductances. C_{pg} and C_{pd} represent the pad capacitances. R_g , R_d and R_s represent the parasitic resistances. The intrinsic chip models the device itself. The Pospiezsalski model assign an asociated a temperature T_g to the gate resistance R_i and T_d to R_{ds} . Parasitic resistances are asociated with the physical temperature of the device.

and C_{gs} represent the geometrical capacitances between gate, drain and source, R_{ds} represent the channel resistance and R_i represent the gate resistance. The model also incorporates the parasitic effects due to the ohmic contact (R_g , R_d and R_s), conexion pads capacitances (C_{pg} and C_{pd}) and inductance of contacts (L_g , L_d and L_s). The model can be extracted from transistor S-Parameters measurements. The process for extract a lineal model from measured data is presented in [45] [46].

Pospiezsalski Noise Model

The lineal model presented above only accounts for the S-Parameters of the transistor. To include the noise features it is necessary to use another model. Several models for the noise can be found [47] [48], being of particular interest to us the noise model proposed by Marian Pospiezsalsky [28] [49]. The advantage of this model is that it can be easily implemented in a computer aid design (CAD) software by asigning an associated temperature to the resistor present on the linear model, as shown in Figure 3.7. The parasitic resistances R_s , R_d and R_g are at ambient temperature, while the intrinsic chip resistance R_{gs} and conductance g_{ds} are asociated with equivalent gate temperatue, T_g , and drain temperature T_d . Experience have proved that T_g is almost equal to ambient temperature while T_d scales linearly with drain current. Using these parameters the noise model can be adjusted by only determining the equivalent circuit based on S-Parameters measurements and using one parameter (T_g) to fit

the measured noise figure of the device at 50 Ω .

The obtained values for noise parameters (defined in section 3.2.4) of the intrinsic chip are:

$$R_{opt} = \frac{f_t}{f} \sqrt{\frac{r_{gs} T_g}{g_{ds} T_d}} \quad (3.16)$$

$$X_{opt} = \frac{1}{\omega C_{gs}} \quad (3.17)$$

$$g_n = \left(\frac{f}{f_t}\right)^2 \frac{g_{ds} T_d}{T_0} \quad (3.18)$$

$$T_{Min} = 2 \frac{f}{f_t} \sqrt{g_{ds} T_d r_{gs} T_g} \quad (3.19)$$

where $f_t = \frac{g_m}{2\pi C_{gs}}$ is the cut-off frequency of the device. Notice that these expressions represent the noise of the intrinsic chip, then the noise contribution from parasitic contact resistances should be added.

3.3.5 Fabrication of LNA

Once defined the adequate technology for the desired application the LNA has to be designed and built. There are two strategies to built microwave amplifiers. The first is to use hybrid technology, also known as microwave integrated circuit (MIC) or chip and wire circuits. In this technology the amplifier is built using discrete devices and bond wires. This technique allows to tune each amplifier, e.g. by slightly modifying the bonding lengths, to achieve the best possible noise. The fabrication of an hybrid amplifier needs a relatively large time as each component should be placed and bonded by hand and, if an optimization is performed, more time is needed. This is only possible when limited numbers of amplifiers are required.

The second alternative is using microwave monolithic integrated circuit (MMIC) technology. In this case the amplifier is completely built over the same substrate with the active devices. This procedure allows, in principle, the fabrication of thousands of amplifiers with similar performance in a short time. The process of design a MMIC starts with the choice of technology. The issues to be considered are the material used in the foundry and the gate lengths they can offer. In case of LNA for radio astronomy, the main issue is to achieve the lowest noise. Therefore, low-noise processes as InP HEMT or GaAS M-HEMT are the best options.

Once the foundry is selected the design process can start. This process is done with the assistance of some specialized softwares as Advanced Desing Suite (ADS), Cadence or

Microwave office (AWR). The design is based on the models of the active and passive components that can be fabricated with the selected technology. Some foundries have good and reliable models to offer to the designers, while others have not, and the work has to be done in close cooperation with the foundry team. Anyway, most of the models offered have been extracted for room temperature. Therefore, when cryogenic application is desired much more work is necessary in order to produce reliable cryogenic models.

After the design is finalized and verified the fabrication process starts. It can take some time as the fabrication process includes several steps and in some cases a second iteration of fabrication is needed. Finally, the MMICs are delivered to the designer and they have to be tested (most times only on-wafer DC measurements) and assembled in the final working components. The main advantage of the use of MMIC amplifier is that the fabrication of a series of LNA becomes easy, as only one chip has to be mounted and bonded. The time in assembling a MMIC-based LNA can be many times lower than for a hybrid amplifier [50] at the penalty of noise, which is higher by 30% than a hybrid amplifier [51].

Chapter 4

LNAs for Band 1

Low noise amplifiers are the key components of a radio receiver. As demonstrated previously in section 3.1.1 the noise level of the first amplifier dominates the noise of the complete receiver. Consequently, the efforts on development of low noise technologies are greatly recompensed by the increase in sensitivity of the instrument. As part of the Band-1 development program at Universidad de Chile a project for design and construction of cryogenic LNAs was started. It included the installation of new facilities at the Millimeter Wave Laboratory and the training of specialized personal on different areas. In this section we present the main achievements of this project. To start the discussion we offer a complete analysis of the Band-1 LNA problematics, reviewing the technologies that can be used and the expected results and problems for each one. Then, we present the achievements of the project in setting up the LNA facilities and expertise.

4.1 Band 1 LNAs problematic

Considering a 7 K contribution from the optics to the receiver noise temperature, the specification for an ALMA Band-1 LNA is to have a noise of 10 K over 80% of the band, and a relaxed specification of 21 K over 100% of the band. Other specifications arise from the architecture of the receiver. The first of these specifications is that the gain should be around 30-35 dB, to allow the following stages of down-conversion to be at ambient temperature. The second specification concerns the input return loss (S_{11}) which should be lower than -10 dB over the complete band, to avoid the use of cryogenic isolators between the OMT and the LNA. Finally the output return loss (S_{22}) is required to be lower than -5 dB. The LNA should also be unconditionally stable for frequencies up to 80 GHz.

If we compare these specifications with the results from the 30 GHz Planck amplifiers [52], which have the best reported noise temperature near the frequency range of Band 1, we conclude that ALMA Band-1 LNAs should have the same noise performance (5 times quantum limit) but over a wider band (36% instead of 20%). The big difference between both cases, is that in the case of ALMA a batch production of amplifiers is needed since it will require 66 receivers working on dual polarization. Therefore, if the LNAs have enough gain

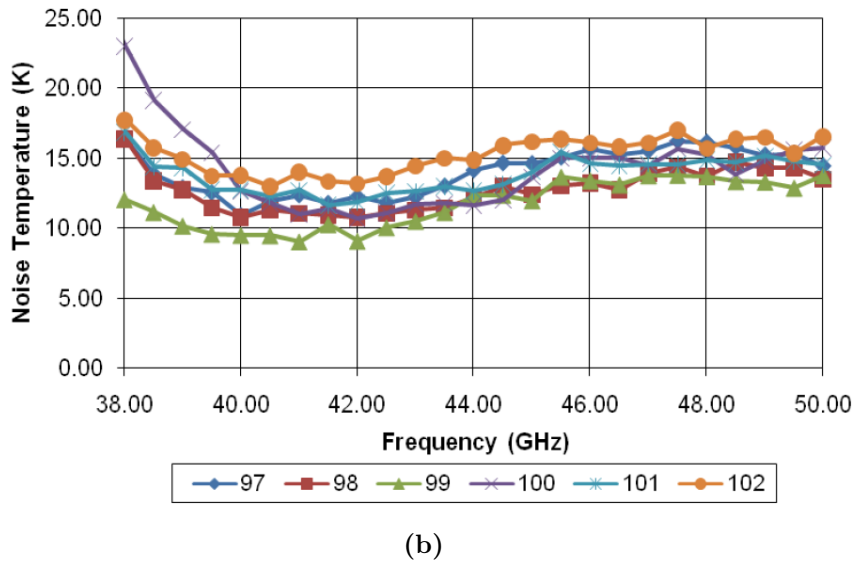
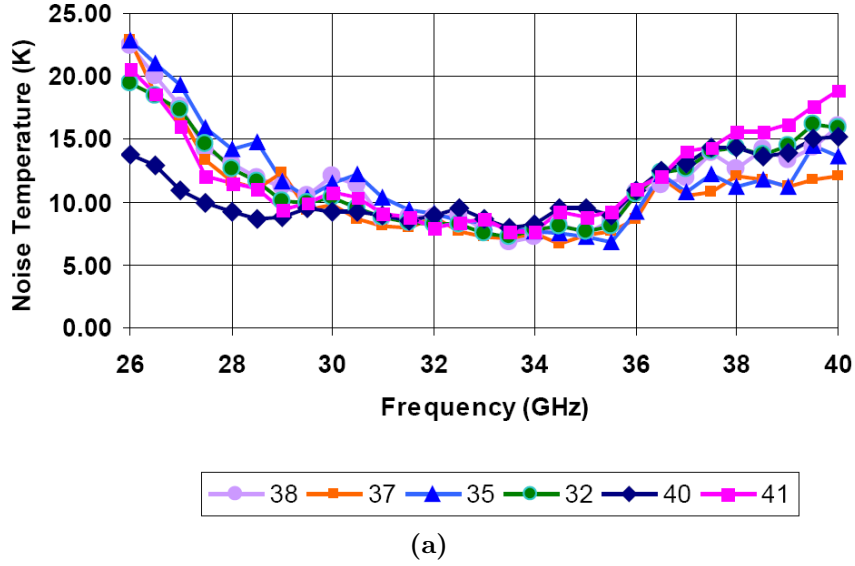


Figure 4.1: LNA noise temperature for EVLA receivers (courtesy of M. Pospieszalski). The noise temperature of the LNA is 8-10 K at the band center for Ka Band (a), and 10-15K for Q Band (b).

(30 to 35 dB), as to use one amplifier per polarization receiver, 132 amplifiers are needed plus some spares. This fact constrains the time that can be used on tuning each amplifier for the best possible noise performance. A useful case to see what is expected for a complete series of LNAs are the amplifier made at the National Radio Astronomy Observatory (NRAO) for the EVLA. In Figure 4.1 the measured noise for the EVLA LNAs shown. We see that the ALMA Band-1 noise specifications are met by the Ka receiver, but in the case of ALMA Band 1 an additional contribution to the receiver noise of 10 K has to be considered due to the warm optics configuration. We can summarize the LNA specifications for Band 1 as presented in Table 4.1.

There are two main ways for designing the Band-1 LNAs. The first is to use hybrid technology. In this technology the amplifier is built using discrete devices and bond wires.

Number of amplifiers	150
RF range	31.3-45 GHz
Noise Temperature, 80% of the band.	10 K
Noise Temperature, 1000 % of the band.	17 K
Gain	35 dB
Gain Flatness	8 dB
Reflection Losses	better than -7 dB.

Table 4.1: Specifications for ALMA Band-1 amplifiers.

The second alternative is using Microwave Monolithic Integrated Circuit (MMIC) technology. In this section a brief discussion about using MIC/Hybrid or MMIC technology for ALMA Band 1 is presented.

4.1.1 Hybrid technology

The first step to produce a LNA for ALMA Band 1 is to choose the right transistor. ALMA Band 1 will need 140 5-stage LNAs (128 + 10% of spares). The use of 5 stage amplifiers will allow the LNAs to have more than 30 dB of gain. The implication is that around one thousand transistors are need (128 amplifiers * 5 stages + 50% contingency). Their gate length should be around 0.1-0.08 μm to have a high enough f_{max} and good stability. Possible sources of transistors for this project are:

- “Cryo-3” from Northrop Grumman Corporation (NGC), formerly TRW. These InP devices were fabricated in 1999 and at the present time they still show the best noise figure for cryogenic operation [53].
- “IHER” or “Cryo-N” from NGC. These InP were fabricated after the Cryo-3 run using the same process. Anyway the transistors proved to be good but not as good as Cryo3 series [53].
- Hughes Research Laboratory (HRL). These InP devices were built at HRL for NRAO and were used in the Wilkinson Microwave Anisotropy Probe (WMAP) [54]. The noise figure is excellent but not as good as the cryo-3 run. Various of this transistors are still available with different gate lengths, including 0.1 μm .
- The Swiss Federal Institute of Technology Zurich (ETH) has developed a process for 0.1um InP HEMT [55]. This is an experimental process but the results up to now have been promising. The noise for an amplifier based on these devices is also expected to be similar to HRL or Cryo-N devices.
- United Monolithic Semiconductors (UMS) offers low noise 0.15 μm devices [56]. This GaAs HEMT is commercially available, but they have a high power consumption as they are pseudomorphic GaAs devices and not InP or Metamorphic GaAs.

In our opinion the best alternative is to use a suitable device, like HRL or ETH for the amplifier, but to reach the noise of 10K a Cryo-3 device should be used as the front-end component. If the hybrid approach is chosen the manufacturability of the amplifiers has to

be considered. The process of fabrication and tuning of the amplifiers is well known as time consuming. Our estimations indicates that 6 person years of work is needed to build and test them. The production should need around 24 months. Anyway some prototype devices should be fabricated and tested to adjust this initial estimation to the real time that will be necessary to produce ALMA Band-1 amplifiers.

In the project of fabricating Band-1 LNAs testing times should be carefully considered. In fact, testing consumes a considerable amount of time, being similar to the fabrication time of an hybrid LNA. A fully automated test setup is highly recommended. In the case of Band 1 a proper measurement system should therefore be installed. For the range of frequencies of Band 1 the noise setup could use hot-cold method or a cold attenuator method [30] [57] [58].

4.1.2 MMIC Technology

The noise of a MMIC chip with current InP technology is expected to be 15-18K at Band-1 frequencies [51]. Probably the noise will increase by 1-2 K when the MMIC is packaged. To achieve the noise of 10 K a first stage transistor could be used before the MMIC. The main advantage of the use of MMIC amplifier is that the fabrication of a LNA module can take 1 day [50]. Then, a complete serie of LNA for Band 1 could be fabricated in a time span of 6-8 months. Anyway, the testing time of this amplifiers should be carefully considered to fit in the production plan. As in the case of hybrid amplifiers, it is recommended to carefully plan the test systems and procedures to allow testing all modules needed for ALMA Band 1 in a reasonable time.

In the case that a “wafer run” of MMIC fabrication is done, a time of 10 to 12 months needs to be considered between the end of the design stage and the reception of MMIC chips. In the decision the specific regulation of every foundry had to be considered. There are several foundries that offer processing with gate lengths lower than 0.15 μm . A brief review of them and their expected cryogenic performance is:

- HRL, have an InP 0.1 HEMT process. This process have been used in several cryogenic MMIC [59]. Some of these designs have been used in cryogenic applications for Deep Space Network and radio-astronomy applications. The expected noise temperature for a Band-1 MMIC is 15-18K.
- NGC, 0.10 μm InP HEMT. As the 0.1 μm process from HRL this technology has been used in several cryogenic amplifiers [51]. The expected noise temperature at Band 1 for these MMICs is around 15-18K.
- NGC, 0.035 μm InP HEMT. This new non-commercial process is reported to have a noise figure as low as 22 K at W band [60], allowing MMIC based LNA with noise figure of an hybrid amplifier.
- OMMIC, this European foundry has a 0.07 μm GaAs mHEMT technology [61].
- Win Semiconductor, they have a non commercial 0.15 μm GaAs mHEMT process for low Noise application [62]. ASIAA is using this technology for a Band-1 amplifiers.
- At the Fraunhofer Institute (IAF) a M-HEMT process has been developed [37][38]. They have gate lengths down to 50 nm and MMIC up to 320 GHz have been pro-

duced [36]. Preliminary data indicates that the transistor cryogenic performance is comparable with NGC or HRL devices [63] [64].

4.2 LNAs development at Universidad de Chile

To setup our amplifier development facilities we started a first project consisting on packaging commercially available GaAs MMIC amplifiers into a LNA module. The main objective was to gain experience on the fabrication and testing of LNAs modules and in the assembling of MMICs to larger systems. As an output of that project an order-zero solution for Band-1 amplifiers was produced. Detailed results are presented in Section 4.2.2. Afterwards, a second project started whose goal was to produce hybrid amplifiers. For this we started with the transistor modeling process, following with the design stage of the amplifiers, which were successfully assembled at our laboratory. A detailed report on this second project is presented in Section 4.2.3. This second project has given our group the necessary knowledge on LNA techniques to start working with more advanced technologies as InP devices. Along with the process of design and built amplifiers a series of testing procedure were developed in order to accurately measure the proposed devices. These test setups are presented in Section 4.2.1.

4.2.1 LNA characterization test setup

The first step of our development effort has been to set up the appropriate facilities for measurements of noise and scattering parameters.

Noise temperature setup

A dedicated test setup was built to measure the noise figure of our amplifiers using the Y factor method. The procedure consists in measuring the power spectrum at the output of the device under test (DUT) when cold and hot loads are placed in front of the device. The output power of the DUT when looking at the cold load is

$$P_{Cold} = kT_{Cold} + kT_{Noise} \quad (4.1)$$

while for the hot load the output is

$$P_{Hot} = kT_{Hot} + kT_{Noise} \quad (4.2)$$

Finally the noise temperature of the device under test is

$$T_{noise} = T_{Hot} - Y T_{Cold} / (Y - 1) \quad (4.3)$$

where $Y = P_{Hot} / P_{Cold}$.

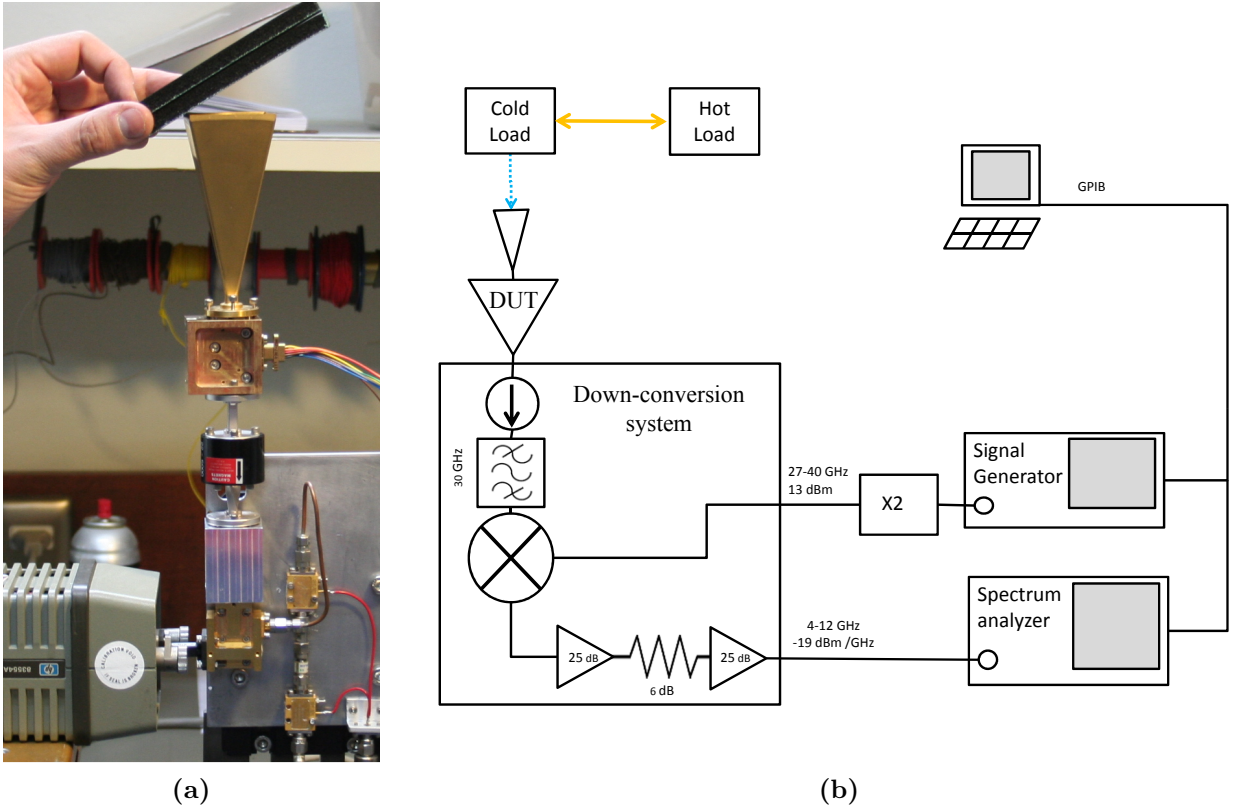


Figure 4.2: The experimental setup. Left: Picture of the down conversion plate, DUT and hot load. Right: Schematic of the experimental setup.

Initially our system used a hot load consistent of a piece of absorber at room temperature (293 K), while the cold load correspond to an absorber embedded in liquid nitrogen. A standard gain horn was used to collect the radiation from this black bodies into the LNA¹. As the output power of the devices is too weak to be directly detected by our instruments it is preprocessed by a Q-Band down converting and amplification system. It consists of an isolator, a 30 GHz high pass filter, a Schottky mixer and two 4–12 GHz LNAs. The local oscillator signal to drive the down converter is generated by a 20 GHz source followed by a doubler. The output power is then measured by a spectrum analyzer. To cover the complete range from 30 to 50 GHz the LO had to be set at different values from 27 to 38 GHz. The complete test setup is depicted in Figure 4.2. The spectrum analyzer and the LO generator are controlled by a PC with LabView using a general purpose interface bus (GPIB). The spectrum analyzer is set to have a resolution bandwidth (RBW) of 10 MHz and to sweep from 2 to 12 GHz. The measurement are binned by the software in 100 MHz channels and stored for further calculations.

The measurements have to be calibrated to remove the effect of the down converting stages. For this purpose the noise and power levels of the down converting stage, T^{sys} , P_h^{sys} and P_c^{sys} have to be measured and stored. Then, the DUT is connected to the system and the noise of the system and DUT is measured. The calibrated noise and gain of the DUT

¹ In a final stage of this thesis a new equipment was acquired to perform the same measurement by using a noise source switching between a electronic loadsw at 293K and near 10.000 K. The rest of the experimental setup and data manipulation is very similar to the described method.

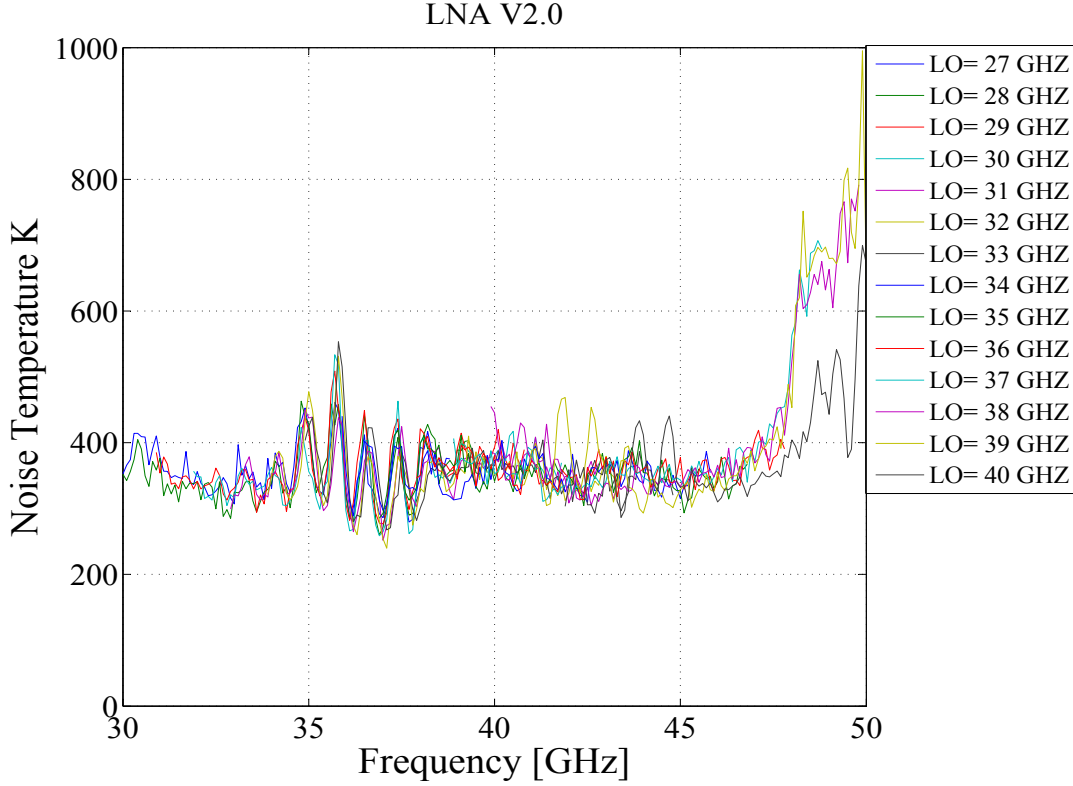


Figure 4.3: Unprocessed set of data for a MMIC based LNA. It can be observed that data for different LO settings at the measuring system have good matching. This data are averaged in order to have a good estimation of the noise temperature value and measuring errors.

are:

$$G^{DUT} = \frac{P_h^{DUT+sys} - P_c^{DUT+sys}}{P_h^{sys} - P_c^{sys}} \quad (4.4)$$

$$T^{DUT} = T^{DUT+sys} - \frac{T^{sys}}{G^{DUT}} \quad (4.5)$$

This process is repeated for different LO settings. It has to be noted that the software has to discard some portions of data that are contaminated by sideband signals which are not filtered out by the down-converting stage. As a result a complete set of noise and gain curves are produced, each curve for different LO setting. Since the contribution from the LO and down converting stages is removed by the calibration process, the final data set for the amplifier should agree and can be averaged to reduce errors. This is clearly shown on Figure 4.3 which presents some unprocessed set of data for a MMIC based LNA.

The standing wave between 34 to 38 GHz is due to reflexions between the load and the horn. To avoid this problem the load should be positioned in an angle of 30°. Another option is to place an isolator between the loads and the DUT. In this case the final data correspond to the noise of the DUT and the isolator. The noise of the DUT can be extracted as [58]:

$$T^{DUT} = \frac{T^{DUT+isolator} - T^{isolator}}{G^{isolator}} \quad (4.6)$$

The noise and gain of the isolator, or any passive component, can be estimated from the S-parameters measurements as:

$$G^{isolator} = |S_{12}|^2 \quad (4.7)$$

$$T^{isolator} = T_{physical} * (1 - |S_{12}|^2 - |S_{11}|^2) \quad (4.8)$$

,where $T_{physical}$ is the physical temperature of the isolator.

Cryogenic Measurements

An old cryostat was adapted to serve as test cryostat at our laboratory. The inputs of the cryostat were modified for using WR-22 waveguide inputs. Vacuum windows for the waveguide ports were built using mylar films. Stainless steel waveguides bring the signals from the 293k to the inner 12 K plate with a thermalization stage at 80 K stage. The system uses a two stages (12 and 80 K) APD system which is cooled by water. The necessary facilities to run such equipment were installed at the laboratory. Despite a small working area, the new cryostat demonstrate to be functional and it was extensively used for cryogenic testing along this project. A more flexible and practical solution was designed which is expected to be implemented in the near future. For cryogenic measurement of S-parameters the system is calibrated using standard S-parameters calibration procedure.

4.2.2 LNA based on commercial chips

The first task of this project was to identify the existing commercial chips that cover the Band-1 frequency range. Three sources were identified:

- Northrop Grumman developed a line of GaAs products (Velocium) for high frequency range applications (20-50 GHz). One of this products , the LNA ALH376 can cover the Band-1 range with a noise figure of 2.2 dB. This line has been sold to Hittite microwave corporation.
- United Monolithic Semiconductor offers LNA MMICS for the 36-44 GHz ,CHA2194, with a noise figure better than 3 dB.
- Avago Tech offers a LNA for the 23-43 GHz range of frequency, AMMC-6241. The noise is about 2.7 dB (250 K) and the gain is 20 dB. The cost of this chip is about US\$ 25. At the high end of the amplifier range (40-45 GHz) the chip will exhibit some gain, but the noise figure will be higher (more than 3 dB).

Table 4.2 summarizes the main differences between these three alternatives. Based on the excellent noise figure of the ALH 376 we chose to build our MMIC modules. These chips had to be integrated into a block which assures mechanical support to the MMIC. We defined that the input and output of the amplification block to be WR22 waveguides with standard

Feature	ALH376	AMMC-6241	CHA2194
Frequency	35-45GHz	23-43GHz	36-44GHz
Noise Figure	2.2dB	2.7dB	3dB
Return loss	< -8dB	< -10dB	< -9dB
Gain	20dB	20 dB	20dB

Table 4.2: Comparison between commercially available LNA. In all cases the specifications are for ambient temperature.

circular flanges (UG-383/U). In that way we assured the mechanical compatibility with the previous component (OMT) avoiding the use of adapters which degrade the performance of the amplifier. The RF signal is coupled from the waveguide into a microstrip line by a RF probe. Furthermore, the chip is biased by only one +5 V signal.

LNA module design

One of the mechanical specifications for the LNA is to have the input and output port on the same axis. This feature allows an easy integration of the LNA into the complete Band-1 receiver. We chose to use the configuration shown in Figure 4.4 which allows to use perpendicular probes, which are easier to fabricate than on axis probes [65]. This specification is achieved by incorporating waveguide E-Bend to the input and output waveguides. The radius of the curvature was optimized to minimize the return losses of the structure. The complete structure of a LNA module, showing its main internal dimensions, is depicted in Figure 4.4.

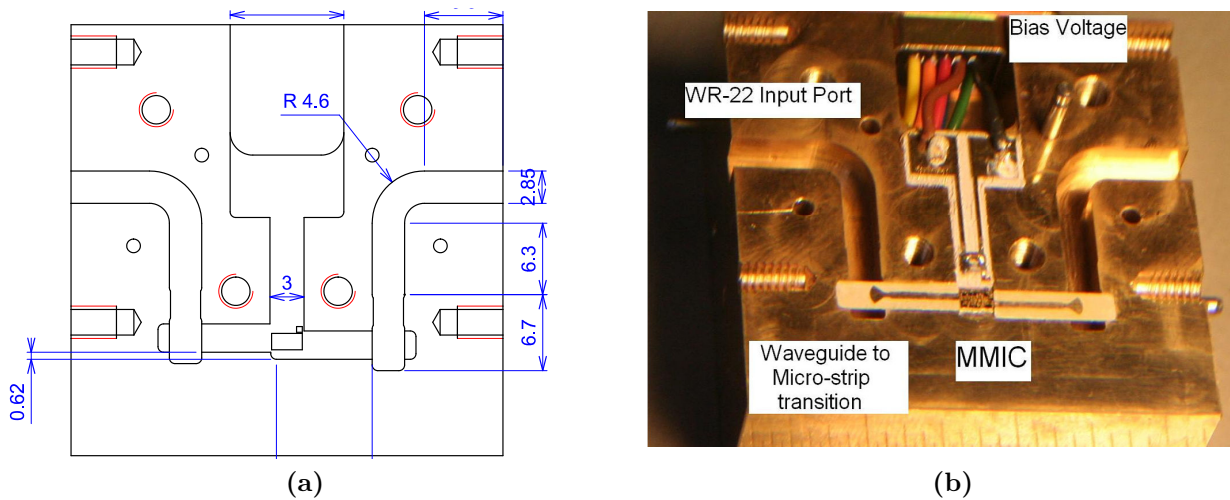


Figure 4.4: The LNA based on GaAs chip. (a) shows the main dimension of the amplifier. (b) shows a photography of the assembled amplifier showing its different parts with labels.

Pin1	+5V
Pin2	Return (GND)
Pin 3 to 9	Unused

Table 4.3: Pin configuration for LNA module.

Bias network

As stated before, the chip is biased by only one +5 V signal. The return line of the chip is connected with its backside through via holes. Therefore, the ground connection of the MMIC is done through the bottom side of it which is connected, by using conductive epoxy H20, to the chassis of the amplifier. We have used a 9-pins Micro-D connector (ITT Canon MDM-9). The pin configuration is presented in Table 4.3. The bias card receive the bias signals from the connector and and distributed to the MMIC, located in the core of the module. It has two ceramic capacitors (0.1 uF and 10 pF) to decouple the bias. A final decoupling stage is done by a single layer 10 pF capacitor (Dielectric Laboratories D20) located as near as possible to the bias pad. The connections from the bias card to the decoupling capacitors and to the MMIC are done trough bond-wires. For this reason the bias card has to be gold plated to assure the correct adherence of bond wires to the surface. The chassis is connected to the return line by several bond wires from the bias card to the chassis. The bias box is inserted in a cavity of the chassis whose dimensions were chosen to avoid mm-wave radiation to propagate on it.

RF probes

The RF probes are a fundamental component of any MMIC based LNA amplifier. They are intended to adapt the signal which is propagating through a waveguide into a signal propagating in a stripline. We designed a transition based on a radial probe [66] which proved to have broader bandwidth than traditional rectangular probes [67]. The substrate used to support the microstrip line and probes is Duroid 6002² with a thickness of 10 mils and a gold plated copper clad of 35 um. The advantage of this substrate are its low losses, easiness of machining, cryogenic operation and low cost.

The RF probes were designed and optimized using HFSS³. The final dimensions and expected results are presented in Figure 4.5. After the design extensive experimentation was needed to determine the best way to fix the antennas to the substrate, achieving the most reliable results by using cianoacrylate (discussion and methodology presented in [68]).

Results

We have built four LNA modules based on this technology. The first one, named version 1 (V1) and described in [68], was the first attempt to package MMICs at our laboratories. It

²Rogers corporation, <http://www.rogerscorp.com/>

³Ansoft corporation, Available: <http://www.ansoft.com>

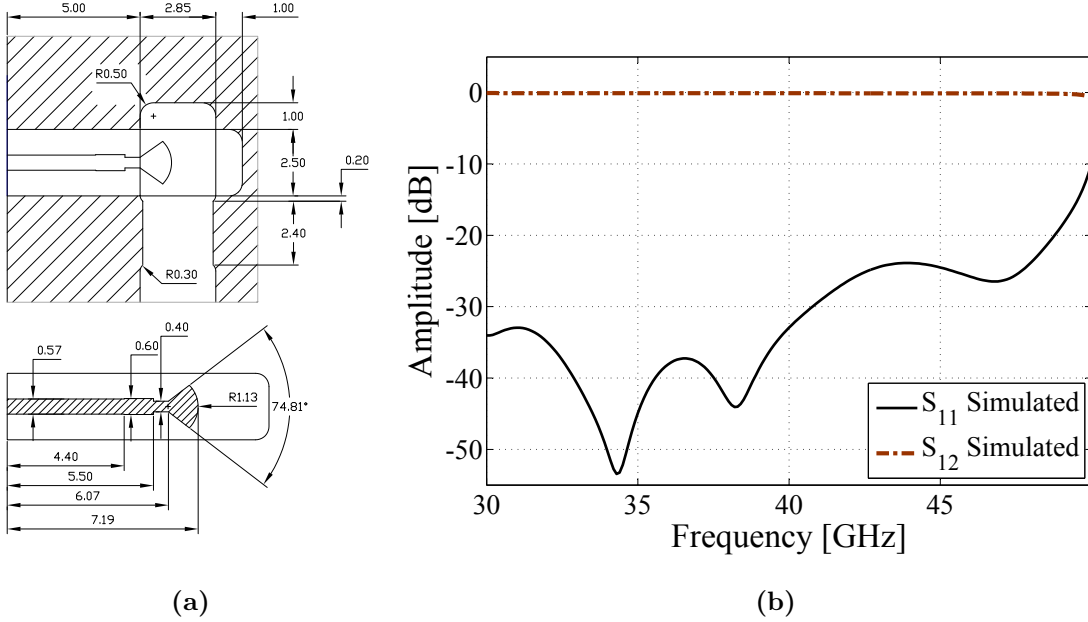


Figure 4.5: Waveguide-to-microstrip transition. (a) The dimensions of the radial probe are given in detail. (b) Simulated performance of the probes.

presented several problems which were solved prior to complete the design that is presented in this thesis, named version 2 (V2). Among these improvements in the design we have to mention the incorporation of waveguide bends to have on axis configuration, the material (gold plated brass instead of aluminum), the use of better quality capacitors for decoupling, and the gold plating of RF probes which assure correct adherence for the bond wires. Three modules were produced using this improved technology (V2.0, 2.1 and 2.2). One of them (V2.1) did not work due to the poor quality of the gold plating. The S-parameters of the amplifier were tested using the VNA up to 45 GHz. To measure the noise of the units a noise meter setup was used. The design and principles of operation of this noise meter are presented in Section 4.2.1. Figure 4.6 shows a comparison between the three working units, showing that the improvement in the fabrication process allows us to have better results on each iteration of design and fabrication.

The results of the LNAs version 2 are presented in Figure 4.7. The gain of the unit is around 18 dB with a gain flatness of 7 dB all over the Band (31 to 45 GHz). The return losses are better than -7 dB all over the band, while the isolation is around -40 dB. The noise figure, depicted in Figure 4.6, is flat all over the band with an average value of 3 dB, equivalent to 290 K. It has to be noticed that an excellent reproducibility is achieved. The results are coherent with the specified performance of the MMIC.

To test the LNA at cryogenic temperatures an old cryostat from the Cosmic Background Imager (CBI) was modified to serve as test cryostat at our laboratory. Using this facility the LNAs were tested at cryogenic temperatures. The complete set of results is presented in Figure 4.8. As expected, the gain of the unit increase by 4 dB due to the improvement in carrier mobility at low temperatures. On the other hand, the reflection losses degraded to -5 dB as the amplifier matching network was designed for transistors operating at room temperature. However, by far, the problem of this unit when operating at cryogenic temperatures arises

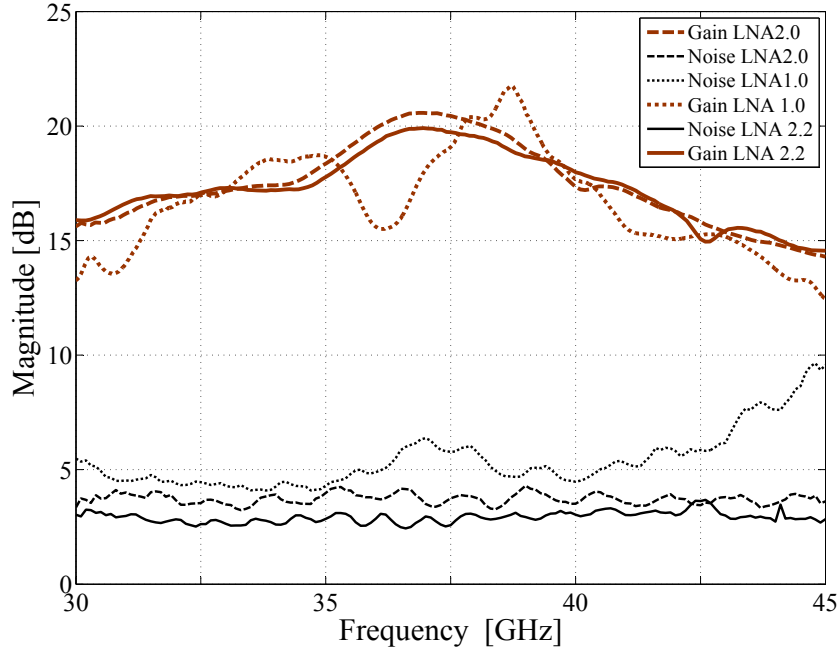


Figure 4.6: Comparison between the performance of three different LNA modules.

by its high power consumption which prevents them to be cooled below 25 K, being 8 K the limit of our test system without any active load.

The power consumption of the LNA is 88 mA at 4 V, equivalent to 382 mW. The reasons for that are related to the MMIC design. Commercial units are usually designed for easy use and acceptable performance. Therefore they have a single supply (4 V) and the internal bias signals for gates and drain are generated through resistor networks, dissipating a large amount of power on them and avoiding to tune the LNA for optimal operation. Moreover, the MMIC is a balanced amplifier which makes the LNA to have a good input matching, but consuming twice the power than a single-end configuration.

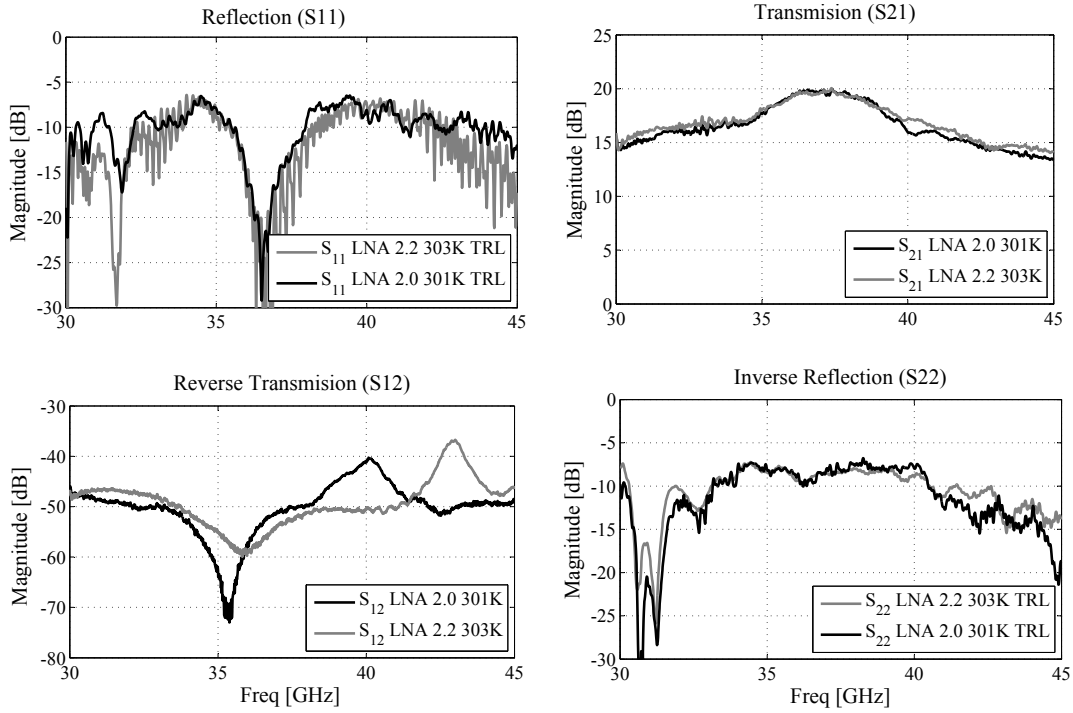


Figure 4.7: Room temperature S-Parameters of LNA V2.

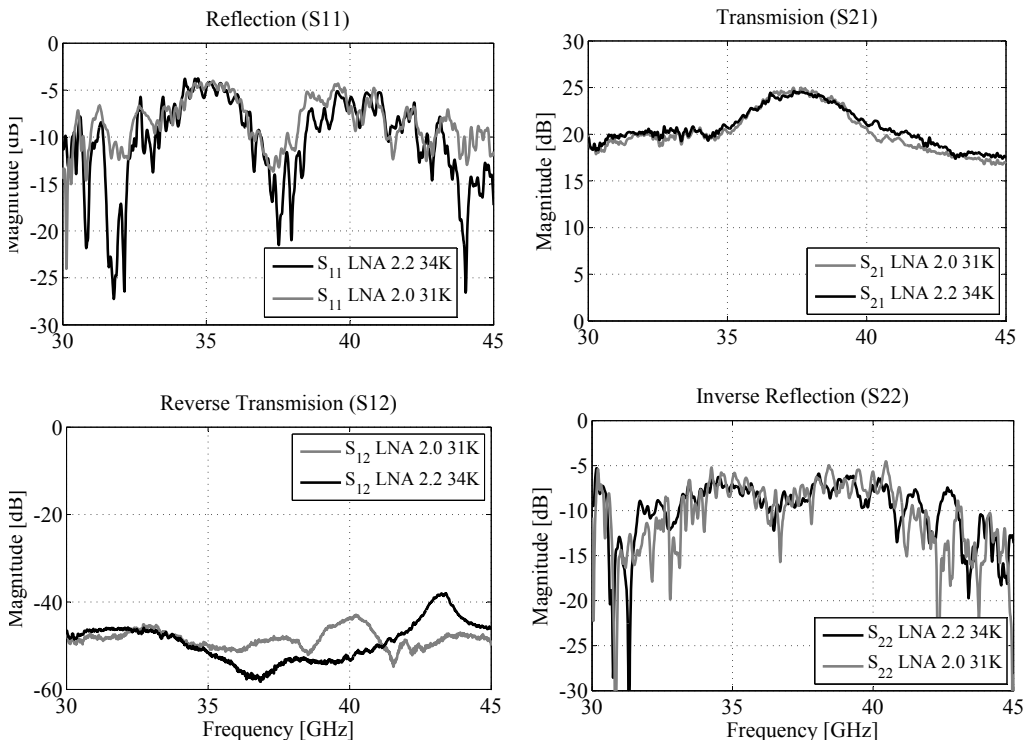


Figure 4.8: Cryogenic temperature S-Parameters of LNA V2.

4.2.3 LNA amplifier using UMS transistors

United Monolithic Semiconductor is an European foundry that offers GaAs devices to the microwave market. They are focused on the MMIC market, but they also have some discrete devices available. The chosen transistor was the EC2612 which is a 6 finger $0.15 \times 120 \mu\text{m}^2$ GaAs p-HEMT. This device has an excellent noise figure of 1.5 dB at 40 GHz for room temperature operation and the specified gain at 40 GHz is 9.5 dB. The data sheet provides the designer with the noise parameters, a linear model and some sets of S-Parameters. Using this available data a Pospiezalski model was built and used during the first stage of design of the LNA.

Transistor measurement

The UMS transistors were measured to investigate their performance and validate the model obtained from the foundry data. As a first step a DC test was performed. The results, shown in Figure 4.9, indicate a threshold voltage of $V_g = 0.7 \text{ V}$, a saturation current of around 25 mA and a transconductance gain of 65 mS. All the relevant parameters meets the

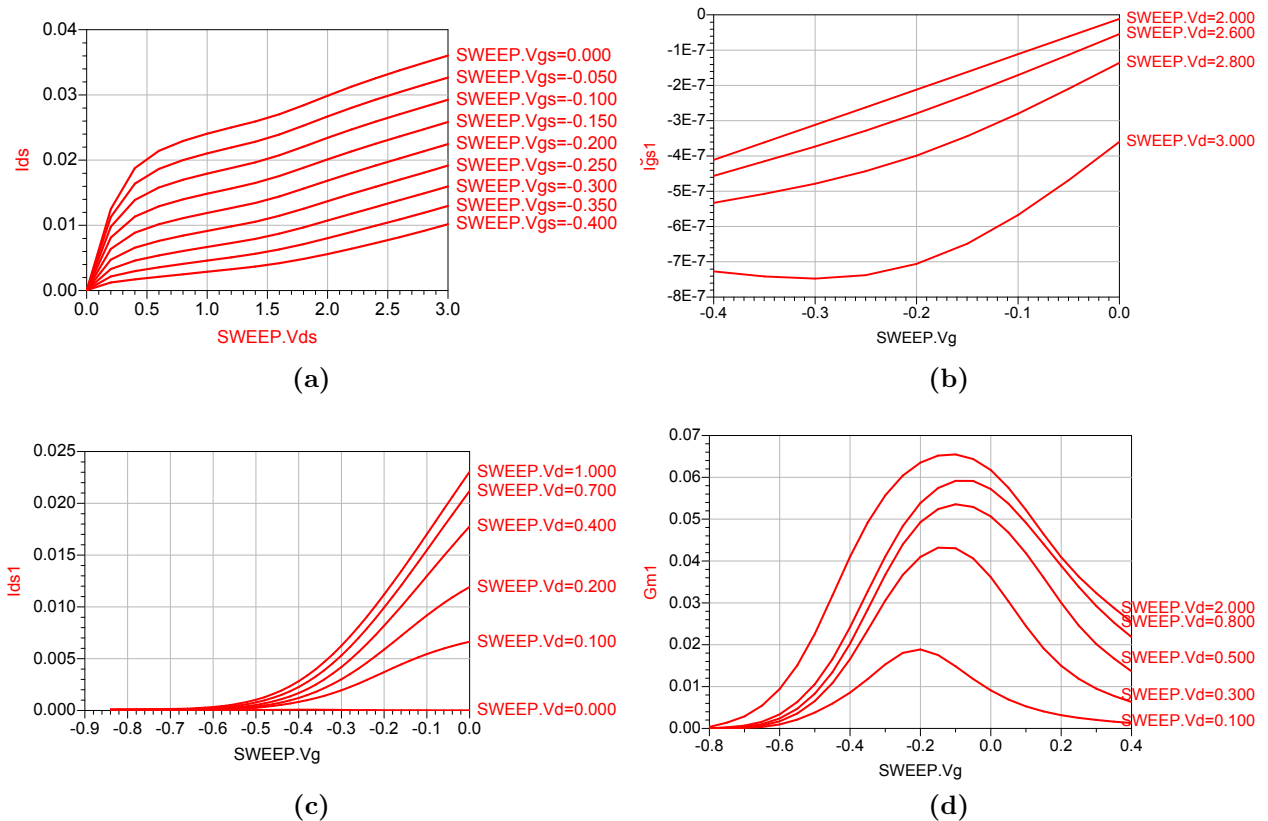


Figure 4.9: DC measurements of UMS EC2612 pHEMT. In (a) the IV characteristic, where the kink effect is clearly observed as an increase on I_{ds} for voltages over 1.5 V. (b) Gate current leakage. (c) Threshold voltage is -0.7 V . (d) DC transconductance of this amplifier is 65 mS.

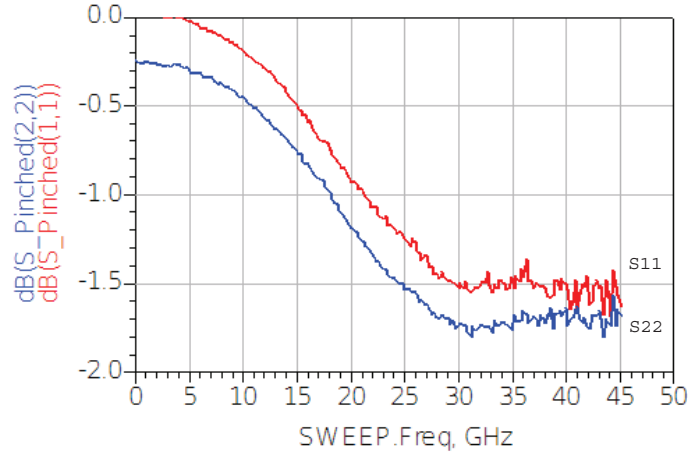


Figure 4.10: Measured S-Parameters of UMS EC2612 at pinched-off condition ($V_{ds} = 0$ V and $V_{gs} = -1$ V). The transistor exhibits a bad quality pinch-off, with S_{22} 0.35 dB lower than S_{11}

specifications presented in the device datasheet. It was pointed out that the devices could present a big variability, as specified values cover a wide range. As an example, for saturated current UMS states that the minimum current is 10 mA and the maximum is 60 mA with a typical value of 35 mA.

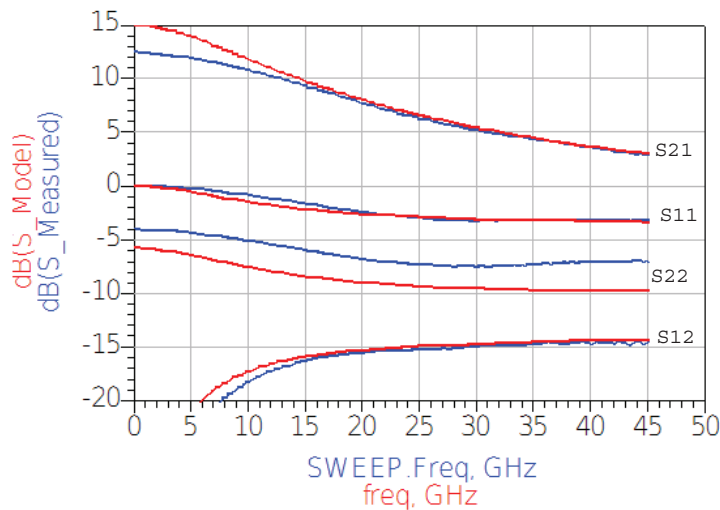


Figure 4.11: Modeled and measured S-Parameters of UMS EC2612 at bias point $V_{ds} = 2$ V and $I_{ds} = 14$ mA. Good agreement between the model and the measured S-Parameter was obtained. The main problem is in S_{22} that is 3 dB lower than the modeled value.

After the DC measurements, RF measurements at several bias points were carried out using a 40-GHz RF probe station at University of Manchester. The pinched-off S-parameters, i.e. RF data with gate voltage under the threshold voltage (V_g minor than -0.7 V), meaning depletion of carriers, of this transistor are presented in Figure 4.10. The bad quality of the pinch-off, reflected on a poor similitude between input and output reflection losses, is an indicator off a not outstanding noise performance when cooled at 20 K [49]. After this preliminary analysis the S-Parameters of the devices were measured at different bias points (shown in Figure 4.11). The measurement were compared with the model we have previously used for the preliminary LNA design. The expected behavior agrees with the measurement, except for S_{22} which is higher than the simulated values. Considering this fact we decided to use the device model only in the early stages of the design and then replace the model by the actual measured data of the transistors.

Low Noise Amplifier design

The amplifier was designed in several iterations. In the first design ideal components, as transmission lines, were used to model bondwires and microstrip lines. The transistors were simulated using the derived Pospieszalski model. In a second stage of design, more accurate physical models were used for each component. We chose to build the RF circuits using 5 mils quartz substrate as it have low losses at Q-Band. For the bond wires we used 1 mil gold wires as they are currently available at our laboratory. It was also decided to include the radial probes to the input matching circuit, based on the good result we have obtained previously using this kind of transitions. In a final stage of the design the transistor model were replaced by the measured data to increase the degree of accuracy of our model. The first two stages were replaced by the transistor at $V_{Drain} = 2$ V and $I_{Drain} = 15$ mA which is the bias point for lowest noise according to the datasheet. The third and fourth stages were replaced by transistor biased at $V_{Drain} = 3$ V and $I_{Drain} = 30$ mA which provides more gain, allowing the amplifier to have around 30 dB of gain.

As usual, when designing low noise amplifiers, the first and second stages of the amplifier were optimized for low noise and good S_{11} , while stages three and four were designed for high gain and good gain flatness. Between all stages a 0.1 pF capacitor provides decoupling of the drain and gate bias voltages.

To avoid the amplifier to be unstable, the bias networks were properly designed. The unstable behavior arises from the excessive gain that the transistors have at low frequencies. Therefore, the bias network should act as a path to ground at lower frequencies and a high impedance line at the frequency of interest. This is achieved by using a $\lambda/4$ bond wire followed by a capacitor. The $\lambda/4$ wire transforms the low impedance of the capacitor into a high impedance for the band of interest. Using additional inductors and resistances we improved the response of the bias network. Finally, a 1 pF capacitor is used to decouple the bias input. The 70 mil wire is the $\lambda/4$ line.

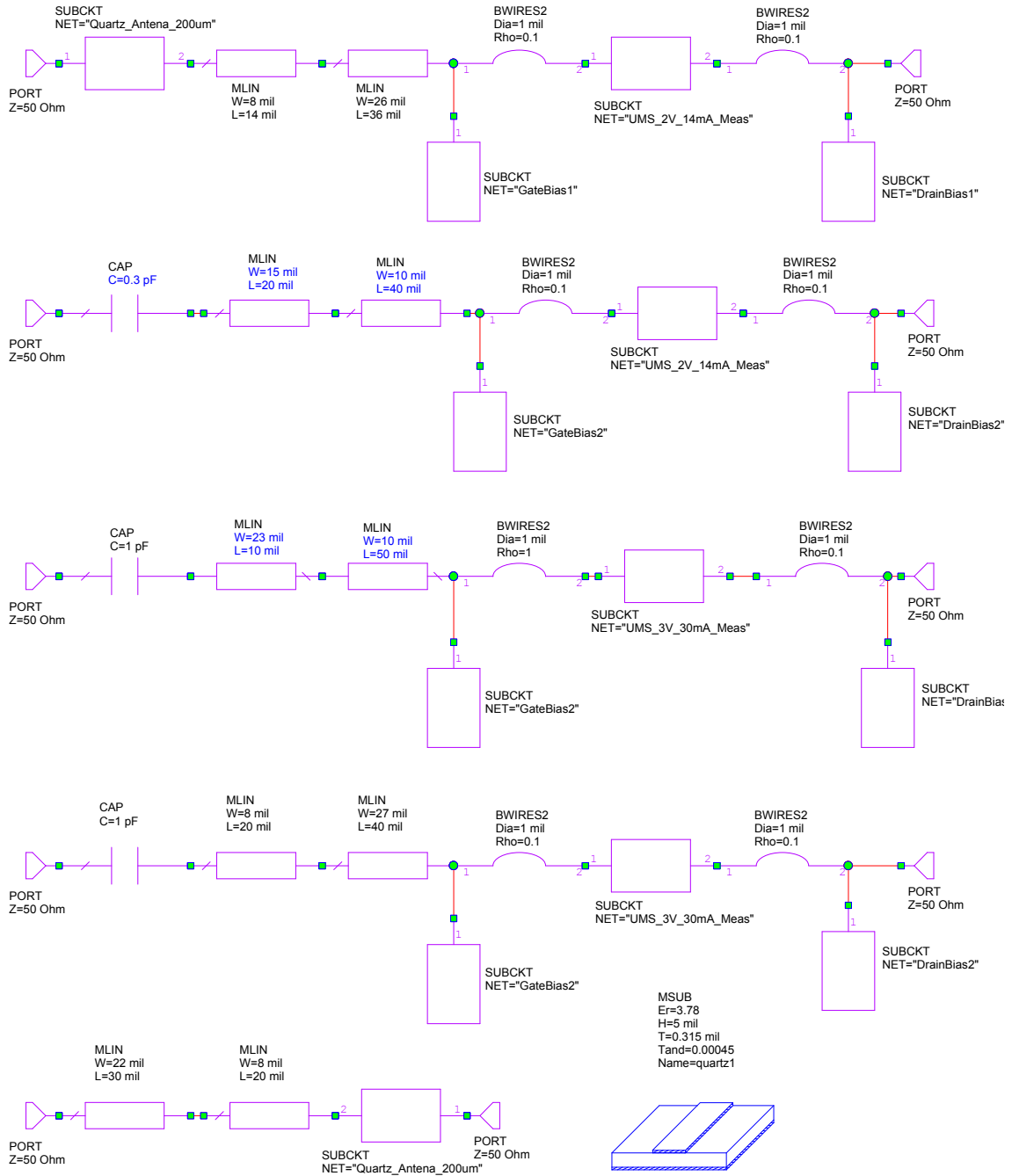
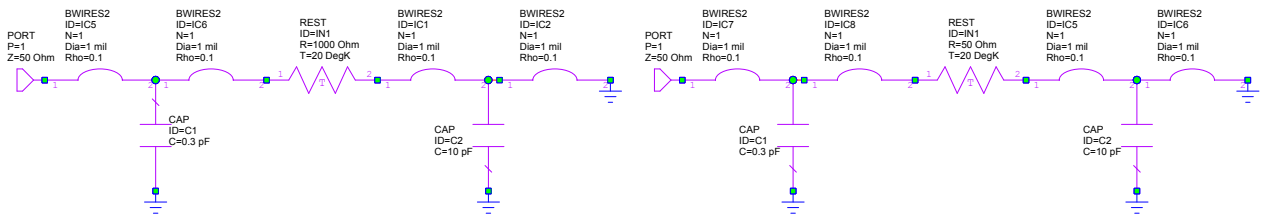


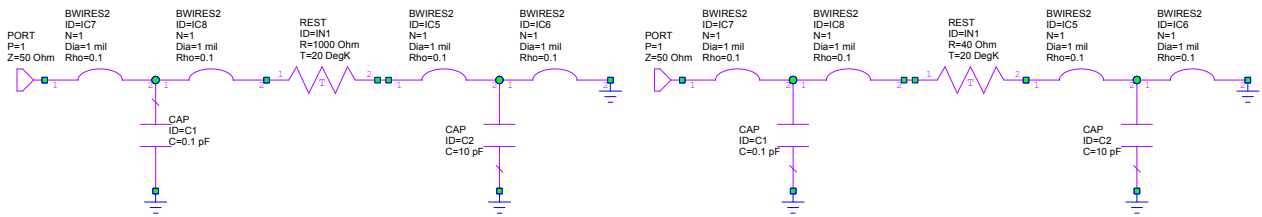
Figure 4.12: Layout of the designed LNA based on UMS devices. From top to bottom: Stage 1 to stage 4. Stages 1 and 2 were optimized for low noise and the transistor is biased at 2 V, 14 mA. Stages 3 and 4 were optimized for high gain and the transistor is biased at 3 V and 30 mA. The input and output stages (1 and 4) include the RF probe, modeled using the values obtained from an electromagnetic simulator.



(a)

(b)

Figure 4.13: Bias networks for the first stage, (a) the gate and (b) for drain. The bias for the first stage, specially for the gate, should also be optimized for low noise contribution to the amplifier. For this reason the rejection of low frequency signals is not as good as the bias network of the following stages.



(a)

(b)

Figure 4.14: Bias networks for stage three and for, (a) the gate, and (b) for drain.

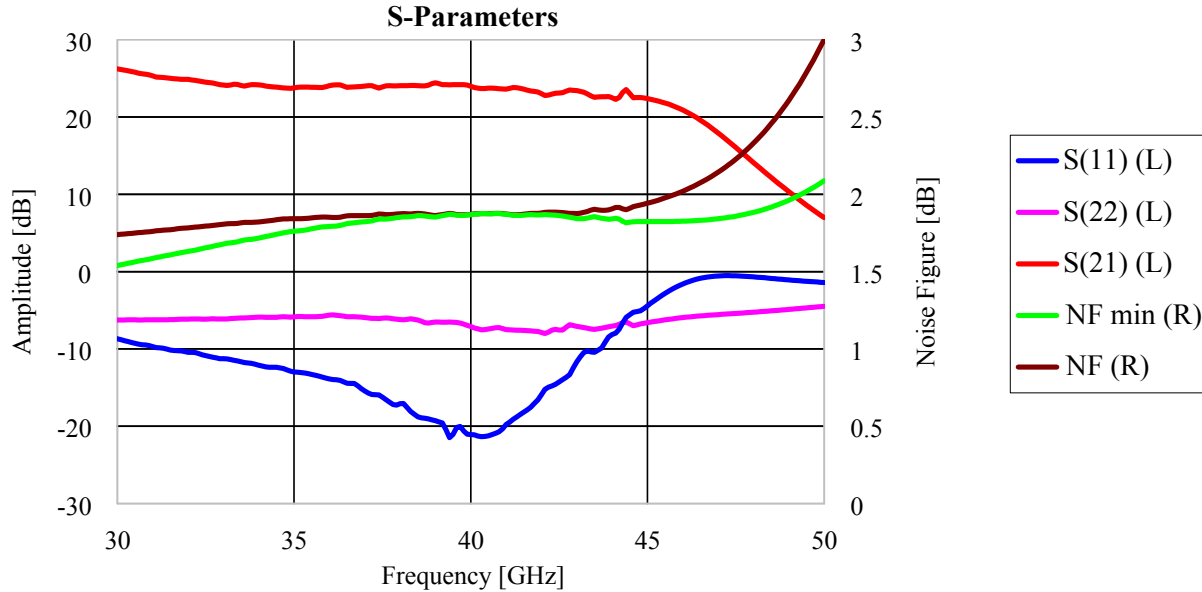


Figure 4.15: Simulations of the designed LNA. The gain is almost 25 dB over the complete Band-1 range. Return losses are better than -5 dB while the isolation of the LNA (not showed) is around -70 dB. The noise figure is always below 2 dB and its typical value is 1.8 dB. In the design some gain was sacrificed in order to improve the stability of the LNA.

We have used capacitors from Advanced Dielectric Laboratories⁴ and resistors from State of the Art⁵. To increase the precision of the amplifier model we have included the equivalent circuit provided by the suppliers of capacitors and resistors to the simulations. The stability of the design was checked using the Rollet's stability factor and the conclusion is that the amplifier is unconditionally stable from 1 GHz to 80 GHz. The final amplifier layout is presented in detail on Figure 4.12. As additional information Figures 4.13 and 4.14 presents the complete design of the bias networks for the different amplifier stages. Simulated results are presented in Figure 4.15. The expected gain is around 25 dB while the reflection losses are around -7 dB at the output, and better than -5 dB at the input.

Fabrication

The LNA was built inside a waveguide block whose inputs and outputs are standard WR22 waveguides. The radiation was coupled to the microstrip lines through the RF probes, similar to the design produced for the MMIC-based LNAs. The RF probes were simulated in HFSS and the resultant S-parameters were incorporated to the LNA design. The LNA itself is housed in a small cavity in the core of the LNA block. The dimensions of the cavity (2 mm width by 1 mm height) were chosen to avoid waveguide modes propagating on it, phenomena that causes unexpected feedback between transistors. Several steps built on the chassis allow to correctly align the components during the fabrication process and help to keep the bonding

⁴Dielectric Laboratories, 2777 Route 20 East Cazenovia, NY 13035 , www.dilabs.com

⁵State of the Art inc., 2470 Fox Hill Road State College, PA 16803-1797, www.resistor.com

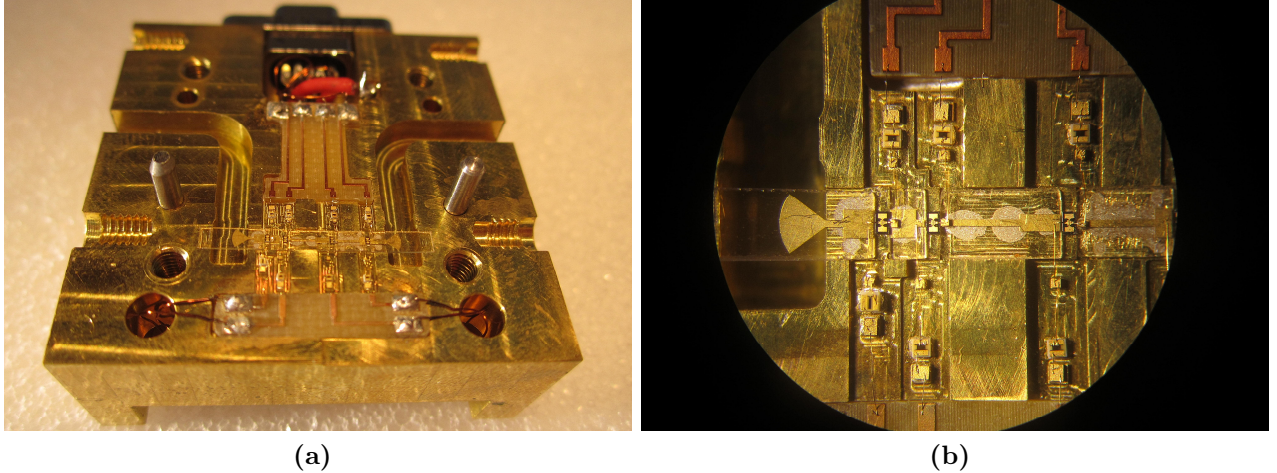


Figure 4.16: (a) General view of the LNA assemble. Overall block dimensions are $40 \times 38 \text{ mm}^2$. (b) Detailed view of the LNA cavity where individual transistors are mounted.

lengths as short as possible. The bias network, housed on small cavities designed to avoid waveguide modes, arrives perpendicularly to the main RF cavity. The microstrip lines were built on 5 mils quartz with a $4\text{-}\mu\text{m}$ gold plating over a sputtered layer of Ti-Pa-gold. The circuits were built at Ion Milling⁶ using plasma etching, obtaining superior accuracy on the dimensions of all RF parts in the LNA. Figure 4.16 shows several details of the fabricated amplifier.

Pin	Signal	Pin	Signal
1	Return (GND)	6	Gate Voltage 4
2	Drain Voltage 4	7	Gate Voltage 3
3	Drain Voltage 3	8	Gate Voltage 2
4	Drain Voltage 2	9	Gate Voltage 1
5	Drain Voltage 1	-	-

Table 4.4: Pin configuration for LNA module.

The bias is provided to the amplifier through a micro-D 9-pin connector. The pin configuration is provided in Table 4.4. The drain voltages arrive directly to the top distribution board, while the gate voltages are routed through the back side of the amplifier to the bottom distribution network. The return signal (ground) is directly connected to the amplifier body by a soldered wire. The reliability of the ground proves to be important since if the return line is lost the transistors would burn out immediately. The distribution boards were made on FR4 and attached to the chassis with epoxic bond.

⁶Ion Beam Milling, 850 East Industrial Park Drive Manchester, NH 03109

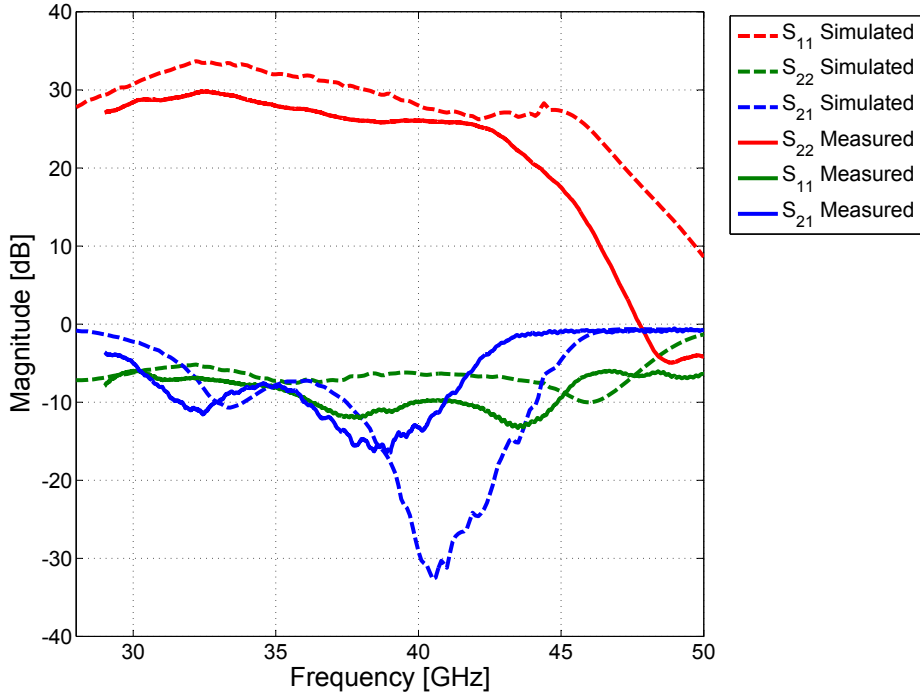


Figure 4.17: Measured and simulated results for the hybrid LNA based on EC2612 transistor. All stages biased with $V_D = 2$ V and $I_D = 15$ mA

S-parameters measurements

To bias the amplifier a standard bias module from ALMA was used. The module can bias 6 independent transistor stages with a drain voltage of 0 to 3 V and drain currents in the range from 0 to 20 mA. The gate voltage is controlled to keep the drain current constant to the specified value. The amplifier was measured using 2 V at drain and a fixed current of 15 mA which gives a total power consumption of 120 mW. Despite the design process check for unstable behaviour between 100 MHz and 80 GHz we had found oscillations of the amplifier at few MHz (variable between 1 and 10 MHz). We have found out that it was caused by inductive coupling between gates and drain originated in the bias cabling. To solve this issue we have included discrete through-hole inductors of 120 μ H in the bias cables, which cancel out this feedback loop. After this modification we could measure the amplifiers at room temperature. The obtained results are presented in Figure 4.17.

The LNA bandwidth is 28–43 GHz instead of the designed 28–45 GHz which is caused by the existence of longer bond lengths than originally specified. A new simulation was performed in order to estimate the effective length of the bond wires. The output of this analysis is shown in Figure 4.18 where the experimental results are presented together with the simulated results using the bonding lengths specified on Table 4.5. The conclusions are that the effective lengths are always longer than the originally specified values. A posterior mechanical analysis indicates that it is not possible to make bonding connections shorter than 7 mils due to the separation between components and the necessary clearance spaces. The best solution is using parallel bondings using a thinner wire (0.7 mils instead of 1 mil). Following this conclusion we are by now purchasing new hardware to modify our bonding

Stage	Specified length	Effective lengthl
Stage 1 input	6 mils	7 mils
Stage 1 output	6 mils	7 mils
Stage 2 input	6 mils	10 mils
Stage 2 output	6 mils	9 mils
Stage 3 input	7 mils	9.5 mils
Stage 3 output	5.5 mils	8 mils
Stage 4 input	5.5 mils	7 mils
Stage 4 output	5.5 mils	7mils

Table 4.5: Specified and effective bond wires length.

machine to work with this thinner gold wires.

A stability analysis of the LNA using the measured S-parameters shows that the amplifier has a Rollet factor greater than 10 all over the band (28 to 50 GHz), being unconditionally stable. No resonances were observed and therefore it is possible to discard the presence of waveguide modes in the cavity.

Noise figure measurements

The noise figure at room temperature of the amplifiers was also measured. The results, presented in Figure 4.19, indicate a noise figure ranging between 2.5 and 3 dB which is higher than the simulated values of around 2.5 dB. This offset can be caused by losses on the substrate or, more likely, by an under estimation of T_{min} in the transistor models. The stationary wave observed in the measured values is caused by the poor quality of the adapter used to convert the noise source output (coaxial 2.4 mm) to the waveguide input of the LNA (WR22). In Figure 4.19 we can also observe that the new model, including the corrected lengths for the bond wires, match better the experimental results than the original one.

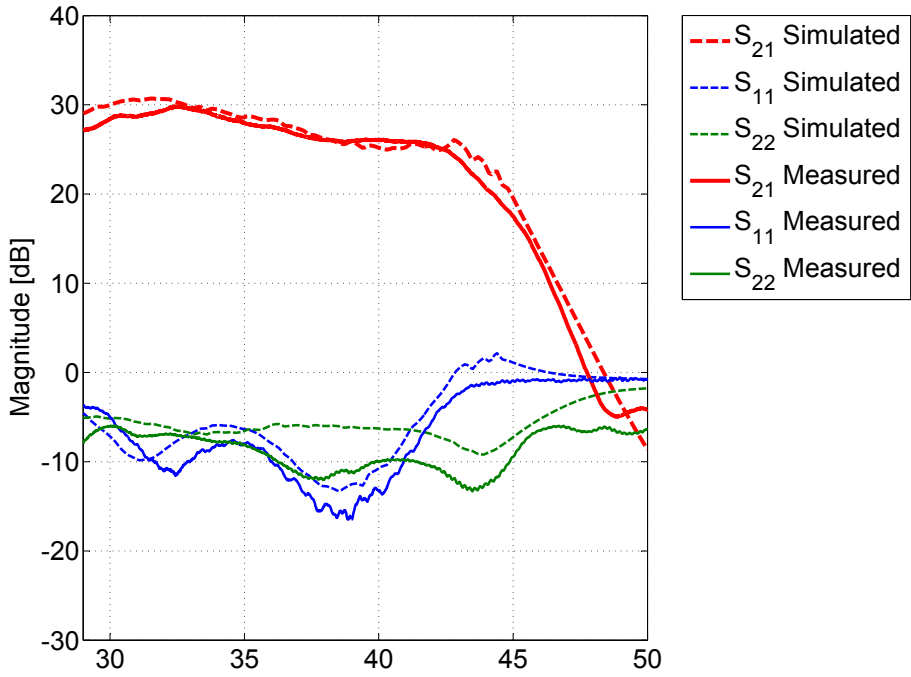


Figure 4.18: Measured results for the hybrid LNA based on EC2612 transistor. They are compared with a model with the lengths of bonding wires fitted to match with measurement.

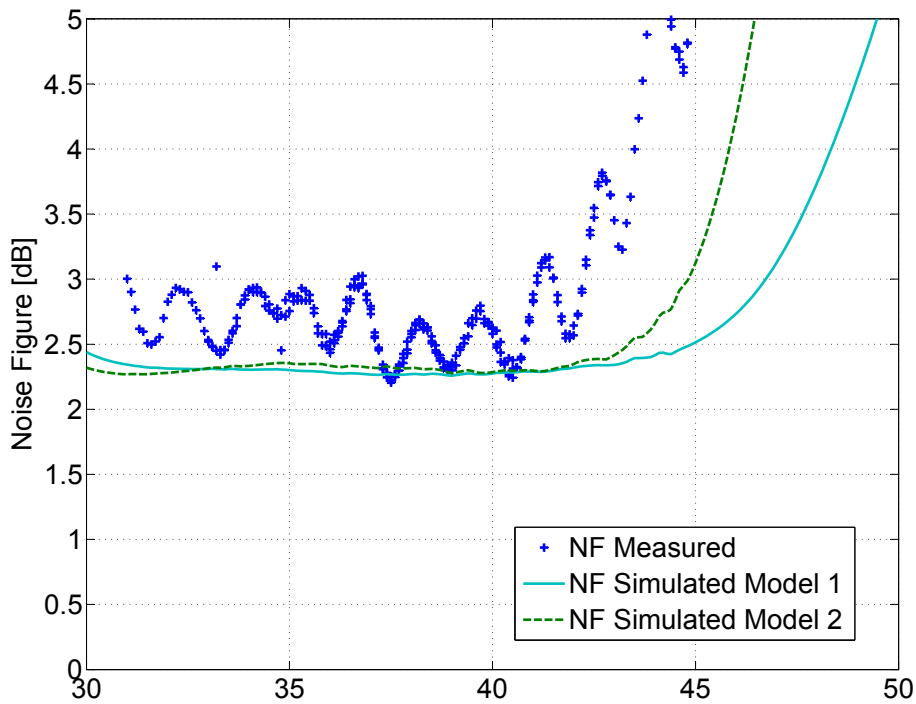


Figure 4.19: Measured results for the hybrid LNA based on EC2612 transistor. They are compared with a model with the lengths of bonding wires fitted to match with measurement.

4.3 Conclusion

After reviewing the specifications for an ALMA Band-1 LNA, an analysis of the advantages of using Hybrid or MMIC technology is done. It becomes clear that an amplifier with a noise temperature of 10–12 K and a gain of 30–35 dB could be achieved by using hybrid technology with the appropriate transistors. Anyway, if this alternative is chosen, a careful analysis of the resources needed to build the 150 LNA in a time span of a couple years should be carried out. The use of a MMIC technology facilitate the task of building the LNA series, but if a traditional process, like InP 0.1 μm is used, the noise of the LNA is expected to be around 18–20 K. There are two alternative to diminish the noise of a MMIC amplifier in order to be competitive with Hybrid amplifiers. The first one is to use a single transistor as a first stage. Working with an appropriate transistor a noise of 10–12K could be achieved. The next alternative is using new MMIC technology, like InP 0.035 μm , which is expected to be competitive with hybrid amplifiers at Q-band.

In the second part of this chapter we have presented our efforts to develop the low noise amplifier technology for high frequencies. In a first stage we have developed housing strategies to package MMIC based amplifiers. We have worked with commercially available GaAs chips which provide an order zero solution to our needs. The transitions from waveguide to microstrip were carefully designed and the overall design was completely analyzed to avoid resonant modes in the RF cavities. Amplifiers with 20 dB of gain and noise figures of 3 dB at room temperature were developed successfully. In a second stage we have designed our own amplifiers based on discrete transistors, achieving a noise figure of 2.5–3 dB and a gain of 20–25 dB over almost the complete band. The necessary facilities were installed, including a bonding machine, noise and S-parameters test facilities, and recently a probe station for transistor measurements.

Chapter 5

Band 1 development

As we have stated before, this thesis is part of a project funded by the Center of Excellence in Astrophysics and Associated Technologies (CATA) to build a prototype receiver for ALMA Band 1. Since the project started in 2008 we found a common interest in Band-1 instrumentation with other groups, as the Academia Sinica Institute of Astronomy & Astrophysics in Taiwan (ASIAA) and the Hertzberg Institute of Astrophysics (HIA) in Canada. In this context, an agreement of cooperation has been signed to work together to achieve the best solution for ALMA Band 1.

This chapter presents a complete overview of the ALMA Band-1 work at Universidad de Chile. After reviewing the interfaces and specifications for a Band-1 receiver, the electronic and mechanical design is discussed. Finally a review of the design and construction of each component is presented. An exception was done with the LNA as it has been extensively discussed in the previous chapter. It is important to remark here that an important part of this project has been to set up the Millimeter Wave Laboratory facilities. Since 2008, when this thesis project started, the laboratory has been equipped with modern instrumental to accomplish the present project.

5.1 Band 1 specifications and interfaces

ALMA is a multinational project, in which different components and assemblies are produced at many places around the world. This fact implies the need for clear specifications and interfaces between the different sub-assemblies. In the case of Band-1 receivers a complete set of specification was written based on high level guidelines. A summary of the main electrical specifications to be accomplished by Band-1 receivers is presented on table 5.1. Other specifications refer to the need for an architecture which allows an easy production of the 66 receivers and the corresponding facilities for maintenance and repairs.

All ALMA receivers are installed in the same cryostat, which was specifically designed to integrate each receiver following the “plug-and-play” philosophy. The space assigned to the Band-1 receiver is fixed and corresponds to a cylinder of 170 mm of diameter and 491 mm

Quantity	Specification
RF Frequency	31-45 GHz
Noise temperature	17K (80% Band) and 28K (100% Band).
Cross Polar level	Better than -25 dB
Image rejection ratio	Better than -10 dB.
LO frequency	27 – 33 GHz.
LO power	15 mW (max).
IF frequency	4 – 12 GHz.
IF Output Power	-30 dBm/GHz when looking at a 290K load.
IF power variation	6 dB peak-to-peak in any 2 GHz portion of the IF band.
IF power variation	10 dB peak to peak across the complete IF band.

Table 5.1: Specifications for ALMA Band-1 receivers

of height. The cylinder includes two fixed positions for the 80 K and 20 K plates which are located at 120 mm and 200 mm above the base plate. These plates are thermally linked to the cryostat during operations and can support the heat load of the receiver (1230 mW at 80 K and 162 mW at 20 K). The receiver base plate contains all the vacuum interfaces of the receiver, including two IF output connectors, two LO input connectors and the bias connector. The leak rate of this plate has to be lower than 1.0^{-8} l/s, measured using a vacuum pressure lower than $1.0e - 5$ mBar. The complete weight of the receiver shall not exceed 8 Kg.

The cover plate of the cryostat is located in the focal plane of the antenna, with each one of the 10 band receivers pointing to a different position of the sky. The center of the cylinder where the Band-1 receiver will be placed is located at 295 mm from the center of the cryostat. The receiver will include a lens to focus the beam from the antenna sub-reflector into the receiver horn. The center position of this lens is located at 255 mm from the center of the focal plane. Giving this distance and considering the separation between the focal plane and the sub-reflector (5.99 m), it follows that the Band-1 optical axis has to be tilted by 2.48° respect to the receiver mechanical axis in order to correctly illuminate the secondary.

All ALMA receivers are monitored and controlled through the same interface, the bias box. It provides bias monitor and control signals for two independent receivers, each one correspondent to one polarization. The signals available for each polarization receiver are to bias and control two LNAs based on HEMTs (four stages per each LNA) and two SIS mixers (not used for Band 1). It also provides signals for temperature monitoring and for identification of the cartridge using an ID code.

5.2 Band 1 proposed design

Figure 5.1 shows the proposed design for the Band-1 receiver. The RF signal is coupled into the receiver by a horn and a lens. Two filters prevent IR radiation to come into the receiver. After the horn the signal is split, by an orthomode transducer (OMT), into two signals with perpendicular linear polarizations. Each polarization signal is then processed by an independent receiver. In the first stage of each receiver the signal is amplified by a

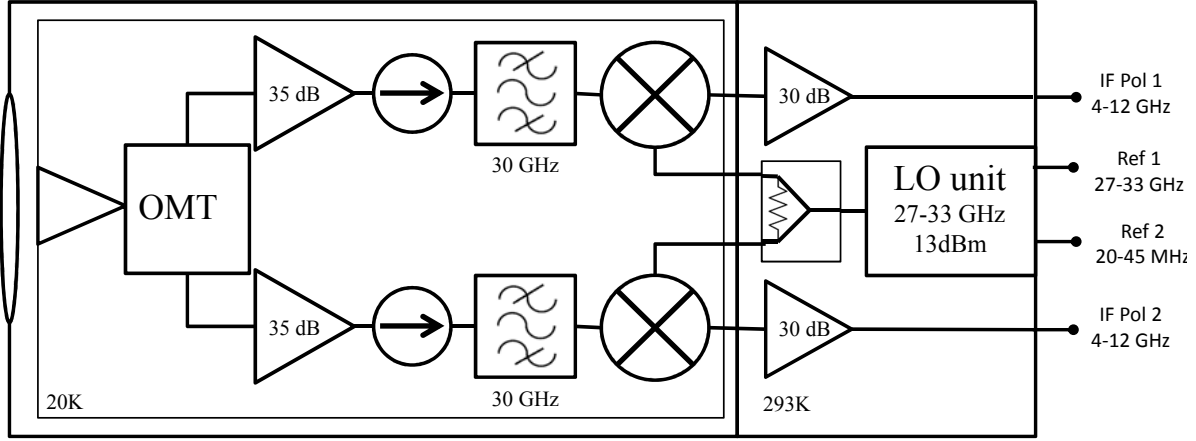


Figure 5.1: Layout of the Band-1 receiver. Although the down conversion stage can be placed at ambient temperature, we are considering to cool down the complete receiver at 20 K. Depending on the performance of the final RF amplifiers, a second amplification stage is also considered.

cryogenic LNA. Our goal is to achieve 30-35 dB of gain in this LNA. An isolator placed between the LNA and the down-conversion system permits a relaxed specification for the output return loss of the amplifier. If not enough gain is achieved in the LNA, an additional amplification stage (amplifier and isolator) must be considered. Before the mixer a high pass filter cancels the image frequency, having an upper sideband (USB) conversion scheme. The down conversion process is carried out by a Schottky mixer. Finally, the IF signal is amplified by a 30-dB LNA working at room temperature.

The local oscillator (LO) module, far right in figure 5.1, provides a tunable signal between 27 to 33 GHz with a power of 13 dBm. The LO is phased locked to two signals that are provided by the ALMA central LO. This signals are used to keep the coherence of all the receivers in the array. This module is not part of the development program at Universidad de Chile as it was developed at NRAO.

Figure 5.2 shows the mechanical drawing for a Band-1 receiver. The use of an improved corrugated spline horn and compact isolators allows having a simple and compact receiver chain for each polarization.

5.2.1 Noise and power budget

Table 5.2 shows the gain and noise estimated for each component of the Band-1 receiver. For the optics we have used the estimations of [69] and [71]. For the passive components as the OMT, filter and isolator we have estimated the noise as $T_{noise} = T_{physical} * (1 - |S_{12}|^2 - |S_{11}|^2)$. For the LNA we have estimated the noise in base of published results [9][12][11] for similar instruments.

Adding the noise temperatures of each component, as indicated in equation 3.6, we obtain a noise temperature of 28 K for the complete receiver. This is well above the specification

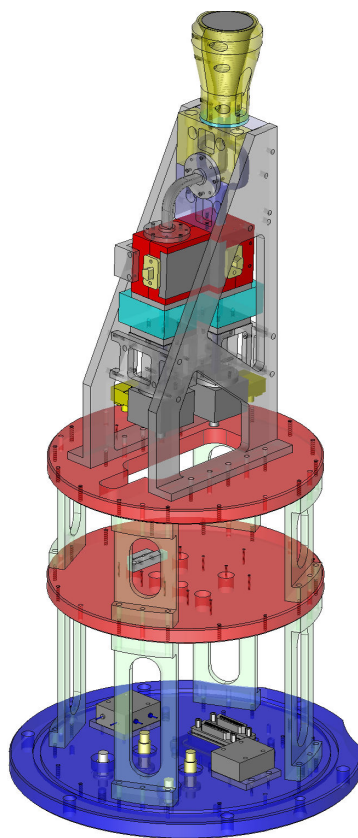


Figure 5.2: Mechanical design of a Band-1 cartridge. From top to bottom: Horn, OMT and HEMT, Isolator and a second stage of amplification, isolator, filter and finally the Schottky mixer. The top plate is at 15 K, The second plate is at 80 K.

of 17 K over 80% of the band. The only way to meet the receiver noise specification would be to diminish the noise contribution of the lens and the LNAs. In the case of the LNA it has been proved in the previous chapter that 15 K is a realistic estimation, while 12 K would be a challenging to achieve on a complete production of amplifiers. Regarding the optics, this contribution can only be lowered by a couple of degrees by using lower loss materials as quartz, which would notably increase the cost and complexity of the optics [71]. With this consideration we propose to relax the noise specification of Band 1 to be 25 K over the 80% of the band and 33 K over the complete band.

Considering the input power of the receiver when looking at a 290 K load as -84 dBm/GHz (calculated as $P_{in} = K * T * \Delta\nu$ where K is the Boltzman constant, T is the physical temperature, and $\Delta\nu$ is the 1GHz analysis bandwidth) we can derive that the Band-1 receiver should have a total gain of around 54 dB to achieve an output power of -30 dBm/GHz as specified.

	Optic	OMT	LNA	Isolator	Filter	Mixer	Cabling	IF Amplifier
Gain [dB]	-0.7	-0.1	30	-0.3	-0.1	-7	-2	35
Noise temperature [K]	7.1	0.3	15	1	0.3	400	50	220

Table 5.2: Noise temperature and gain for each Band-1 receiver components.

5.3 Optics

ALMA antennas are Cassegrain. Ten different receivers are located in the focal plane of the antenna, each receiver covering a different frequency band. A preliminary design of the optics of Band 1 has been done by M. Carter [75]. This design consists of a lens, a series of infra red (IR) filters and a horn. The main problem that presents this solution is the high noise contribution from the lens, around 10K. To address this issue other solutions have been investigated [71], including the use of a dual lens configuration where one lens can be cooled to reduce the emissivity. The results of this work indicates that the best choice to diminish the noise level is to keep the same configuration described above, but changing the material of the lens to a low loss material as quartz. This solution allows to get 6 K contribution from the quartz lens instead of the 10 K contribution of HDPE lens. The problem of this approach is that while HDPE lenses can be easily machined in conventional CNC lathe machines, quartz lenses require a much more complicated and expensive process which is not well suited for production of 66 receivers.

The original design [75] also includes the use of a standard corrugated horn with a 29.9 mm aperture and an axial length of 180.52 mm. We have proposed the use a new corrugated spline horn [76] which is around half the size of the original design, allowing a more compact receiver for Band 1. This new approach also implies a slight modification of the HDPE lens design to focus the new horn beam to the ALMA sub-reflector. An overview of this new design is presented in the next subsections.

5.3.1 Horn

The horn allows the beam, which is traveling in free space, to be confined into a waveguide. There are many designs of horns, but to achieve low cross polarizations levels, as desired for dual polarization receivers, the best option are corrugated horns. A complete analysis on the theory and applications of this horns can be found on [77]. In the case of Band 1 a set of specifications for the horn was agreed as guidelines for the design. They are presented in Table 5.3.

The new design, proposed in [76], is a corrugated spline horn based on the design methodology described on [78]. This new horn design has the advantage, over traditional corrugated horns, of being half the size, keeping at the same time its main features almost unchanged. The horn was designed using mode matching techniques and its performance was double checked using 3D electromagnetic simulator from ANSYS. The input port of the horn is a

Quantity	Specification
Frequency	31-45GHz
Cross Polar level	$< -30dB$
Return loss	$< -30dB$
10dB beam width	

Table 5.3: Specifications for ALMA Band-1 Horn

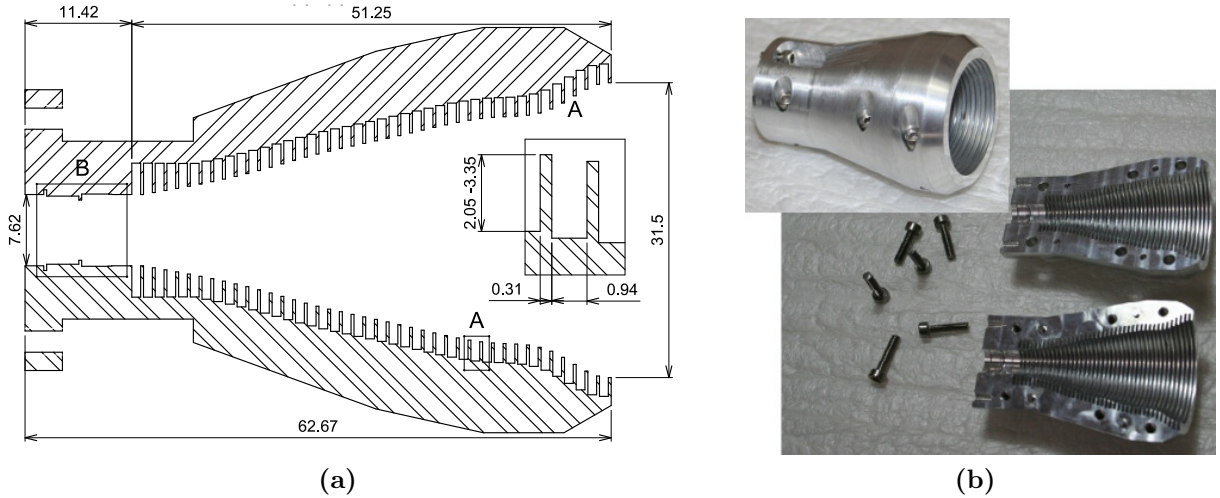


Figure 5.3: (a) Main dimensions of the spline corrugated horn. (b) Picture of the assembled horn (left top) and the two main split-block halves (bottom right).

7.62 mm diameter circular waveguide supporting the TE_{11} mode. The first part of the horn, known as launcher, converts the TE_{11} mode into an hybrid HE_{11} mode. This conversion is done by a series of corrugation with variable depth from $\lambda/2$, equivalent to 3.35 mm in our design, to $\lambda/4$ (2.01 mm in our design). After the launcher the corrugated walls of the horn, with a groove depth constant of 2.01 mm, allows the propagation of the hybrid HE_{11} mode up to the horn aperture, which have a diameter of 31.5 mm. It is important to remark that for achieving a low cross-polar level the electric field at the aperture has to be an hybrid mode HE_{11} without components in the TE_{11} mode. The spline profile of the horn was optimized to obtain a low sidelobe level and a cross-polar level lower than -30 dB at the same time that minimizing the overall horn length. Finally, to improve the return losses of the horn, specially at low frequencies, two ring loads were added to the throat of the horn.

The horn was built in aluminum 2017 at our mechanic shop. Due to the high corrugation-to-throat ratio (corrugation deep = 3.35 mm, throat radius= 3.81 mm) at the inner part of the structure it was decided to build the horn using split block technique, as shown in Figure 5.3. The horn was tested at the Millimeter Wave Laboratory using a near field beam scanner that was custom designed and built for these purposes[79]. The beam scanner measures the electric field at few centimeters from the horn aperture (both polarization E_x and E_y). The measurement plane is around 15×15 cm². This data is used by the software to calculate the far field radiation pattern ($E_{co-polar}$ and $E_{cross-polar}$). The results, presented in Figure 5.5, show an excellent agreement with simulated data, validating the design and measurement procedure. We obtained a horn with low sidelobes levels (always below -25 dB and typically around -30 dB). The cross polar level is below -30 dB, and for higher frequencies is below -40 dB. It is important to remark that we have not noticed any problems in the cross-polar patterns due to the fabrication process, which, being split block, introduces a preferential plane on the structure. The reflexion losses of the horn are lower than -30 dB all over the band as shown in Figure 5.4. Some resonances are observed just below 31.3 GHz which could cause some problems.

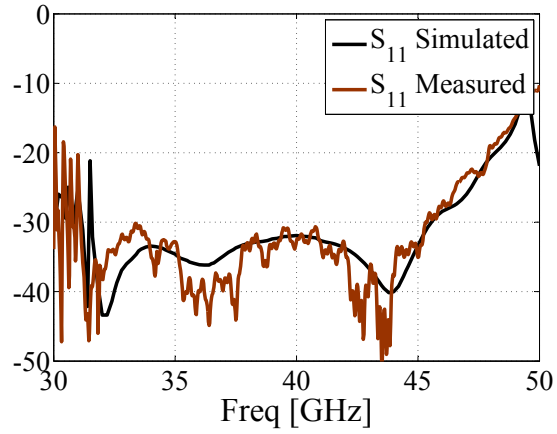


Figure 5.4: Spline-Line corrugated Horn return losses.

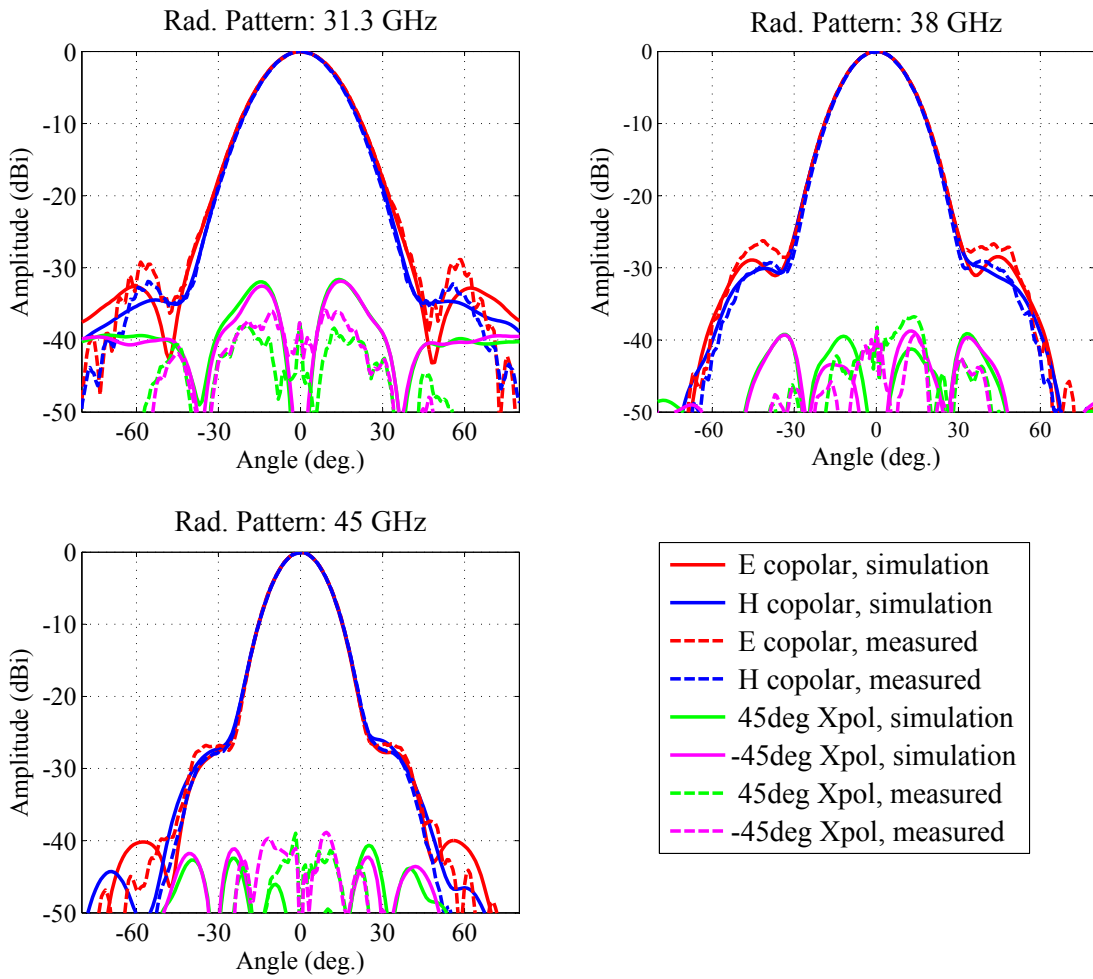


Figure 5.5: Spline-Line corrugated Horn radiation patterns simulation versus measurement results.

5.3.2 Lens

The lens has to refocus the beam from the horn to illuminate correctly the sub-reflector. The lens was designed to have a focal lens of 0.185 m and to be located at 0.196 m from the horn aperture. The illumination taper was calculated to be -12.3 dB at 38 GHz achieving ALMA specifications.

The chosen material for the lens was High Density Poly Etilene (HDPE), which has a refraction index of 1.52 and a loss tangent of 2.7×10^{-4} . To avoid truncation losses at the lens its diameter was set to fully cover the 3σ beam. Therefore, the lens diameter is 0.22 m and its thickness is 0.055 m. A corrugated surface has to be used to adapt the impedance of the HDPE with the free space [70]. Considering this dimensions and the tangent losses of the material the noise contribution from the lens was estimated to be around 8 K [71]. The lens was prototyped, in a first iteration without including the corrugated layer, and installed in our test cryostat. Experimental results of the illumination parameters are presented in section 5.10.2.



Figure 5.6: Left, prototyped lens installed on the test cryostat. Right, IR filters, Top is the 80 K filter and bottom is the 15 K filter.

5.3.3 Infra-red filters

Part of the optics are two infra-red (IR) filters, one at 15 K and the other at 80 K. These filters block the IR radiation from the outside targets get into the dewar, heating it. All the ALMA cryostat IR filter were designed by [69] and are already installed in the ALMA production cryostat. For Band 1 the proposed to use the same set of filter whose main features are:

1. A PTFE filter with a diameter of 60 mm and a thickness of 5 mm for the 80 K radiation shield stage. It includes an anti-reflection layer with triangular profile. It is installed with a 1.5° tilt angle respect to the cryostat axis to avoid standing waves between this components and other optical components.
2. A GoreTex filter with a diameter of 80 mm and a thickness of 3 mm for the 15 K radiation shield stage. It is installed with a 7.5° tilt angle respect to the cryostat axis to avoid standing waves between this components and other optical components.

The filters were procured through ALMA and were installed at our facilities to test the optical performance of the Band-1 system. Figure 5.6 shows a photograph of the units at our laboratory.

5.4 Ortho Mode Transducer

The OMT is a waveguide component which separates the two orthogonal polarizations¹. In the case of band 1 the specifications for this device are stringent. The cross-polar isolation has to be lower than -25 dB. over the complete range from 31 to 45 GHz, giving a fractional bandwidth of 37 %. For an adequate interface of the OMT and other Band-1 receiver components we have set some additional specifications. We aimed to obtain reflection losses below -20 dB and an isolation between the two channels better than -50 dB. There are several designs for an OMT. The most common ones for broadband operation are the Boiffot [80], the turnstile [81] [82] and the dual ridge OMTs [83]. For Band 1 we have decided to implement a double ridged structure, based on a design for Bands 4 and 8 of ALMA [72] [73].

In order to facilitate the assembly of the receiver, the OMT was designed to be directly connected to the Band-1 feed horn [76]. Therefore, the input port of the device consists of an octagonal mode converter, designed to be mated to a circular waveguide with 3.81 mm radius. The two TE_{11} modes present in the circular waveguide (labeled as H and V modes in Figure 5.7) are converted by the octagonal transitions into TE_{10} and TE_{01} modes propagating in the inner square waveguide. The design of this mode converter follows [84] and the ALMA Band-5 solution for the OMT-to-horn transition [85]. The main advantage of using octagonal transitions is that it increases the size of the OMT by only few millimeters, without paying any cost in terms of performance in comparison to traditional square to circular converters.

The two orthogonal TE modes present in the square waveguide are separated by the dual ridge structure, depicted in Figure 5.8. The aim of this structure is to concentrate the V-mode in the narrow space between the two ridges, meanwhile the H-mode is concentrated in the two waveguide structures separated by the central ridge. The V mode continues straight into a reduced height rectangular waveguide, which is in cut-off mode for the H-mode. Meanwhile, the H-mode waveguides are bent and output through two lateral ports with a 180° degree difference of phase. The symmetry of the complete structure is fundamental as it prevents

¹Part of this work has been published in: N. Reyes, P. Zorzi, J. Pizarro, R. Finger, F. P. Mena, L. Bronfman "A Dual Ridge Broadband Orthomode Transducer for the 7-mm Band", Journal of Infrared Millimeter Wave and Terahertz waves, 2012, DOI:10.1007/s10762-012-9942-6.

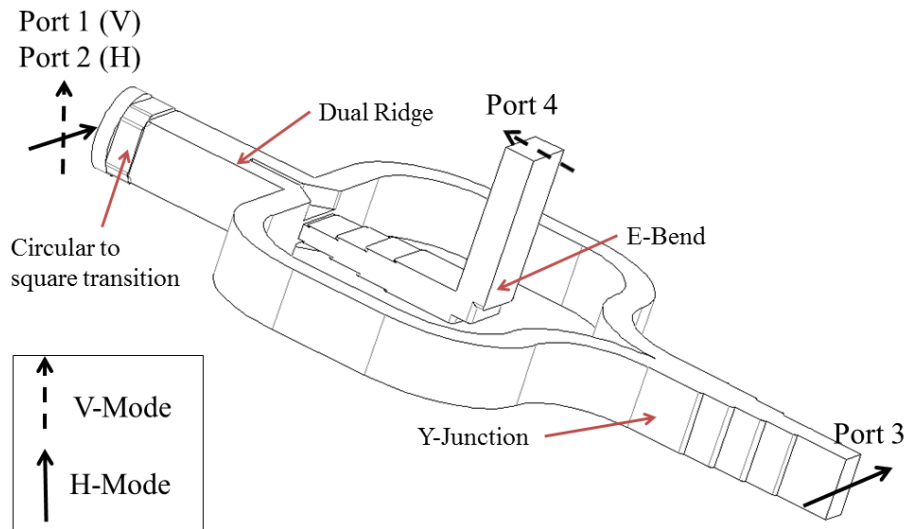


Figure 5.7: Model of the dual ridge OMT. The input port is the octagonal converter which allows the OMT to be directly connected to the circular waveguide coming from the horn. The circular waveguide supports two orthogonal modes (H and V). These modes are converted in square waveguide modes and then separated by the dual ridge structure. H modes are recombined by a Y junction and output at port 3. Mode V continues in the same direction and output through port 4.

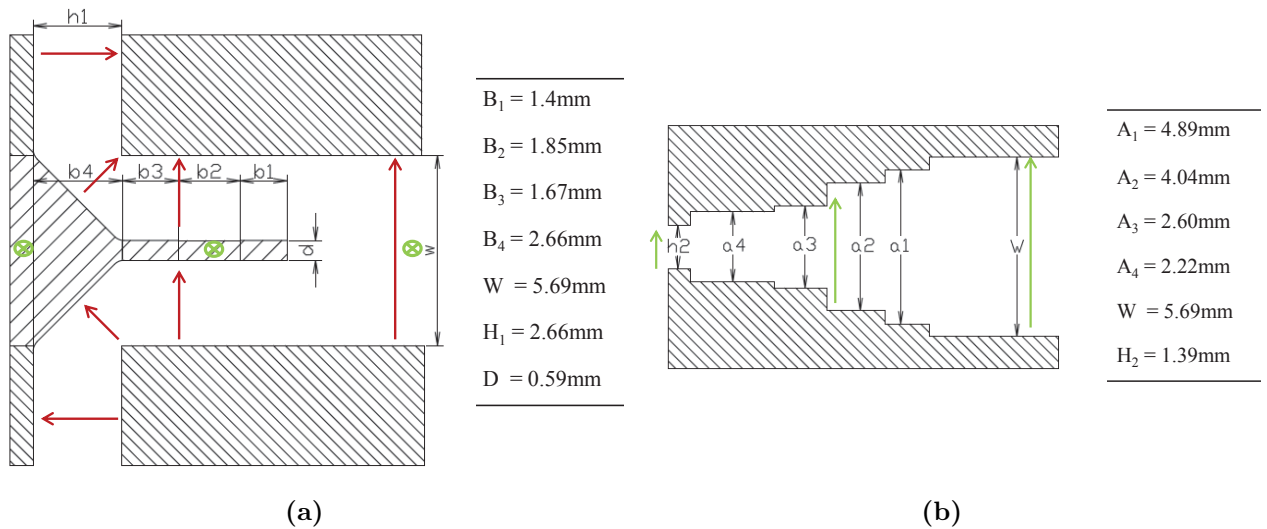


Figure 5.8: Structure and dimensions of the dual ridge structure. (a) presents a top view of the dual ridge structure, showing how the V mode is bended into two symmetric outputs while the V mode continues straight to the single output. (b) shows a section view of the ridge revealing the internal dimensions.

higher order modes, specially the TE_{11} , to appear in the square waveguide causing cross-polar talk.

One of the advantages of the dual ridge structure is its inherent broad-band behavior, allowing the OMT to achieve the specified bandwidth. This structure is the core component

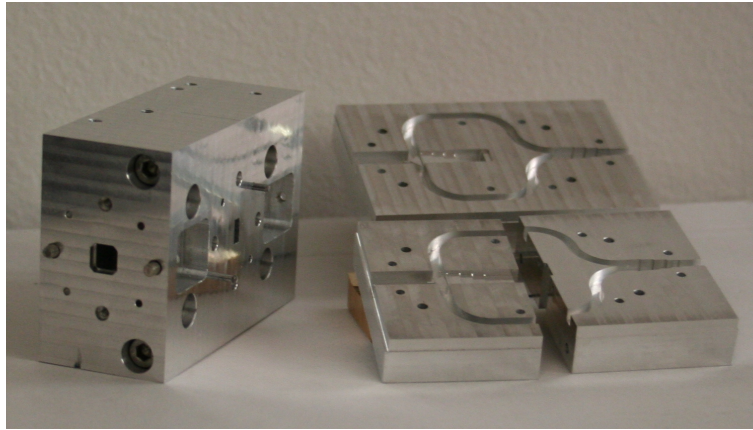


Figure 5.9: The OMT was built using split block technique. At the left side an assembled OMT is shown, where the input octagonal port can be observed. At the right side the three blocks that compose the OMT are shown. The overall block dimensions are $72 \times 30 \times 50 \text{ mm}^3$

of the OMT and the most critical part for broadband operation. We chose to use three steps for the dual ridge as it proves to be enough to cover the specified bandwidth. All the dimensions listed in Figure 5.8 were carefully optimized to achieve the desired specifications.

After the dual ridge the V-mode has to be bent to output by port 4. Meanwhile the H-mode signals have to be recombined in a Y-junction. Both structures were designed based on [74] and were optimized to cover the specified frequency range. The outputs of the OMT are two standard WR-22 waveguide ports, named ports 3 and 4 in Figure 5.7, one for each orthogonal polarization.

Each one of the parts (circular to square transition, dual ridge guide, E-bend and Y-junction) were designed and optimized separately in a 3D electromagnetic simulator². Afterwards, a second iteration was necessary to optimize the performance of the OMT working as a whole. In the simulation we have accounted for the losses on the waveguide walls and for the machining effects, as the fillets in the corners and the surface roughness.

The OMT was built using a high precision CNC milling machine. We have used Aluminum 2017 to produce the units as it is inexpensive, light, resistant to corrosion, and has excellent electrical conductivity. The OMT was constructed in three blocks that are tightened by screws and aligned using stainless-steel alignment pins. The fabricated OMT is shown in Figure 5.9.

The OMT was characterized using a vector network analyzer model E8364C from Agilent. A circular load was designed and built to terminate the input port while measuring the reflection losses at the H and V ports. Transmission and cross polar levels were measured using a rectangular to circular adapter. Isolation was directly measured between the ports H and V of the device while the circular port was loaded. Figures 5.10a to 5.11 summarizes the simulations and experimental results. Both set of results show an excellent agreement, demonstrating the good quality of the fabricated OMT.

²High Frequency Structure Simulator from Ansys

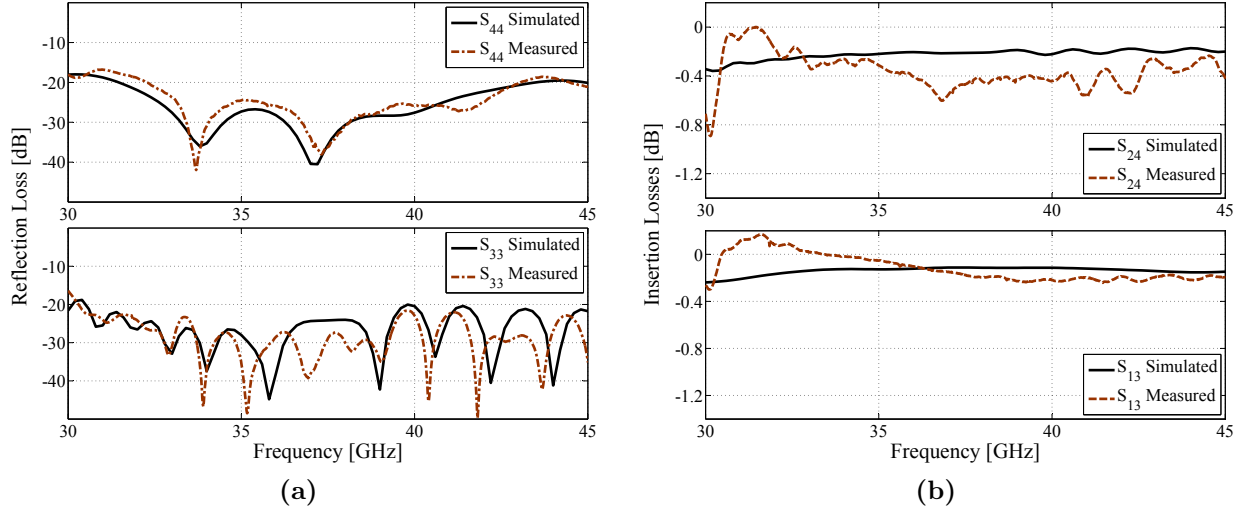


Figure 5.10: (a) Measured and simulated reflection losses for the dual ridge OMT. Reflection losses are below -20 dB all over the band of design. (b) Measured and simulated insertion losses for the dual ridge OMT. We have assumed a conductivity of 3.8×10^{-7} [S.m $^{-1}$] and a surface roughness of $2 \mu\text{m}$ for the Aluminum walls of the OMT model.

In the operation range of 31 to 45 GHz we can summarize the results as following. *(i)* An insertion loss lower than -20 dB both at the H and V port (Figure 5.10a), *(ii)* a transmission of about -0.4 dB (Figure 5.10b) and *(iii)* cross-polar and isolation of -50 dB and -60 dB respectively (Figure 5.11).

It has to be noticed that the new design of the dual ridge OMT allows us to reduce the crosspolar levels previously published by [72] to -50 dB from the original -30 dB. This fact proves that this kind of devices can achieve a cross-polar as low as other reported waveguide OMTs [82] [81]. The new design also provides a compact and effective solution to interface the square waveguide inherent to the double ridge structure to the standard circular input needed to connect a dual polarization horn. Despite being optimized to work between 31 to 45 GHz, the OMT shows a good performance (return losses lower than -17 dB) between 30 to 48 GHz, as shown on Figure 5.12. With such performance this device is a good option for receivers covering the complete Q waveguide band (33-50 GHz).

We have fabricated three units of the OMT with only few mechanical differences between them. The repeatability is excellent for all the units as observed in Figure 5.12.

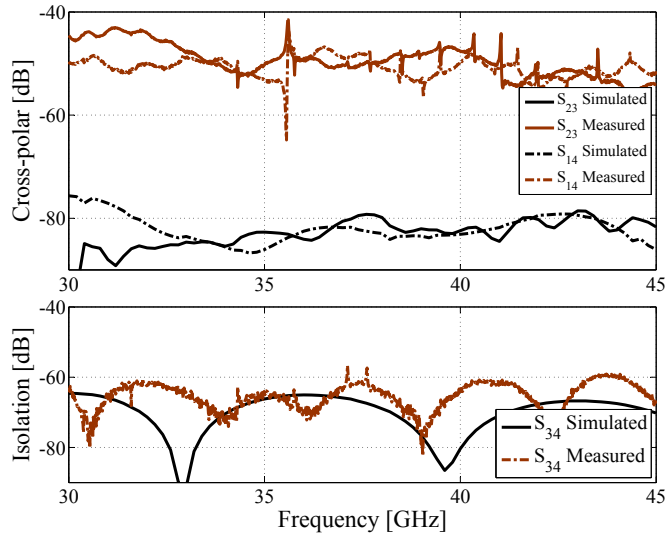


Figure 5.11: Measured and simulated isolation (bottom) and cross-polar (top) for the dual ridge OMT. The cross-polar levels are well below -30 dB, which is according to specification. The difference between simulation and measurements in the cross-polar level is due to instrumental effects and to misalignments between the blocks that constitute the OMT. The isolation, in contrast, is similar to the simulated value of around -60 dB.

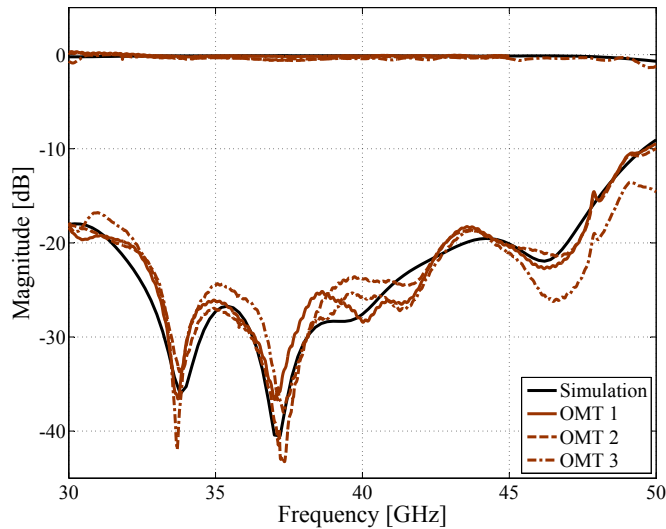


Figure 5.12: Comparison between the three different units that were produced at our laboratory. All units have the same design, but some minor modification in the machining strategies. This explain the small differences that are observed. For clarity the figure shows only S_{24} and S_{44} , Other parameters show the same degree of repeatability.

5.5 Isolator

If the reflexion losses of the LNA are too high it will cause the existence of a stationary wave between the LNA and the optics or between the LNA and the mixer. This situation there would affect the noise figure of the receiver and gain flatness. Even the cross-polar levels can be spoiled if a standing wave is present between the LNA and the optics , as part of the reflected signal can change its polarization status when reflected back by the lens. Fortunately we have not detected this problem in the proposed architecture therefore such isolator can be avoided.

Isolators are microwave components which allows the signal to propagate only into one direction while attenuating the signal traveling in the reverse directions. They are based on the Faraday effect [86] in a ferromagnetic material, and have been used in microwave design for more than three decades. The problem of cryogenic isolators arises from ferrites which tend to scratch with thermal cycles and lose their ferromagnetic properties.

At the Australia Telescope National Facilities commercial Q-Band isolators from Millitech had been tested down to 19 K and no appreciable degradation in performance was measured after several thermal cycles [87]. As the available space for Q-Band is limited these units are not suitable for this project. An interesting option are the isolators designed for the Five Colleges Radio Observatory [88] W-Band receiver. These units were custom designed by Millitech for this project and achieve a good performance keeping at the same time a small size.

As part of our program for Band 1, cryogenic isolators were bought from Channel Microwave. The main goal was to have low insertion loss (better than 0.3dB) over the complete band. The original specifications for this isolator are shown in Table 5.4. After several it-

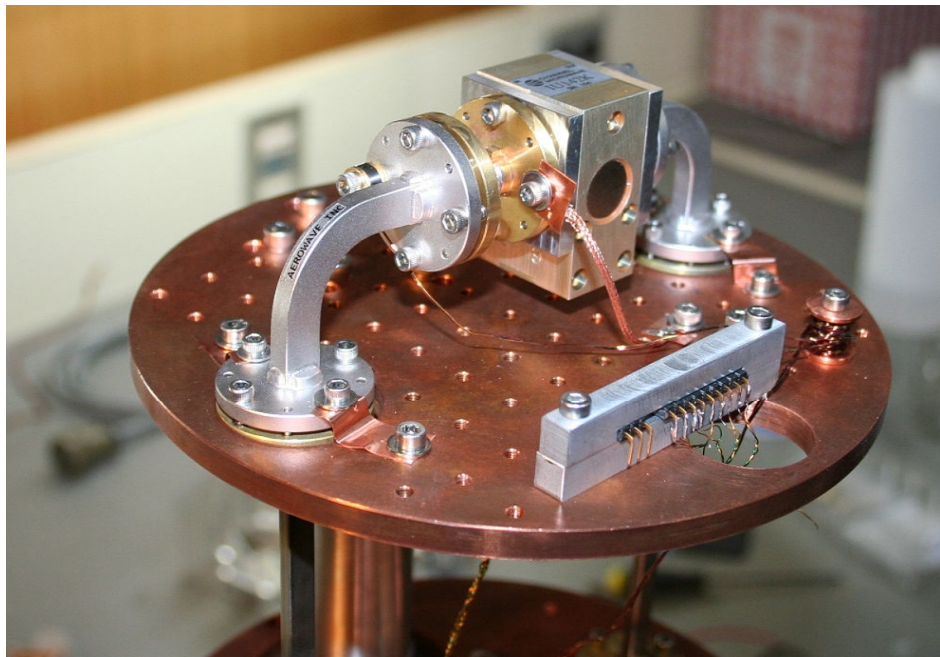


Figure 5.13: Laboratory setup for cryogenic measurements of Band-1 isolators.

Quantity	Original specification (31-45 GHz)	Edge specifications(31-33 & 43-45 GHz)
Isolation	16dB	10dB
Insertion loss	0.7 dB	1.0 dB
Return loss	-15 dB	-9.5 dB

Table 5.4: Specifications for Channel Microwave isolators

erations it was clear that these values cannot be achieved over the complete bandwidth of Band 1. A new specification for the extremes of the band (31 - 33GHz, 43 - 45 GHz) was agreed and is shown in a second column in Table 5.4.

The isolators were received and tested at the Millimeter Wave Laboratory. For this purpose an old cryostat was refurbished to be used as cryogenic test setup. The results are presented in Figure 5.14. It was found that three devices achieve the specified values while the fourth unit did not.

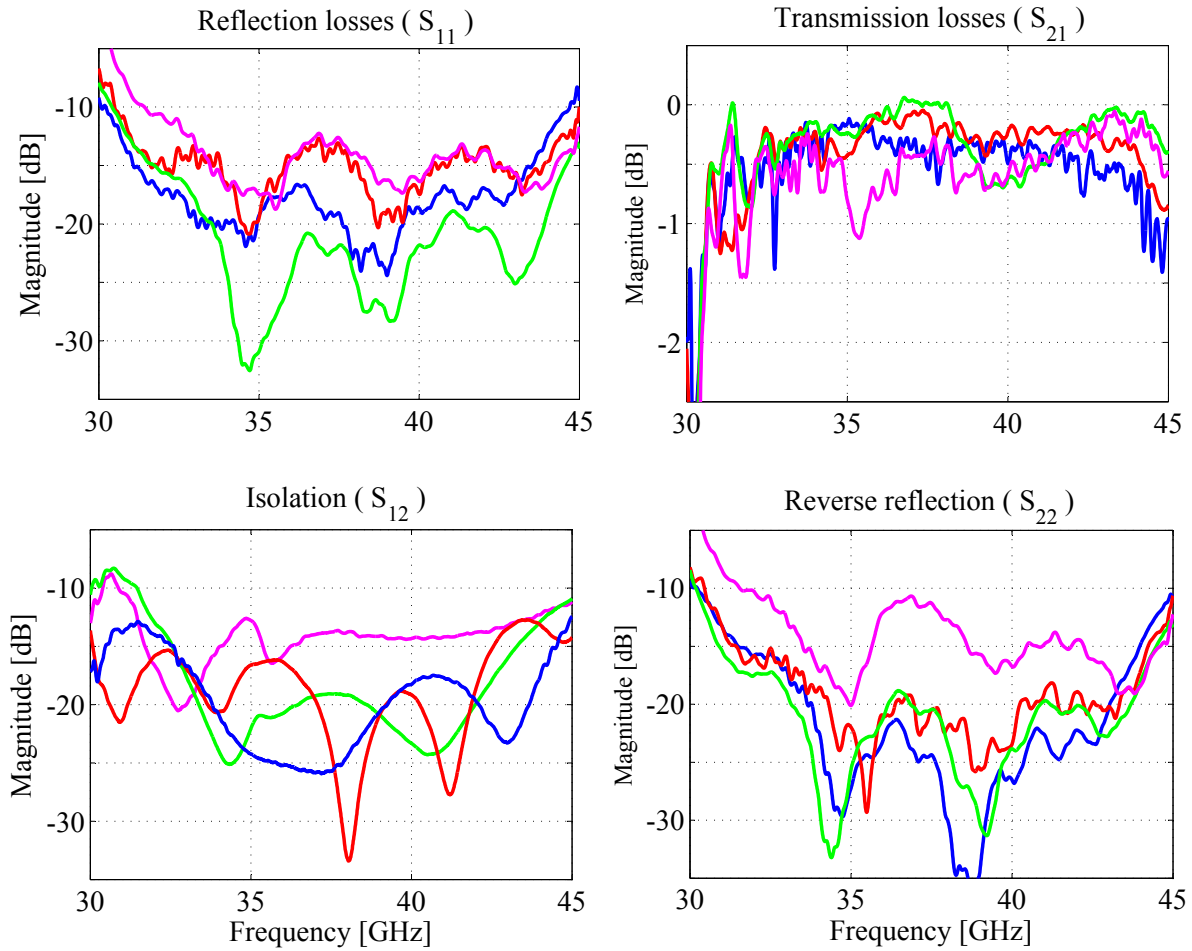


Figure 5.14: Cryogenic measurements of Band-1 isolators. Each panel presents cryogenic measurements of one scattering parameter. Different color traces represents results for a different unit.

5.6 High pass filter

The high pass filter cancels out the LSB signal before the down-conversion. As explained in Chapter 1 of this thesis, the result is a SSB receiver. We need a filter with a cut-off frequency of 30 GHz, with passband at 31-45 GHz and a rejection band with more than 20 dB at frequencies lower than 29 GHz.

To design the filter we have followed [89] and [90]. The filter is compound by several waveguide sections, each one with a width A_i and a length C_i . Each section of the filter is modeled by a transmission line with a propagation constant β_i , and an impedance Z_{0i} .

$$\beta_i = 2\pi \sqrt{\left(\frac{f}{c}\right)^2 - \left(\frac{1}{2A_i}\right)^2} \quad (5.1)$$

$$Z_{0i} = \frac{jf\mu}{\sqrt{\left(\frac{1}{2A_i}\right)^2 - \left(\frac{f}{c}\right)^2}} \quad (5.2)$$

where f is the frequency of simulation. If this frequency is below the cut-off frequency of the waveguide section it will act as an attenuator with an attenuation given by

$$\text{Attenuation} = -8.68\sqrt{2\pi} \frac{A_N}{C_N} \sqrt{1 - \left(\frac{f}{f_c}\right)^2} \text{dB} \quad (5.3)$$

The reflection between two section is calculated as

$$\Gamma_{i,i+1} = \frac{Z_{0i+1} - Z_{0i}}{Z_{0i+1} + Z_{0i}} \quad (5.4)$$

The reflection coefficient for a cascade of sections is

$$\Gamma_i = \frac{\Gamma_{i,i+1} + \Gamma_i e^{-2j\beta_{i+1}C_{i+1}}}{1 + \Gamma_{i,i+1}\Gamma_{i+1} e^{-2j\beta_{i+1}C_{i+1}}} \quad (5.5)$$

then, Equation (5.5) is computed for each section of the filter from left to right. At the end the scattering parameter of the complete filter are computed as

$$|S_{11}| = |\Gamma_0| \quad \text{and} \quad |S_{12}| = \sqrt{1 - |\Gamma_0|^2} \quad (5.6)$$

Using this model, an optimization script was written in MatLab to find the optimum dimensions for the filter. The objective function was to minimize the transmission in the LSB (below 29 GHz) while maximizing the transmission in the passband (31.3-45 GHz). After the optimization process a three stage filter was selected. The final dimensions are shown in Figure 5.15. The performance of the filter was checked using a 3D full electro-magnetic simulator.

The filter attenuation in the rejection band is better than 18 dB. The transmission losses of the filter are negligible over the pass band. The results are summarized in Figure 5.16, where we can also check the correspondence between the simulation and the measured results. Using this filter the sideband rejection ratio of the receiver would be better than 20dB in 99% of the LO configurations. The worst case is a rejection Ratio of -18.47 dB where the LO is at 33 GHz and the observing frequency (RF) is 37 GHz.

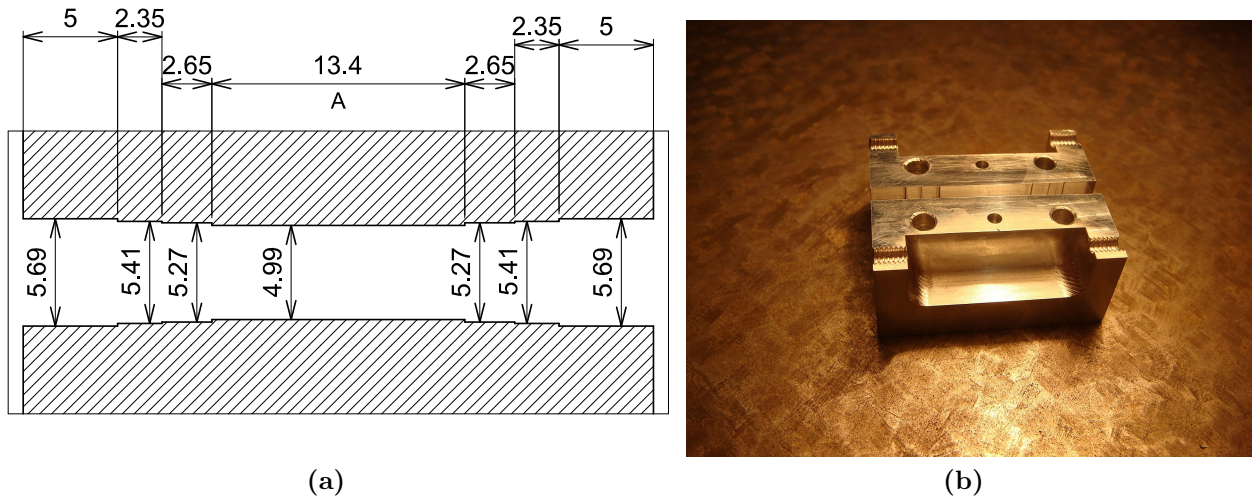


Figure 5.15: (a) High pass filter dimensions (in millimeters). Only the waveguide width (a) is showed, height correspond to $a/2$. (b) Picture of the fabricated filter.

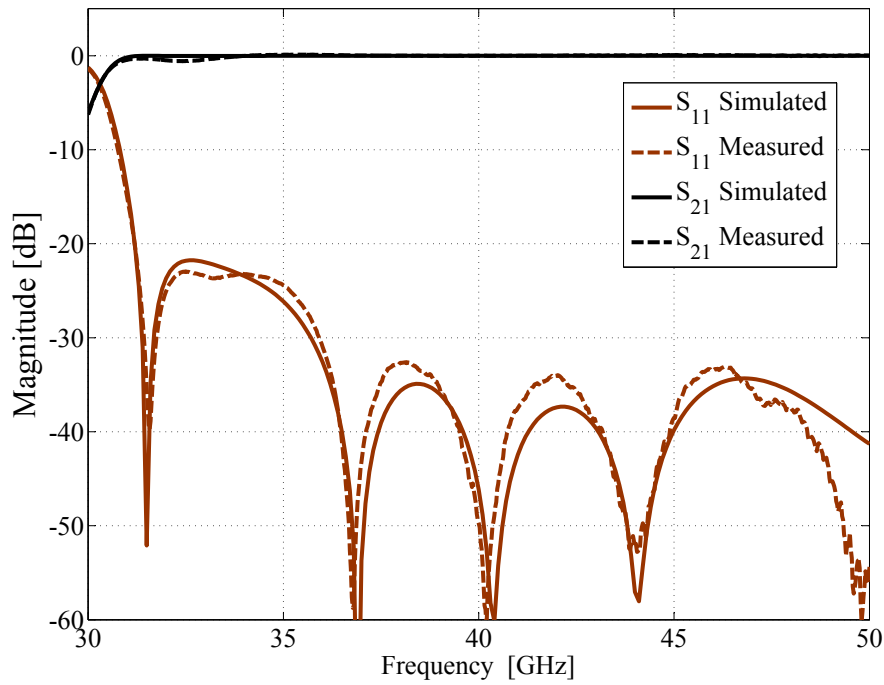


Figure 5.16: High pass filter simulation and measured data. An excellent correspondence between them is achieved.

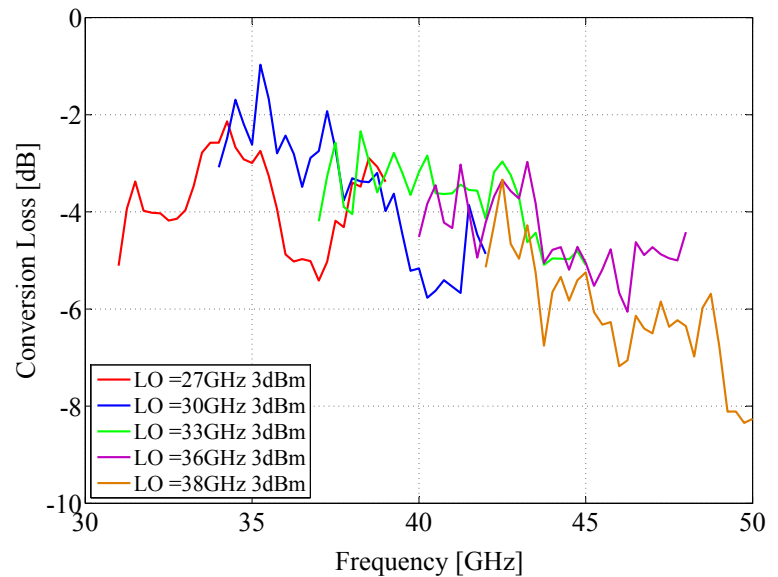
5.7 Mixer

After the filter the signal is down converted to 4 to 12 GHz by a mixer. Since the overall noise figure is dominated by the noise figure of the amplifier, we can use commercially available components without a penalty in noise. In order to avoid using power amplifiers for the LO we need to have a mixer with low power consumption which is achieved by using a biasable balanced mixer based on Schottky diodes. We have acquired a couple of units from Spacek (model M32-8B) and tested their performance at Band 1.

As presented in Figure 5.17b the conversion loss of the mixers is not flat and the average value is around -4 dB when operating with a 3 V bias signal and 3 dBm of LO power. The reflection losses of the mixer are good, but the most problematic part is the IF port which has a reflection loss of -3dB between 10 to 12 GHz as shown in Figure 5.18b. This situation is being evaluated to define if an additional attenuator is needed between the mixer output and the IF amplifiers to minimize standing waves between this two components.



(a)



(b)

Figure 5.17: (a) shows the test setup for mixer characterization. (b) presents the measured Conversion loss of the unit.

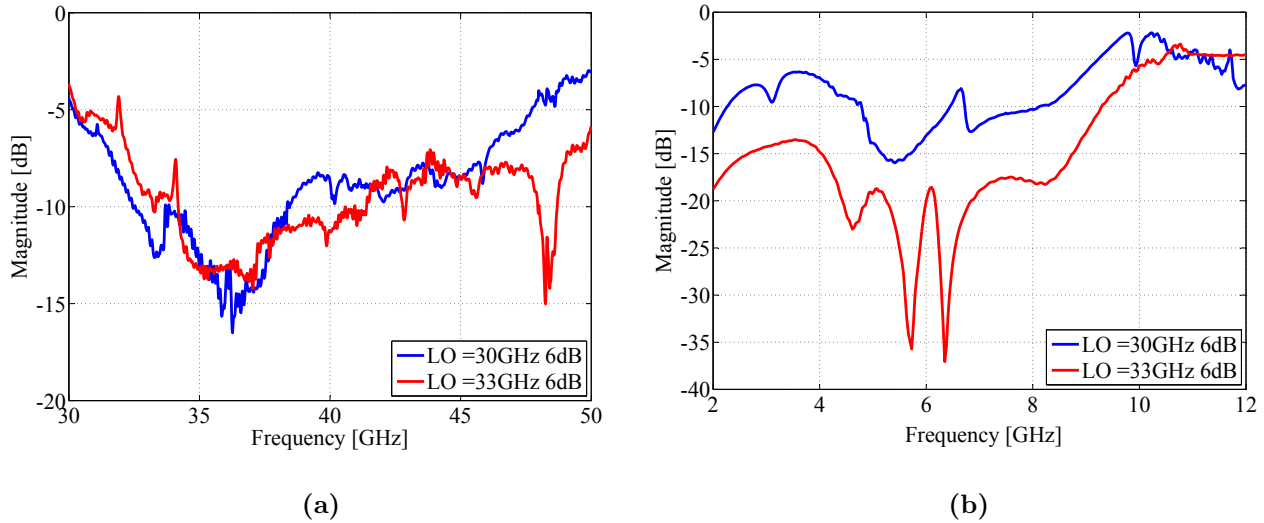


Figure 5.18: (a) and (b) show the reflection losses of the mixer at the RF and IF ports.

5.8 IF Amplifiers

A broad band (4-12 GHz) amplifier is needed to obtain the output power levels required by specifications. There is no need of cryogenic operation since the noise is dominated by the HEMT amplifiers. As first solution we chose the Miteq AMF-4D-02001800-23-10. It provides a gain of 25 dB with a flatness of 1.5 dB. The unit is biased with a +15 V signal with a consumption of 160 mA. It is allocated in the warm space of the receiver.

5.9 Band-1 prototype receiver

After having proposed a receiver architecture and identifying the critical components our development effort was focused in assembling the entire prototype receiver, which is presented in this section. For this reason the results presented here have to be understood as preliminary results, work that is presented here in order to give a complete overview of the Band-1 effort.

The proposed mechanical architecture for Band 1 was carefully analyzed. Vibrational analysis was performed in [91] and the architecture was slightly modified to meet the ALMA mechanical requirements. It has to be highlighted that the proposed solution is very compact and was designed for easiness of assembly and maintenance, qualities that are important when a batch production of receivers is envisioned. The Band-1 prototype receiver was assembled, as show in Figure 5.19. All components presented previously can be identified starting from the spline horn, followed by the OMT, amplifiers, isolators, filter and mixers. Due to the time constraint in this project we choose as amplifier the MMIC based LNA presented in section 4.2.2. Unfortunately, the hybrid amplifier (section 4.2.3) was obtained recently and, at the time of writing, it was not possible to incorporate it to the receiver. Both amplifiers have the same external dimensions and can be easily replaced.

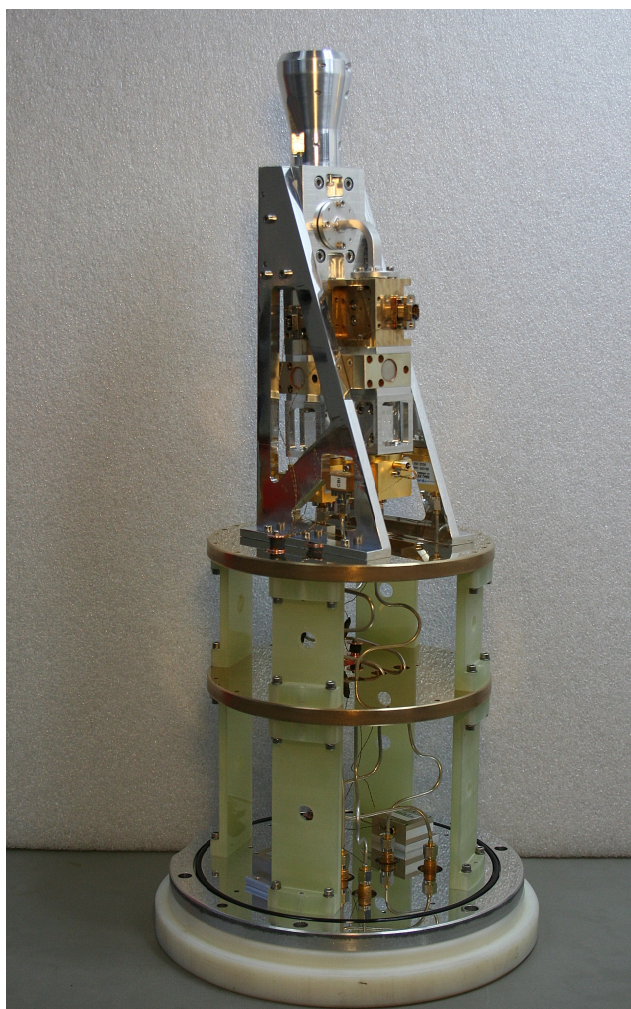


Figure 5.19: Assembled prototype of an ALMA Band-1 receiver

The electronic interface of the receiver is located at the bottom plate and corresponds to four coaxial 2.9 mm connectors which are used to feed the receiver with the two LO signals, one for each polarization, and to extract the two IF outputs corresponding to the two polarization channels. A bias connector brings the signals to bias the mixers and LNAs.

The body of the receiver consists of three plates, the bottom plate (at 293 K), the 80 K plate and the 12 K. They are separated by G-10 fiberglass structures to avoid thermal conduction between them. All these components, along with the receiver support structure, were designed by us and fabricated at a local company³. All structural components are aligned using stainless steel dowel pins in order to keep the tolerances under specifications. RF components are located at the 12 K stage and are connected to the bottom plate through stainless steel coaxial cables, which are thermally linked to the 80 K stage in their middle part. The complete receiver can be assembled in a few hours by trained personnel.

³Pimet, www.pimet.cl, Ñuble 1490 Santiago



Figure 5.20: Test setup for receiver characterization. An ALMA compatible cryostat, developed by NAOJ is used to house the receiver.

5.10 Preliminary results

The prototype was assembled and tested. For this purpose a receiver characterization test setup was built at our laboratory. This setup, shown on Figure 5.20 allows to quickly switch between different measurements as: beam pattern characterization, cross-polar level, noise measurements and IF power levels. The receiver is housed in an ALMA test cryostat developed by the National Astronomy Observatory of Japan (NAOJ) [92]. This cryostat was specially designed for testing purposes of the different ALMA receivers during the development phase. The cryostat was modified to incorporate the ALMA Band-1 optics, consisting of two IR filters and a warm lens. In this section the different measurements are presented along with the hardware implementation of the setup for the different configurations.

5.10.1 Noise measurements

The noise temperature of the receiver is measured using the hot and cold method as presented in section 4.2.1. The cold load corresponds to a microwave absorber embedded into a liquid nitrogen container, while the hot load corresponds to a piece of absorber at room temperature. The output of the cartridge, when observing a 290 K load, will be -43 dBm/GHz. This signal is amplified by the IF electronics and one polarization is selected for measurement using an electronic switch. The output signal is filtered by a tunable YIG filter with a 30 MHz band pass between 4 and 12 GHz. Additional 45 dB amplification was required to increase the

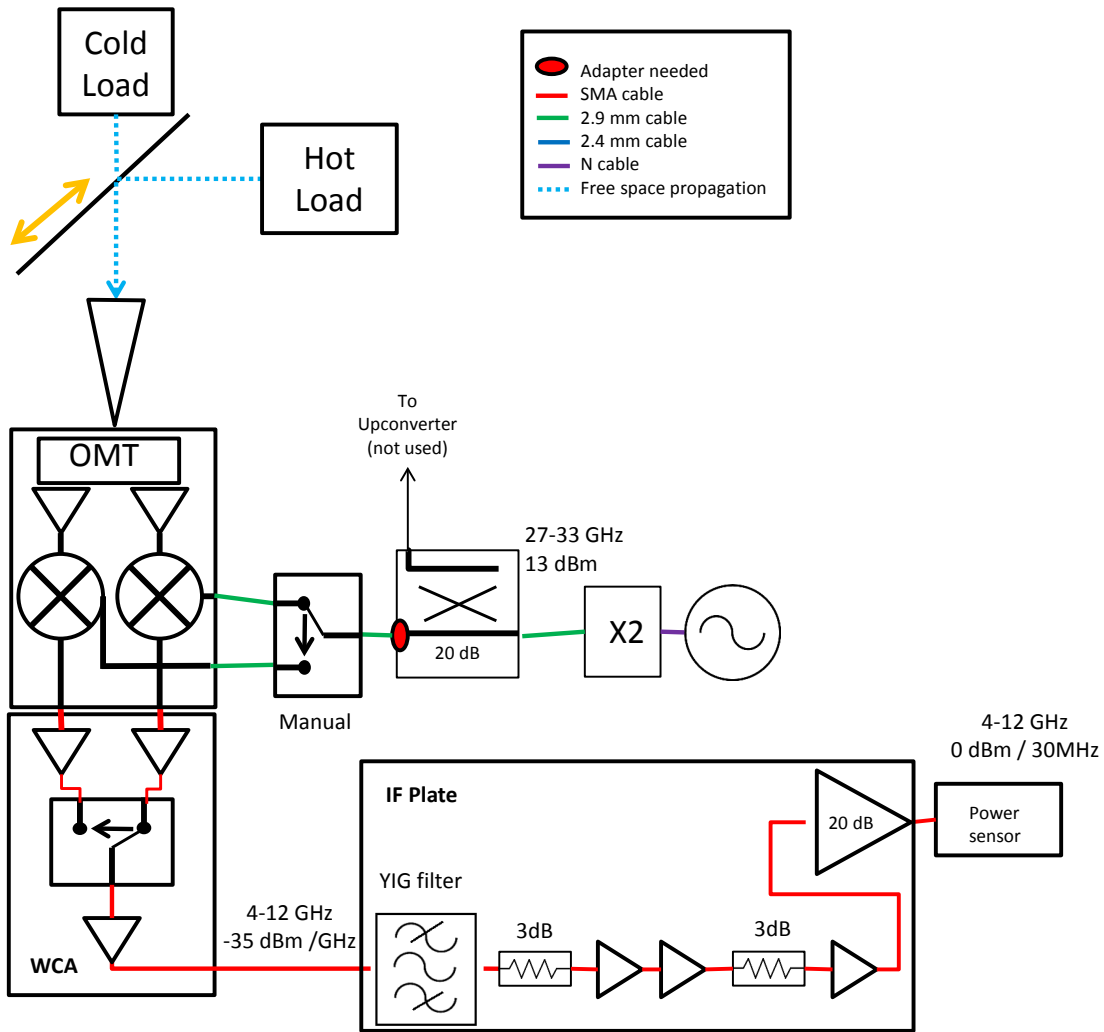


Figure 5.21: Test setup schematic for noise temperature measurements of Band-1 cartridges.

output power to obtain around 0 dBm at the input of the detector. A couple of 3 dB attenuators are used to minimize standing waves between amplifiers. The noise temperature is measured for LO frequencies between 27 and 33 GHz with a resolution of 1 GHz. For each LO, 240 points separated by 33.3 MHz between 4 and 12 GHz are measured. Each measurement has an instantaneous bandwidth of 30 MHz. A schematic of the test setup is presented in Figure 5.21.

The results of extensive tests are presented in Figure 5.22. The noise temperature of the cartridge is around 150-200 K which is considerably higher than specified values. That is explained by the high power dissipation of these GaAs chips (382 mW) which is heating up the HEMT conduction channel rising its physical temperature, and as a consequence its noise level. A second fact is that the MMIC was designed for room temperature operation having no specifications for cryogenics. There is no way to solve this problem except to replace these amplifiers by new amplifiers with better noise performance. We expect, in the near future to replace them by our hybrid designs which exhibit lower noise, higher gain and lower power dissipation.

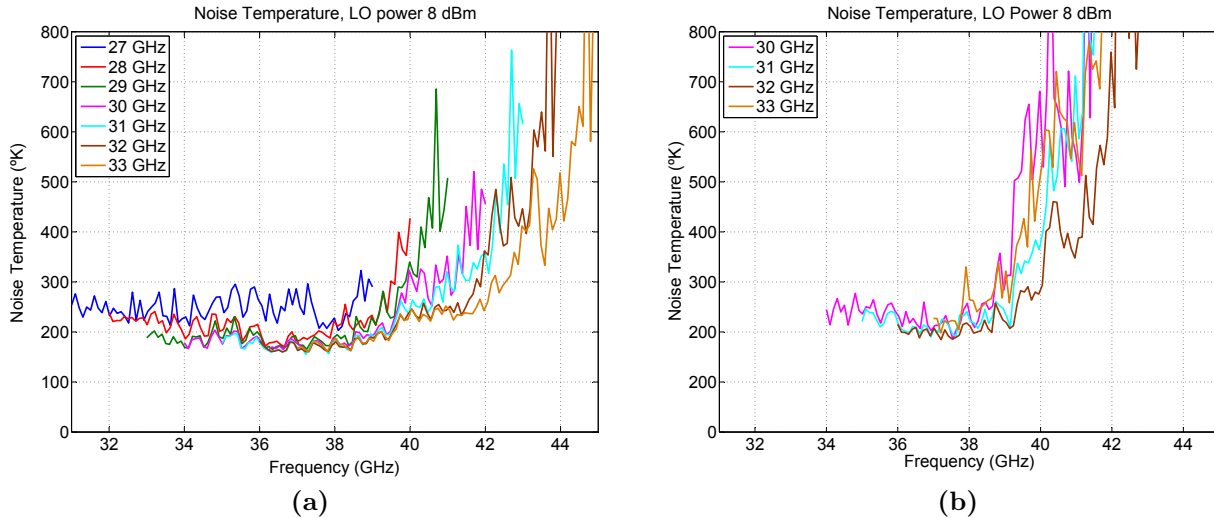


Figure 5.22: (a) shows the noise temperature of the polarization 0 receiver. It can be noted that the LO=27 GHz curve has a higher noise than the following curves. This is caused by the mixer running out of LO power. (b) shows the noise temperatures of polarization1. In this set of data the effect of running out of LO power is more pronounced than in Pol0 data.

A second order analysis of the results is that despite the mixers need a low LO signal (3 dBm) we need to feed the receiver with a strong LO signal (+11 dBm) in order to have the mixers working on their optimal point. Anyway, for some configurations (polarization 1 at 27 GHz LO) the LO power is not enough to run the mixers generating higher noise temperatures. It is suggested for the future to include a power amplifier to boost the LO signal and overcome the losses at the interface, connectors, and cables, assuring that the mixers are correctly pumped. Another problem that was detected is that the overall noise temperature between 40 and 45 GHz is much higher than in the central part of the band. This is probably caused by the low gain of the amplifiers at the higher edge of the band (see Figure 4.6) and can be easily solved using higher gain amplifiers.

5.10.2 Beam Pattern

The beam pattern of the Band-1 cartridge is measured using the experimental setup presented in Figure 5.23. A 4 to 12 GHz test signal generated by the VNA is upconverted to the Band-1 RF range (31-45 GHz). To avoid the receiver being saturated the test signal is attenuated by a 30-dB variable attenuator located before the RF probe. The RF probe is mounted in a X-Y movement stage⁴ with resolution of 1 μm which allows to scan a $60 \times 60 \text{ cm}^2$ area.

The test signal is deflected by a 43.4° deg mirror to finally illuminate the receiver optics where it is down converted by the Band-1 receiver. The output IF is compared by the VNA with the original test signal measuring its phase and relative amplitude. Data are recorded for a measurement plane of 300 mm by 300 mm with a resolution of 2 mm (corresponding to $\lambda/4$ at the center frequency). It is important to highlight that the LO used to feed the

⁴Newmark systems model NLS4-24

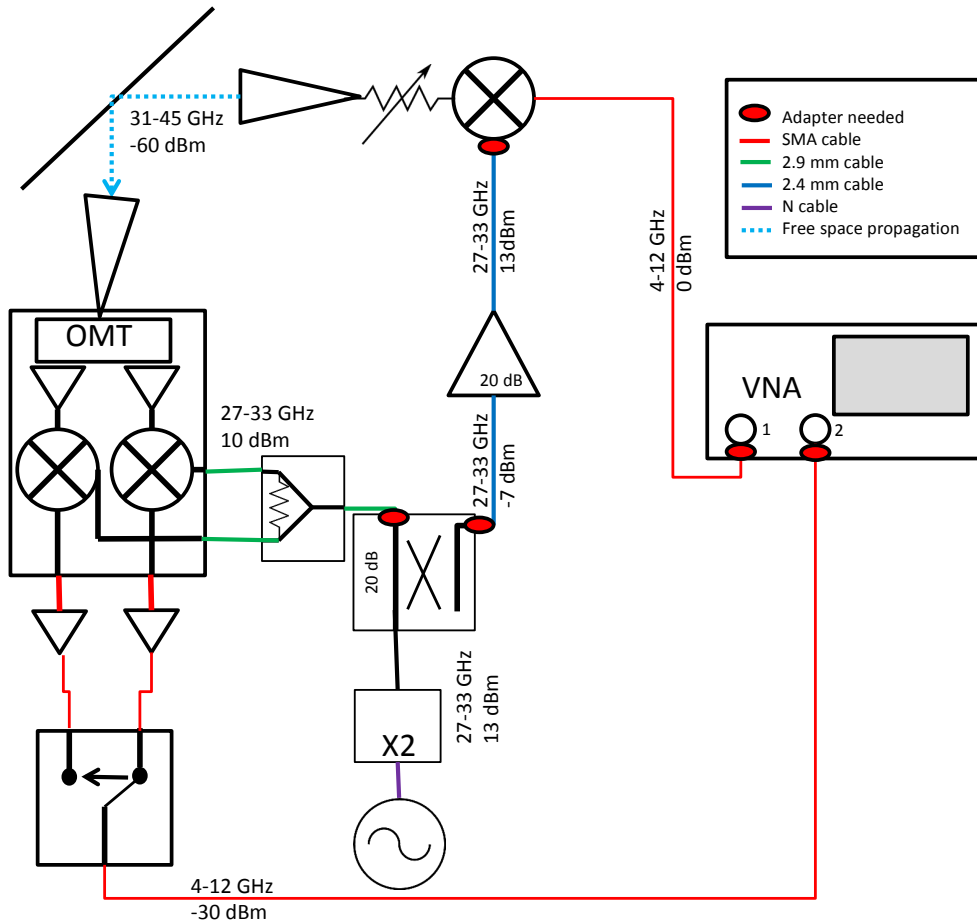


Figure 5.23: Test setup schematic for beam pattern measurements of Band-1 cartridges.

Band-1 receiver is the same used for the up converter. In this way the phase variation due to the LO contribution is canceled out and the measured phase only depends on the position of the RF probe in the measurement plane.

After a careful alignment of the optical system (dual stage, mirrors, cryostat and RF probe), the beam pattern was measured at the edges of the band (31 and 45 GHz) and at the central frequency (38 GHz). Preliminary results for 38 GHz are presented in figures 5.24 and 5.25.

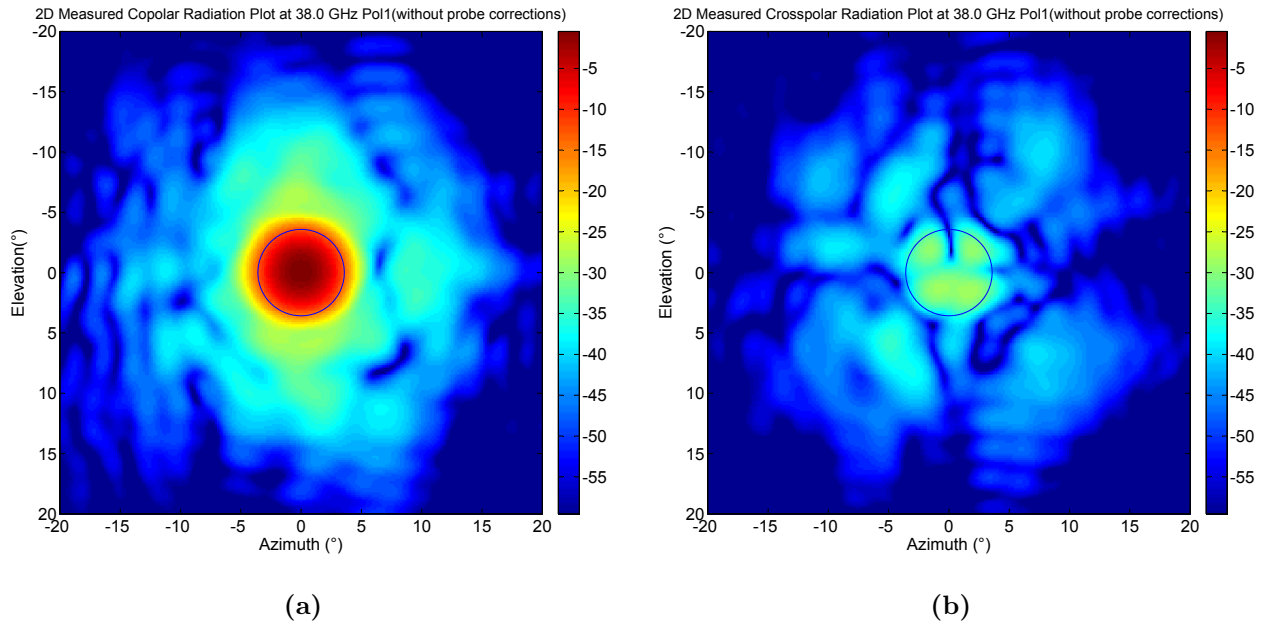


Figure 5.24: Preliminary co-polar (a) and cross-polar (b) beam patterns for Polarization 0 at 38 GHz. Blue circles indicate the position and angular size of the antenna subreflector

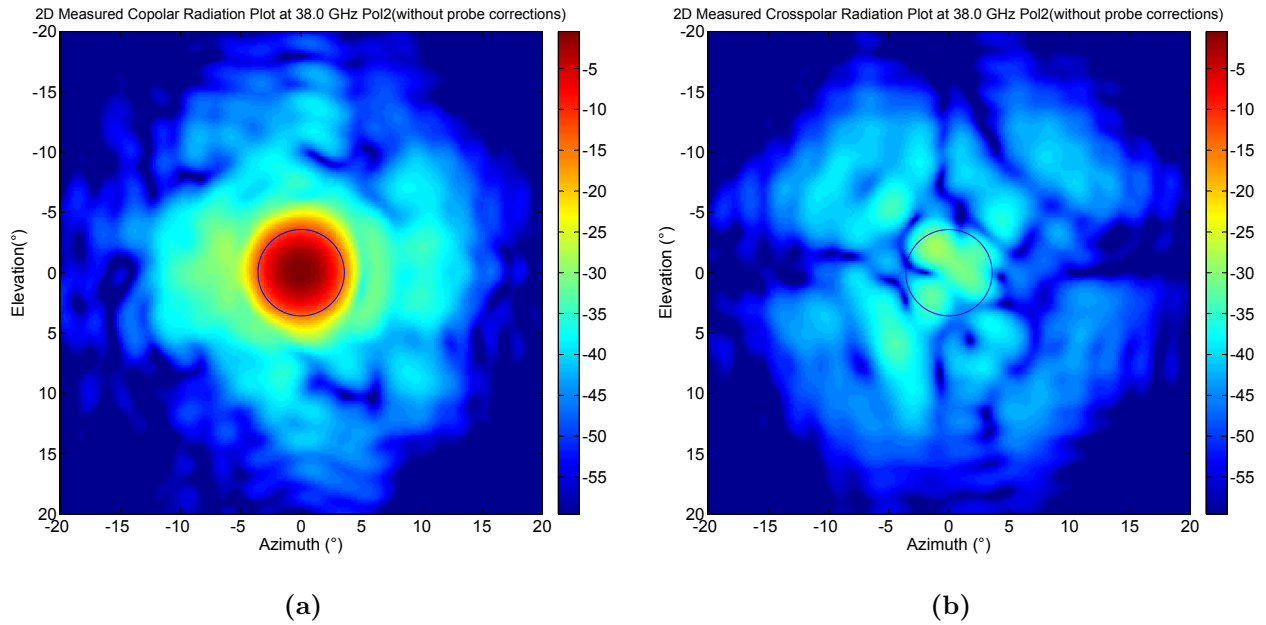


Figure 5.25: Preliminary co-polar (a) and cross-polar (b) beam patterns for Polarization 1 at 38 GHz. Blue circles indicate the position and angular size of the antenna subreflector

5.11 Conclusions

In this chapter we have presented the technologies we have developed for ALMA Band 1. The overall architecture was presented and analyzed, extracting the main specifications for each component of the future Band-1 receivers. Excellent results have been presented for the feed-horn using a spline corrugated technology. This technology also allows to reduce the size of the standard horn by almost a factor of two, allowing the receiver to easily fit into the allocated space for Band 1. The proposed OMT present excellent results in terms of cross-polarization and insertion losses over a broad frequency range, having at the same time an excellent manufacturability using a conventional CNC machining. Both results, horn and OMT, have been published in specialized journals [76] [93].

The work on LNAs has permitted our group to acquire capabilities in design, fabrication and testing of active microwave components. The work presented here corresponds to the first generation of amplifiers fully designed and built within our group and we hope that in the near future we can obtain state-of-the-art results using more advanced technologies. Following this path we have recently installed (2012) new facilities consisting in an automated noise figure analyzer and a microwave probe station. This complementary equipments will allow us to work on device characterization and modeling, fundamental step to start working with transistors especially designed for microwave low-noise operation.

We have also identified components that are already available in the market where no research effort is needed. In this case we have selected the best candidates for the receiver and have tested extensively to study their performance. This is the case of cryogenic isolators, mixers and IF amplifiers. Results of this evaluation components have also been presented.

Finally, A complete receiver was assembled to serve as technological demonstrator for the proposed Band-1 technologies. A complete test setup was designed and built at our laboratory in order to measure the main parameters of the prototype receiver. Preliminary results show a smooth overall operation, with the optics showing results better than specification. Ongoing work should provide amplifiers with better cryogenic performance than the actual LNAs. In this sense we have started new projects and collaborations in the area of low noise devices to follow up our efforts in this particular area.

Chapter 6

Conclusions and perspectives

The central motivation of this work has been the study of technologies that allow the implementation of a Q-Band receiver at the Atacama Large Millimeter Array (ALMA). This receiver corresponds to the lowest spectroscopic band devised for ALMA, the so-called Band 1. Initial specifications set the frequency coverage of this band to be 31 to 45 GHz. This band was not implemented during the first construction phase of the telescope, but is included within the second development phase. Such instrument will enhance the actual capabilities of the interferometer by adding new possibilities to the scientific community using ALMA. The main applications among many interesting topics, described deeply in Chapter 2, are the detection and study of high redshifted molecular gas from external galaxies and the study of medium size (few millimeters) dust components in protoplanetary disks.

During the past years our group at Universidad de Chile has been working on the development of different technologies to cover this band complying with the demanding ALMA specifications. Among the most burdensome challenges are the stringent specifications on noise temperature, the large required bandwidth, and the limited space available for this receiver within the ALMA cryostat. To achieve the desired results, state of the art performance components have to be designed specially for this application. We have identified the design of the optics, ortho mode transducer (OMT) and low noise amplifiers (LNA) as science enabling technologies and our efforts were focused on developing such technologies.

Special emphasis during this thesis project was to develop cryogenic LNAs based on High Electron Mobility Transistors (HEMTs), technology that presents the best noise figures for the millimeter-wave band up to date. Amplifiers based on commercial microwave monolithic integrated circuits (MMICs) were produced as a first approximation to the problem. This first design allows us to develop advanced waveguide to microstrip probes and to gain experience on microelectronic assembly and design of millimeter-wave active components. The obtained results were according to the chip specifications but some issues, as the large power dissipation, prevented their use in cryogenic low-noise receivers. A second design based on hybrid approach was started. It included a six-month training at University of Manchester to learn about design and testing of low noise cryogenic amplifiers for the millimeter wave range. As an outcome a design of an hybrid amplifier based on GaAs HEMT was produced and built at our laboratory. During this process numerous technical problems were solved

allowing our group to start working on millimeter-wave microelectronics. As a result we obtained a LNA with 25–30 dB of gain and a noise figure of 2.5 dB.

Another important part of this thesis work was the assembly and testing of a prototype receiver using the developed technology along with high performance commercial solutions for the non-critical components. The receiver architecture is based on a single side band configuration. The RF signal is coupled into the receiver by a horn and a lens. Two filters prevent IR radiation to come into the receiver. After the horn the signal is split by the OMT into two signals with perpendicular linear polarizations. Each polarization signal is then processed by an independent receiver. In the first stage of each receiver the signal is amplified by the cryogenic LNA. An isolator placed between the LNA and the down-conversion system avoids standing waves between them. Before the mixer a high pass filter cancels the image frequency, obtaining an upper sideband conversion scheme. The down conversion process is carried out by a Schottky mixer. Finally, the IF signal is amplified by a 30-dB amplifier at room temperature. A mechanical configuration for the receiver was also proposed including the vibration analysis of the solution. The proposed architecture is fully compatible with ALMA standards.

It is important to highlight that as part of this effort a new laboratory for millimeter wave instrumentation was set and several equipments were bought and installed. The most important are a vector network analyzer, cryogenic test equipments, signal generators and a close cycle helium refrigerator. A precision workshop was equipped with a 5 axis precision CNC milling machine, which allows us to have a short time between design and prototyping stages. The installation of the laboratory continues with the recent acquisition of a last-generation spectrum analyzer and a probe station that will boost our measurement capabilities. Important part of this thesis work has been the installation of appropriate measuring and fabrication practices which are critical when working at the millimeter wave range.

As an outcome of this project a consortium was created by the institutions interested on Band 1 for ALMA, the Academia Sinica Institute of Astronomy and Astrophysics (ASIAA) in Taiwan, the Hertzberg Institute for Astrophysics in Canada, the National Radio Astronomy Observatory (NRAO) in USA and the University of Chile. In 2011 a joint study was submitted for Band-1 production and a cooperative work has started in order to produce 70 receivers between 2014 and 2018. In this final Band 1 design it was considered, as a suggestion from the scientific community, to shift the frequency range from the original 31–45 GHz to 35–50 GHz. This change has been implemented in order to take advantage of the high quality site compared with other Q-Band facilities as the Extended Very Large Array (EVLA). Our work is now focused on redesigning and optimizing the previously designed components to work on this new frequency range and in improving its manufacturability to lower the production costs of the final 66 Band-1 receivers.

Appendix A

Acronism index

ALMA	Atacama Large Millimeter Array
CBI	Cosmic Background Imager
CMB	Cosmic Microwave Background
CNC	Computer Numerically Controlled
DC	Direct Current
DUT	Device Under Test
EVLA	Extended Very Large Array
ETH	Swiss Federal Institute of Technology Zurich
FET	Field Effect Transistor
GPIB	General Purpose Interface Bus
IAF	Fraunhofer Institute
HDPE	High Density Poli-Ethilene
HEMT	High Electron Mobility Transistor
HFSS	High Frequency Structural Simulator
HRL	Hughes Research Laboratory
IF	Intermediate Frequency
LNA	Low Noise Amplifier
LSB	Lower Side Band
LO	Local Oscillator
MBE	Molecular Beam Epitaxy
MIC	Microwave Integrated Circuit
MMIC	Monolithic Microwave Integrated Circuit
MOCVD	Metal Organic Vapor Deposition
m-HEMT	metamorphic High Electron Mobility Transistor
NGC	Northrop Grumman Corporation
NAOJ	National Astronomy Observatory of Japan
NRAO	National Radio Astronomical Observatory
OMT	OrthoMode Transducer
p-HEMT	pseudomorphic High Electron Mobility Transistor
PTFE	Poli Tetra Fluor Etileno (Teflon)
PWV	Precipitable Water Vapor

QUIET	Q/U Imaging Experiment
RBW	Resolution Bandwidth
RF	Radio-Frequency
SSB	Single Side Band
SZ	Sunyaev Zel'dovich
UMS	United Monolithic Semiconductor
USB	Upper Side Band
VLBI	Very Long Base Line Interferometry
VNA	Vector Network Analyzer
YIG	Yttrium iron garnet

Appendix B

List of publications

Articles

1. Nicolas Reyes, Pablo Zorzi, Jose Pizarro, Ricardo Finger, F. Patricio Mena and Leonardo Bronfman, “A Dual Ridge Broadband Orthomode Transducer for the 7-mm Band”, Journal of Infrared Millimeter wave and terahertz waves, 2012, DOI:10.1007/s10762-012-9942-6.
2. P. Zorzi, C. Granet, F. Colleoni, N. Reyes, J. Pizarro, P. Mena, L. Bronfman, “Construction and measurement of a 31.3-45 GHz Optimized Spline-profile horn with corrugations”, Journal of Infrared Millimeter wave and terahertz waves, October 2011.

Conferences

1. N. Reyes, P. Zorzi, C. Jarufe, F. Navarrete, F. Colleoni, J. Pizarro, F.P. Mena and L. Bronfman, “ALMA band 1 development at Universidad de Chile”, in Millimeter and Submillimeter Detectors and Instrumentation for Astronomy V, edited by Wayne S. Holland; Jonas Zmuidzinas, Amsterdam, July 2012.
2. R. Rodriguez, R. Finger, P. Vasquez, R. Bustos, N. Reyes, P. Zorzi, L. Bronfman, F. P. Mena, “New capabilities for the Southern 1.2-m mm-Wave Telescope” in Millimeter and Submillimeter Detectors and Instrumentation for Astronomy V, edited by Wayne S. Holland; Jonas Zmuidzinas, Amsterdam, July 2012.
3. N. Reyes, P. Zorzi, C. Jarufe, P. Altamirano, F. P. Mena, J. Pizarro, L. Bronfman, J. May, C. Granet, and E. Michael. “Construction of a Heterodyne Receiver for Band 1 of ALMA”. Proceedings of the 21th International Symposium on Space Terahertz Technology, Oxford, March 23-25, 2010.
4. N. Reyes; C. Jarufe; F. P. Mena; J. Pizarro; L. Bronfman; J. May, “Amplification system of ALMA Band 1”, in Millimeter and Submillimeter Detectors and Instrumentation for Astronomy V, edited by Wayne S. Holland; Jonas Zmuidzinas, USA, July 2010.

5. N. Reyes, P. Zorzi, F. P. Mena, C. Granet, E. Michael, L. Bronfman, and J. May, “Design of a Heterodyne Receiver for Band 1 of ALMA”, Proceedings of the 20th International Symposium on Space Terahertz Technology, Charlottesville, USA, April 20-22, 2009.

A Dual Ridge Broadband Orthomode Transducer for the 7-mm Band

Nicolas Reyes · Pablo Zorzi · Jose Pizarro ·
Ricardo Finger · F. Patricio Mena · Leonardo Bronfman

Received: 24 July 2012 / Accepted: 8 October 2012
© Springer Science+Business Media New York 2012

Abstract In this work we present a Q-band waveguide orthomode transducer (OMT) based on a dual ridge structure. It was designed to be used in astronomical projects where an excellent broad-band performance is mandatory. Of particular interest is the case of ALMA Band 1 (originally set at 31–45 GHz) project which will need several OMTs with outstanding performance and demonstrated manufacturability. By using a symmetrical structure, low cross-polar level and good input matching are achieved over a broad bandwidth (37 %). The proposed design incorporates an octagonal mode converter which allows the unit to be directly mated with the horn avoiding cross-polar issues at the interface. The OMT was designed to have a compact configuration and easiness of fabrication, both crucial features in projects where several units (up to 70) have to be constructed.

Keywords Orthomode transducer · Waveguide components · Dual ridge structure · Q-band components

1 Introduction

The Atacama Large Millimeter Array (ALMA) is the largest array of radio-astronomical antennas ever devised. Each antenna will cover the spectroscopic window from 30 to 950 GHz with ten different receivers. The lowest-frequency band (so-called Band 1), which will cover the 7-mm range, was not implemented during the first construction phase of the telescope, but will be included during a second upgrading phase. Band 1 will allow the study of several important radio-astronomical phenomena, like molecular gas in high red-shift galaxies, high resolution CMB, dust in proto-planetary disks, and conventional observations of southern hemisphere targets [1].

The specifications set by ALMA for its receivers are stringent. All the receivers should work on a dual-polarization configuration with a cross-polar isolation lower than -25 dB. Moreover, the frequency coverage of every band is rather large. In the particular case of

N. Reyes (✉) · P. Zorzi · R. Finger · F. P. Mena
Department of Electrical Engineering, Universidad de Chile, Av. Tupper 2007, Santiago, Chile
e-mail: nireyes@u.uchile.cl

N. Reyes · J. Pizarro · R. Finger · L. Bronfman
Astronomy Department, Universidad de Chile, Camino el Observatorio 1515, Las Condes, Chile

Band 1 the proposed frequency range is 31 to 45 GHz, giving a fractional bandwidth of 37 %. Given these specifications we have selected as polarization splitter a waveguide orthomode transducer (OMT). For an adequate interface of the OMT with other Band-1 receiver components we have set some additional specifications. We aimed to obtain reflection losses below -20 dB and isolation between the two polarization channels better than -50 dB.

There are several designs for an OMT. The most common ones for broadband operation are the Boiffot [2], the turnstile [3, 4] and the dual ridge OMTs [5]. The main advantage of the latter over other designs is its simple fabrication process using conventional CNC milling machines, without the need of high-precision alignments, or the need for high precision pins and septum. Specifically, we have decided to implement a double ridged structure, similar to the design for Bands 4 and 8 of ALMA [6, 7]. We improved the original design by, first, incorporating a built-in compact circular to square waveguide adapter at the input port and by, second, redesigning and optimizing the complete structure with special emphasis on the dual ridge structure which dominates the cross-polar level and reflection losses of the device. We have found that a critical dimension to improve the cross-polar level was the distance between the dual ridge and the octagonal mode converter. The radius of curvature of the two arms was also optimized in order to get best results in the lower part of the band. In this way we have achieved the desired broad-band performance and diminished the previously published cross-polar levels [6].

2 OMT Design

Figure 1 shows the overall layout of the designed dual ridge OMT. The input port of the device is an octagonal mode converter, which converts the input from a circular to a square waveguide supporting the two orthogonal polarization modes. These orthogonal modes are separated in the dual ridge structure, which is the core component of the device. One polarization mode is bent by an E-Bend structure, while the other is recombined by the Y-Junction. Finally the outputs of the OMT are two standard WR-22 waveguide ports, named

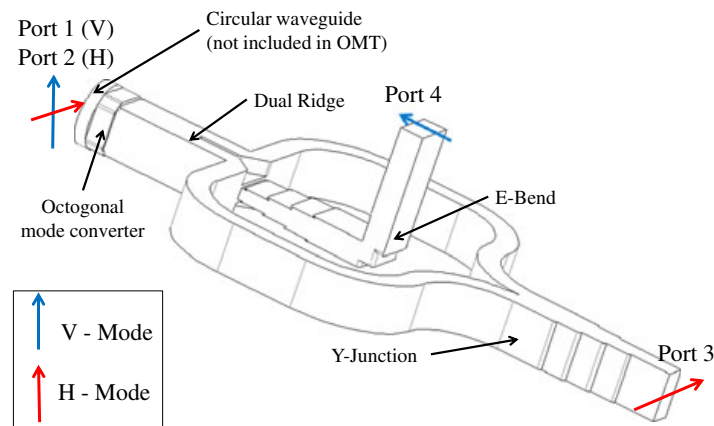


Fig. 1 Model of the dual ridge OMT. The input port is the octagonal converter which allows the OMT to be directly connected to the circular waveguide coming from the horn. The circular waveguide supports two orthogonal modes (H and V). These modes are converted in square waveguide modes and then separated by the dual ridge structure. H modes are recombined by a Y junction and output at port 3. Mode V continues in the same direction and output through port 4.

ports 3 and 4, respectively, one for each orthogonal polarization. In the following section the design and performance of each part is reviewed.

2.1 Octagonal Mode Converter

To facilitate the assembly of the receiver, where the device will be used, the OMT was designed to be directly connected to a conical corrugated horn with circular waveguide input (Fig. 2). A solution for the Band 1 horn was previously published in [8]. In order to avoid excitation of higher order modes, which will cause an increment in the cross-polarization value, it is important to assure that the transition keeps the symmetry of the structure. We decided to use an octagonal mode converter, designed to be mated to a circular waveguide with a radius of 3.81 mm. This dimension allows the two orthogonal TE₁₁ fundamental modes (labeled as H and V modes in Fig. 1) to propagate between 30 and 50 GHz. The TE₁₁ modes present in the circular waveguide are converted, by the octagonal mode converter, into orthogonal TE₁₀ and TE₀₁ modes propagating in the inner square waveguide. The design of the mode converter follows reference [9] and the ALMA Band-5 solution for the OMT-to-horn transition [10]. The advantage of using octagonal transitions is that it increases the size of the OMT by only few millimeters, without paying any cost in terms of performance when comparing to traditional square to circular converters [11]. To assure the correct alignment of the mode converter with the rest of the OMT, it was built in the same block, avoiding alignment issues during the assembly of the device.

2.2 Dual Ridge

The two orthogonal TE modes present in the square waveguide are separated by the dual ridge structure, depicted in Fig. 3. The purpose of this structure is to concentrate the V mode into the narrow space between the two ridges and the H mode into the two waveguide structures separated by the central ridge. The V mode continues straight into a reduced height rectangular waveguide, which is in cut-off mode for the H mode. Meanwhile, the H mode waveguides are bent and output through two lateral ports with a 180 degree difference

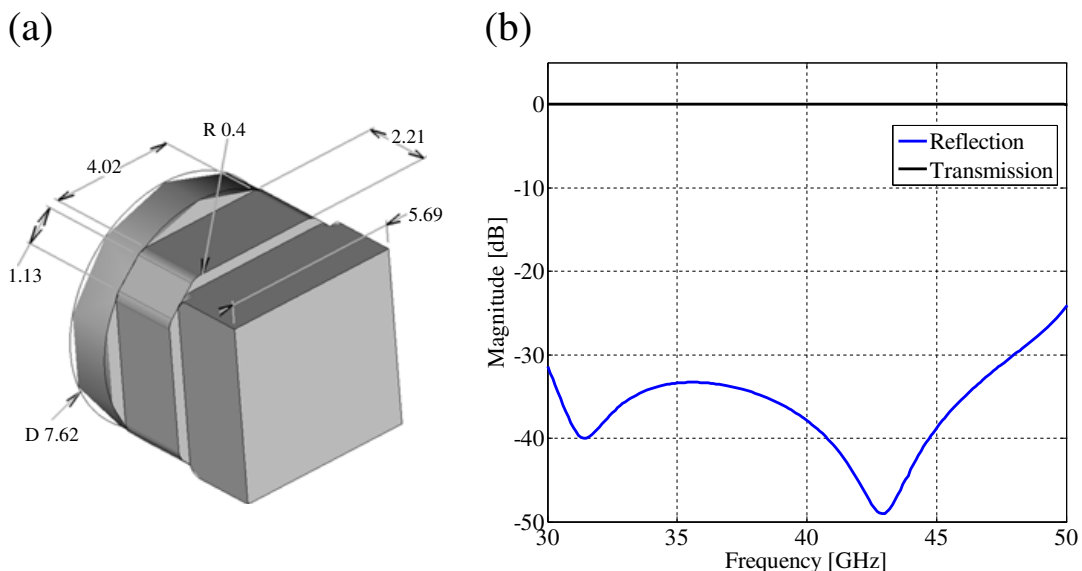


Fig. 2 (a) Structure and (b) simulated results of the octagonal mode converter.

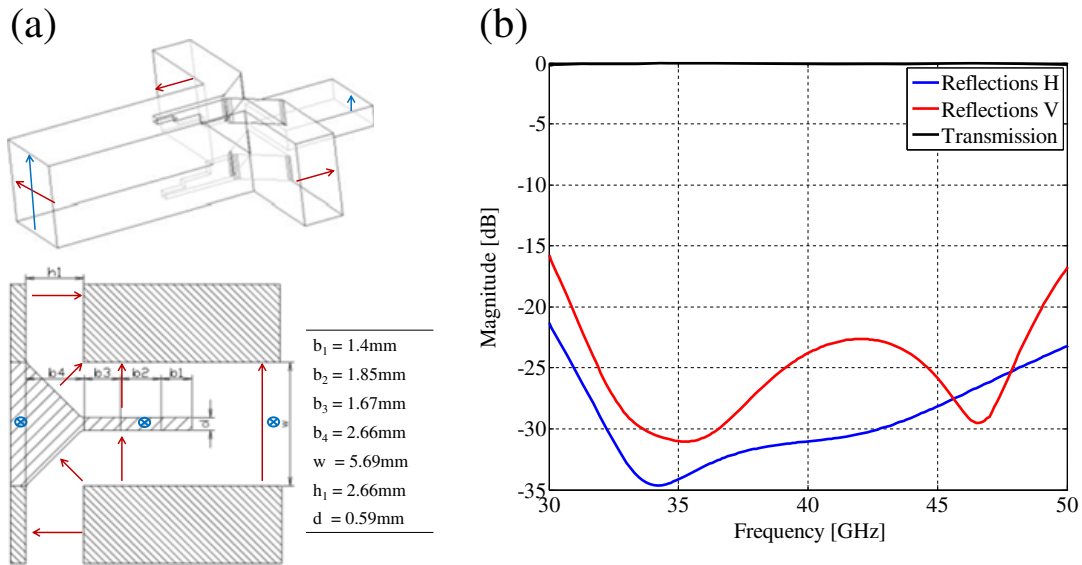


Fig. 3 Dual ridge structure. (a) Isometric and top view of the dual ridge structure showing how the H mode (red arrows) is bent into two symmetrical outputs while the V mode (blue arrows) continues straight to the single output. (b) Simulated results for the dual ridge structure.

of phase. The symmetry of the complete structure is fundamental as it prevents higher order modes, specially the TE₁₁, to appear in the square waveguide causing cross-polar talk.

One of the advantages of the dual-ridge structure is its inherent broad-band behavior, allowing the OMT to achieve the specified bandwidth. This structure is the core component of the OMT and the most critical part for broad-band operation. It was carefully designed and optimized to reduce the return losses from this structure below -25 dB all over the frequency range. We have decided to use three steps for the dual ridge as it proves to be enough to cover the specified bandwidth. The final dimensions of the proposed structure are listed in Fig. 2 which also shows the simulated reflection losses of the structure.

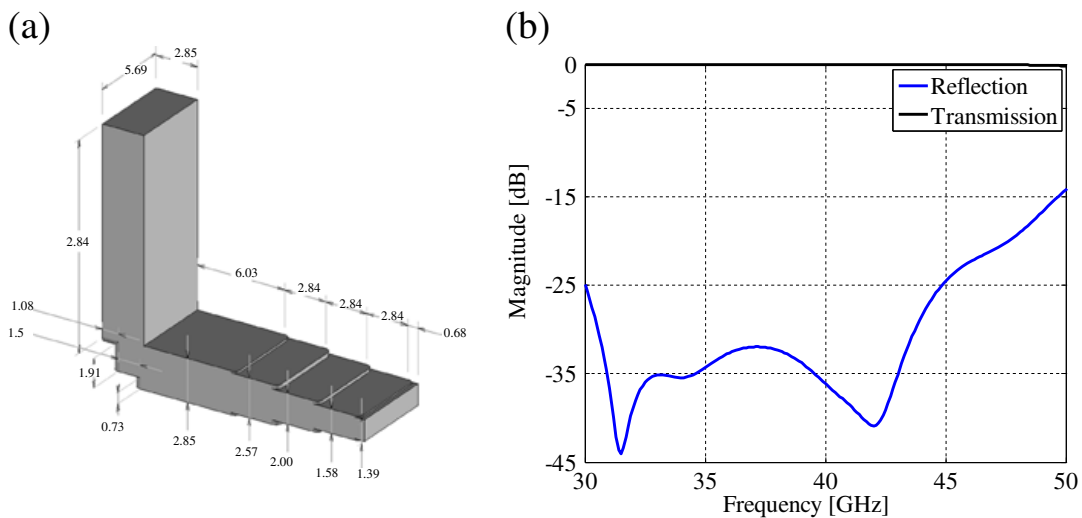


Fig. 4 The E-Bend drives the H signal to the output located in the top part of the OMT. (a) 3-D view of the E-bend. (b) Return losses and transmission of the structure.

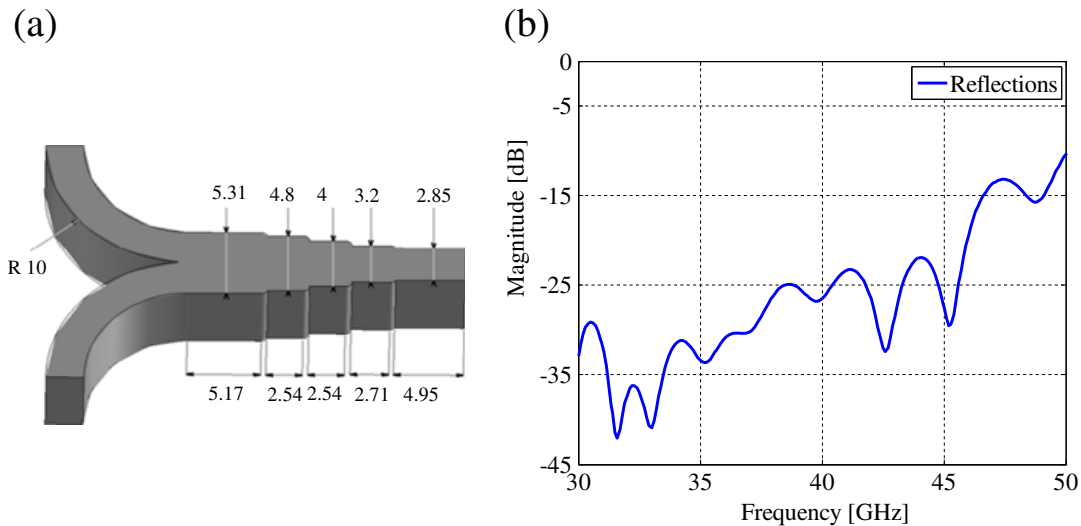


Fig. 5 The Y junction has to recombine the two H signal coming from the dual ridge. (a) 3D view and its most important dimensions. (b) Simulated return losses of the structure.

2.3 E-Bend and Y- Junction

After the dual ridge the V-mode is bent by an E-bend structure and output through port 4. The design and simulated results of this structure are presented on Fig. 4. The reflection losses introduced by this structure are negligible, being below -30 dB all over the band of interest. Meanwhile, the two H-modes signals have to be recombined in a Y-junction whose dimensions and simulated results are presented in Fig. 5. Both structures, the E-bend and the Y-junction, were designed following [12] and were optimized to cover the specified frequency range.

Each one of the parts (circular to square transition, dual ridge guide, E-bend and Y-junction) were designed and optimized separately in a 3D electromagnetic simulator (High Frequency Structure Simulator from ANSYS). Afterwards, a second iteration was necessary to optimize the performance of the OMT working as a whole. Special emphasis was exercised during this final optimization process to avoid resonant behaviors in the cross-polar and isolation features. The final simulation results, presented in the following section, account for the losses on the waveguide walls and for the machining effects, as the fillets in the corners and the surface roughness.

Fig. 6 The OMT was build using split-block technique. At the left side an assembled OMT is shown, where the input octagonal port can be observed. At the right side the three blocks that compose the OMT are shown. The overall block dimensions are $72 \times 30 \times 50 \text{ mm}^3$.

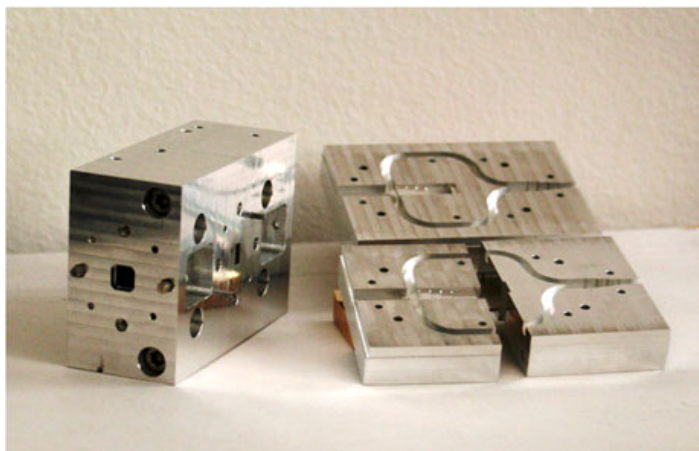
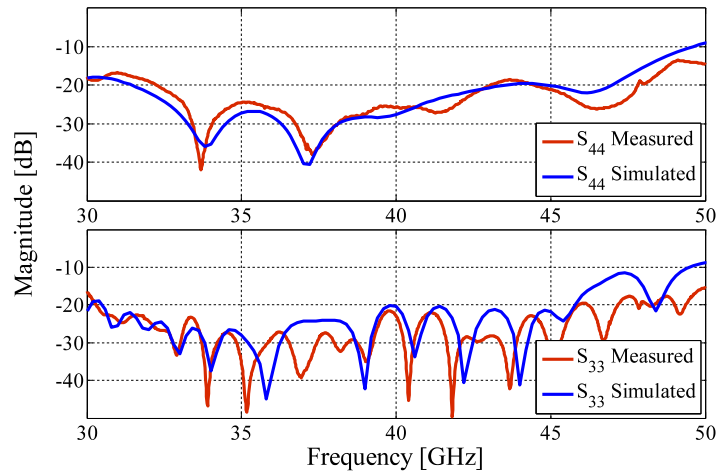


Fig. 7 Measured and simulated reflection losses for the dual ridge OMT. The agreement between them is excellent. Reflection losses are below -20 dB all over the band of design (31–45 GHz).



3 Construction and Measurements

The OMT was built using a high precision CNC milling machine. We have used Aluminum 2017 to produce the units as it is inexpensive, light, resistant to corrosion, and has excellent electrical conductivity. The OMT was constructed in three blocks that are tightened by screws and aligned using stainless-steel alignment pins. The octagonal mode converter is built in the same block, avoiding further alignment issues. The fabricated OMT and its three constitutive parts are shown in Fig. 6. We have fabricated three units of the OMT with only few mechanical differences between them. The repeatability was excellent for all the units proving that the fabrication process of this OMT is not only easier than other reported devices but is also reproducible.

The devices were characterized using a Vector Network Analyzer model E8364C from Agilent. A circular load was designed and built to terminate the input port while measuring the reflection losses at ports 3 and 4. Transmission and cross-polar levels were measured using a rectangular to circular adapters which were designed using octagonal transitions. The adapters were characterized to discount their effect on the OMT insertion loss measurements. Isolation was directly measured between ports 3 and 4 of the device while the circular input port was loaded.

Fig. 8 Measured and simulated insertion losses for the dual ridge OMT. We have assumed a conductivity of 3.5×10^7 [S.m⁻¹] and a surface roughness of $2 \mu\text{m}$ for the aluminum walls of the OMT model.

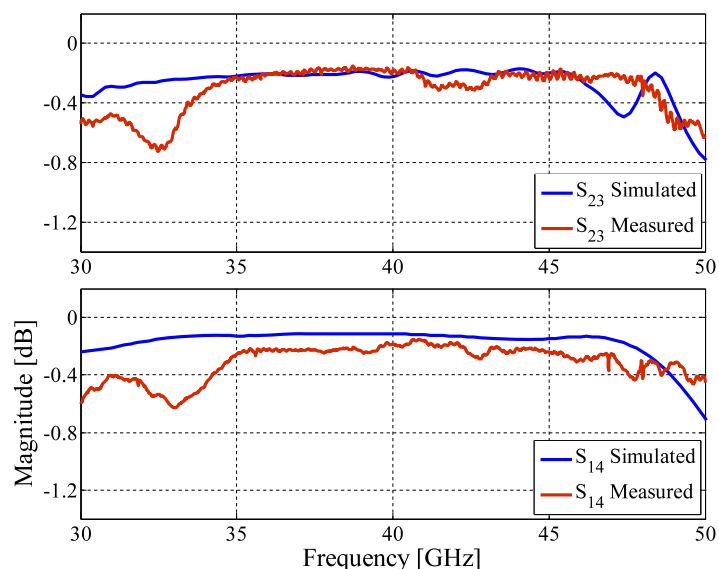
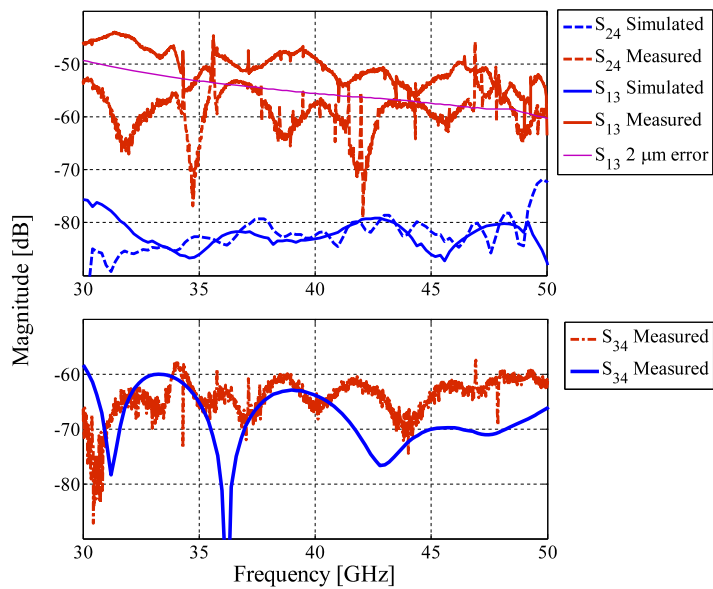


Fig. 9 Measured and simulated isolation (*bottom*) and cross-polar (*top*) for the dual ridge OMT. The cross-polar levels are well below -30 dB, which is according to specification. The difference between simulation and measurements in the cross-polar level is due to instrumental effects and to misalignments between the blocks that constitute the OMT. The isolation, in contrast, is similar to the simulated value of around -60 dB as it does not use any transitions when measuring.



Figures 7, 8 and 9 summarize the simulations and experimental results. Except for cross-polar measurements, all set of results show an excellent agreement with the simulation, demonstrating the good quality of the fabricated OMT. The differences found in the cross-polar measurements can be explained by the cross-polar contribution of the adapters used to characterize the device and by a slight misalignment between the blocks that make the OMT. In fact, the measurements are consistent with simulations that incorporate a misalignment of $2\text{--}4\ \mu\text{m}$. It is important to notice that the misalignment does not affect any other of the S-parameters. Indeed, it only affects the cross-polar levels because it breaks the inherent symmetry of the OMT. Simulations also indicate that misalignment errors of up to $20\ \mu\text{m}$ keep the overall cross-polar lower than -30 dB allowing this OMT to be scaled to higher frequencies keeping under control the alignment errors between blocks.

In the operation range of 31 to 45 GHz we can summarize the results as follows:

- (i) A return loss lower than -20 dB both at the H and V port (Fig. 7),
- (ii) A transmission of about -0.4 dB (Fig. 8), and
- (iii) Cross-polar and isolation of -50 dB and -60 dB respectively (Fig. 9).

It has to be noticed that the new design of the dual ridge OMT allows us to reduce the cross-polar levels previously published by [6] to -50 dB from the original -30 dB. This fact proves that this kind of devices can achieve a cross-polar as low as other reported waveguide OMTs [3, 4]. The new design also provides a compact and effective solution to interface the square waveguide inherent to the double ridge structure to the standard circular input needed to connect the horn.

Despite being optimized to work between 31 to 45 GHz, the OMT shows a good performance (return losses lower than -17 dB) between 30 to 48 GHz. With such performance this device is a good option for receivers covering the complete Q waveguide band (33–50 GHz).

4 Conclusions

A dual ridge OMT was designed to cover the ALMA Band-1 frequency range. The device was prototyped and tested showing an excellent RF performance all over the rather broad band of interest (37%). Within this band the OMT reaches -20 and -45 dB of reflection and

cross-polar level, respectively. In this way it improves previous results using the same technology and demonstrate that can achieve similar performance as other more popular waveguide OMTs but more difficult to be implemented. Moreover, the design shows good results out of the band of design, showing potential operation in a wider bandwidth. This is of particular interest for instruments that aim to cover the complete Q-band. Finally, the repeatability of the design is also outstanding, allowing the OMT to be used in projects, as it is the case of ALMA or future arrays of detectors, where a batch production of OMTs is needed.

Acknowledgments We remember J. May (R.I.P) for his unconditional support to this project. This work was funded by the Chilean Center of Excellence in Astrophysics and Associated Technologies (PBF 06), and by the ALMA-CONICYT Fund for the Development of Chilean Astronomy (Projects 31080003 and 31080004).

References

1. D. Johnstone, J. Di Francesco, B. Matthews, N. Bartel, S. Casassus, S. Chitsazzadeh, G. Duchene, A. Hales, M. Houde, P. M. Koch, R. Kothes, S-P. Lai, T. Maccarone, G. Moriarty-Schieven, A. M. M. Scaife, D. Scott, H. Shang, S. Takakuwa, J. Wagg, A. Wootten, “The Science Case for Building a Band1 Receiver for ALMA”, arXiv:0910.1609v2 [astro- ph.IM], (Submitted on 8 Oct 2009(v1)).
2. AM Boifot, E Lier, T Schaug-Pettersen (1990) “Simple and broadband orthomode transducer”. *Proc Inst. Elect Eng* 137(6):396-400
3. A. Navarrini and R. L. Plambeck, “A turnstile junction waveguide orthomode transducer”, *IEEETrans. Microw. Theory Tech.*, vol. MTT-54, no. 1, pp. 272- 277, Jan. 2006.
4. G Pisano, L Pietranera, K Isaak, L Piccirillo, B Johnson, B Maffei, S Melhuish (2007) “A broadband WR10 turnstile junction orthomode transducer”. *IEEE microwave and wireless components letters* 17(4), 286-288
5. A. Dunning, “Double Ridged Orthogonal Mode Transducer for the16-26 GHz Microwave Band”, *Proc. of the Workshop on the Applications of Radio Science*, February 20-22, 2002.
6. S. Asayama, M. Kamikura, “Development of Double-Ridged Waveguide Orthomode Transducer for the 2MMBand”, *Journal of Infrared and Millimeter Waves*, Volume 30, Issue 6, pp 573–579, 2009.
7. M. Kamikura, M. Naruse, S. Asayama, N. Satou, W. Shan, Y. Sekimoto, “Development of a Sub-millimeter Double-Ridged Waveguide Ortho-Mode Transducer (OMT)”, *Journal of Infrared Millimeter and Terahertz Waves*, Volume 31, Issue 6, pp 697-707, 2010.
8. P. Zorzi, C. Granet, F. Colleoni, N. Reyes, J. Pizarro, P. Mena, L. Bronfman, “Construction and measurement of a 31.3-45 GHz Optimized Spline- profile horn with corrugations”, *Journal of Infrared Millimeter and Terahertz waves*. Volume 33, Issue 1, pp 17-24, 2012.
9. A. Mediavilla, J.L. Cano, K. Cepero, “On the octave bandwidth properties of octagonal shaped waveguide mode transformer”, *IEEE Transactions on Microwave Theory and Techniques*, Vol 59, No. 10, pp 2447-2451, October 2011.
10. Asayama S., Private communication, May 2010.
11. P. Fuerholz and A. Murk, “Design of broadband transition using the constant impedance structure approach,” *Progr. Electromagn. Res. Lett.*, vol. 7, pp. 69–78, 2009.
12. A. R. Kerr, “Elements for E-plane split-blocks waveguide circuits”, *Nat. Radio Astronomy Observatory, ALMA Memo 381*, Jul. 2001. [Online]. Available: <http://www.alma.nrao.edu/memos>

Construction and Measurement of a 31.3–45 GHz Optimized Spline-profile Horn with Corrugations

**Pablo Zorzi · Christophe Granet ·
Franco Colleoni · Nicolas Reyes · Jose Pizarro ·
Fausto-Patricio Mena · Leonardo Bronfman**

Received: 28 July 2011 / Accepted: 13 September 2011
© Springer Science+Business Media, LLC 2011

Abstract A corrugated spline-profile horn has been designed to meet the stringent specifications and constraints of a receiver for Band 1 (31.3–45 GHz) of the Atacama Large Millimeter Array (ALMA). Given the physical restrictions of the receiver, the horn will be located behind a focusing lens placed 191 mm over its aperture. After this first focusing stage, the horn must have a reflection coefficient less than -20 dB and the cross-polarization not exceeding the -30 dB level in the entire frequency range. The side-lobes should be less than -25 dB at all frequencies and its half power beamwidth must be approximately 24° at 31.3 GHz and 16° at 45 GHz. The horn has been constructed using the split-block technique and characterized in a near-field scanner setup. The results show an excellent performance complying with all the requirements.

Keywords Spline-profile · Corrugated horn · Radiation pattern · Cross-polarization · Phase center · Quasi optics · Radio receiver

P. Zorzi (✉) · F. Colleoni · N. Reyes · F. P. Mena
Department of Electrical Engineering, Universidad de Chile,
Av. Tupper 2007, Santiago, Chile
e-mail: pzorzi@ing.uchile.cl

C. Granet
BAE Systems Australia Pty Ltd, 40-52 Talavera Road, North Ryde, 2113 NSW, Australia

J. Pizarro · L. Bronfman
Astronomy Department, Universidad de Chile, Camino el Observatorio,
1515, Las Condes, Chile

1 Introduction

The Atacama Large Millimeter Array (ALMA) is the largest millimeter and sub-millimeter astronomical array ever built. It is under construction in the altiplano region of northern Chile. This is an extremely dry plateau at an altitude of 5,000 m, making it one of the best sites on earth for radio astronomy. ALMA combines an array of 66 antennas (54×12 m and 12×7 m diameter antennas) designed to perform interferometry and spectroscopic measurements of the early Universe with an angular resolution accuracy of $1''$ [1]. It will also reveal new information about the birth of stars and planets and the formation of galaxies. In general, ALMA will provide high sensitive and precision imaging between 30 and 950 GHz in 10 bands of the Southern Hemisphere sky (<http://almascience.eso.org/alma-science>). This telescope will be already functional in 2011 although with only 16 antennas and 4 bands implemented.

The aim of this paper is to present the details of the design, construction and testing of a 31.3 45 GHz spline-profile corrugated horn that will be used in an ALMA Band-1 receiver. The horn is used to feed a high-density polyethylene (HDPE) bi-hyperbolic lens 194 mm in diameter and located at 191 mm from the aperture of the horn. Furthermore, the outgoing radiation from the lens will subsequently illuminate a 750 mm diameter subreflector, located 5.79 m from it, with a uniform Gaussian beam efficiency of -12.3 dB at all frequencies.

2 Design

In order to achieve the stringent specifications imposed over the horn, in particular its large coverage bandwidth, two different profiles were studied using mode-matching techniques and the optimization procedure defined step by step in [2] and [3]. The first was based on a smooth-walled profile while the

Fig. 1 Profile of the spline-profile corrugated horn. The dimensions are given in Table 1.

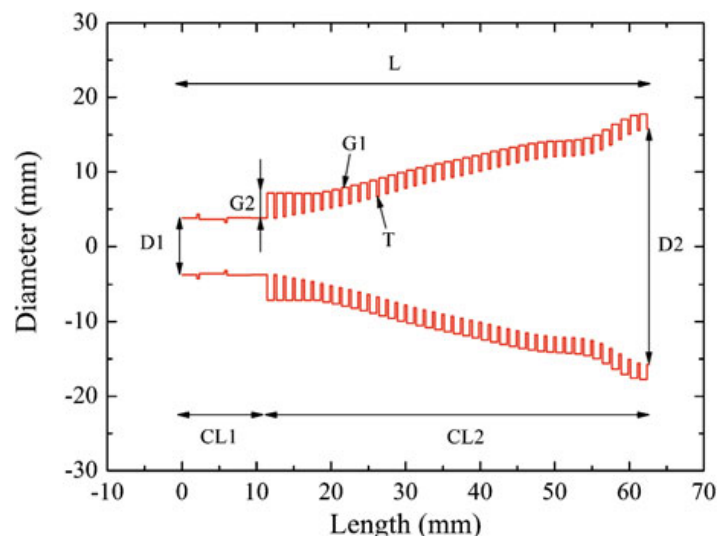


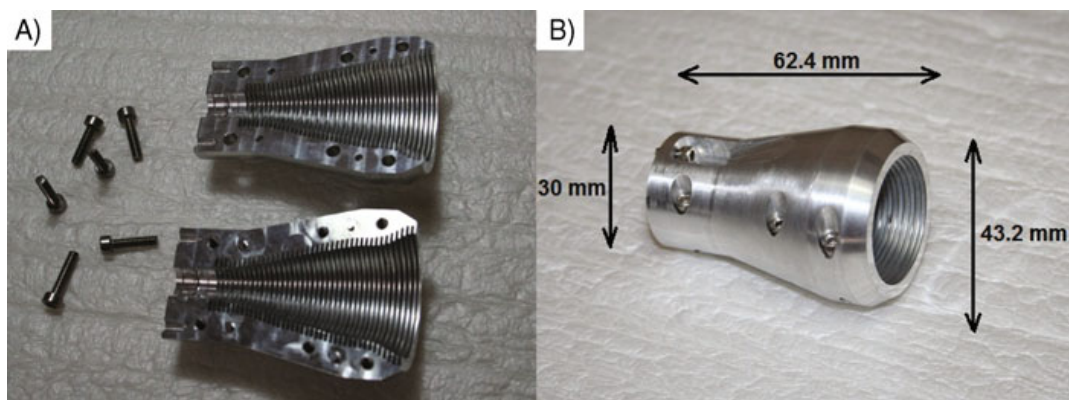
Table 1 Dimensions of the different sections of the corrugated horn.

Index	Section	Dimension (mm)
L	Horn total length	62.37
CL1	Circular waveguide length	11.42
CL2	Corrugated section length	51.25
D1	Input diameter	7.62
D2	Output diameter	31.50
T	Teeth width	0.94
G1	Grove width	0.31
G2	Grove depth	2.01–3.35

second model used was a corrugated spline-profile horn. As it was shown in [4], the spline-profile corrugated horn design was the best choice to construct since it met all the specifications in a much better way than the simple smooth-walled horn. As an additional advantage, the corrugated spline-profile horn resulted in a total length which is almost half of that of the conventional conical corrugated horn [5], making it easier to be implemented in the Band-1 receiver. This is particularly important in ALMA as the available space for implementing the receiver is limited [6]. After the design, all the results were corroborated using HFSS (<http://www.ansoft.com/products/hf/hfss>). The corrugation profile of the selected horn is shown in Fig. 1 and Table 1 summarizes its physical dimensions.

3 Construction

The spline-profile corrugated horn was constructed using the split-block technique. Both split sections were milled using a five-axis high-precision CNC milling machine (<http://www.kern-microtechnic.com>). The horn was milled in aluminum due to its good machinability and suitability for cryogenic applications. The corrugation profile at the split plane was checked with an optical microscope. No construction errors and misalignment of the corrugations were found. This sets the construction and alignment precision in less than 10 μ m.

**Fig. 2** Fabricated horn. **a** The two split-block halves. **b** Assembled horn and final dimensions.

Instead of using standard alignment pins, four pins were machined directly in one of the block surfaces minimizing in this way the alignment errors once the horn was assembled. The horn is presented in Fig. 2.

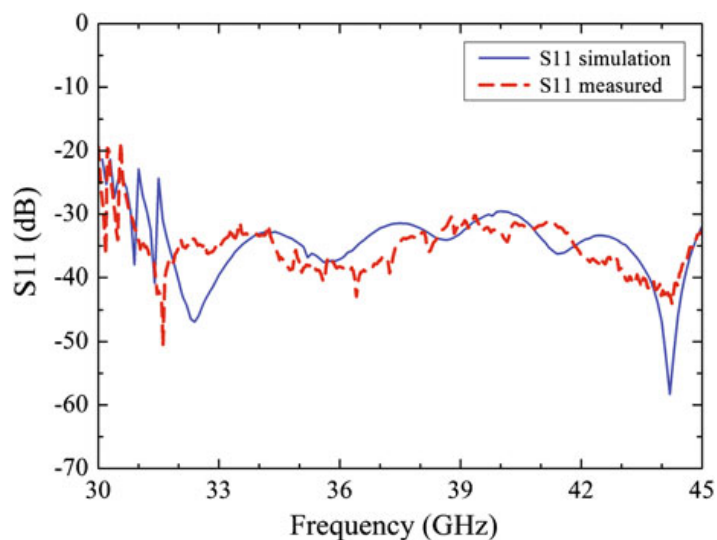
4 Measurements, results, and discussions

For the characterization of the horn, a vertical planar near-field beam-pattern measurement setup was designed and built [7, 8]. The near to far-field data transformation algorithm, which uses a Fast Fourier Transform (FFT) on the near-field measured data, and the probe amplitude pattern corrections were adapted from [9]. The resulting measured far-field data were consistent within a dynamical range of greater than 50 dB. For determining the phase center a phase model with amplitude weighting correction was used [10]. In this section we present the measured reflections at all frequencies, and the co-polar and cross-polar radiation pattern, phase and phase center location at 31.3, 38 and 45 GHz. All the measured data presented here includes the corresponding HFSS simulations for comparison purposes.

4.1 Reflection coefficient

Figure 3 presents the measured reflection losses at the input port of the horn. The measurements correspond to the real circular waveguide input. The contribution of the rectangular-to-circular waveguide transition was subtracted using a previous calibration step. The measurements show that the reflection losses are less than -20 dB for the complete band of interest in excellent agreement with the simulations.

Fig. 3 Measurements of the horn input reflections (red line) compared to the HFSS simulated expected S11 values (blue line).



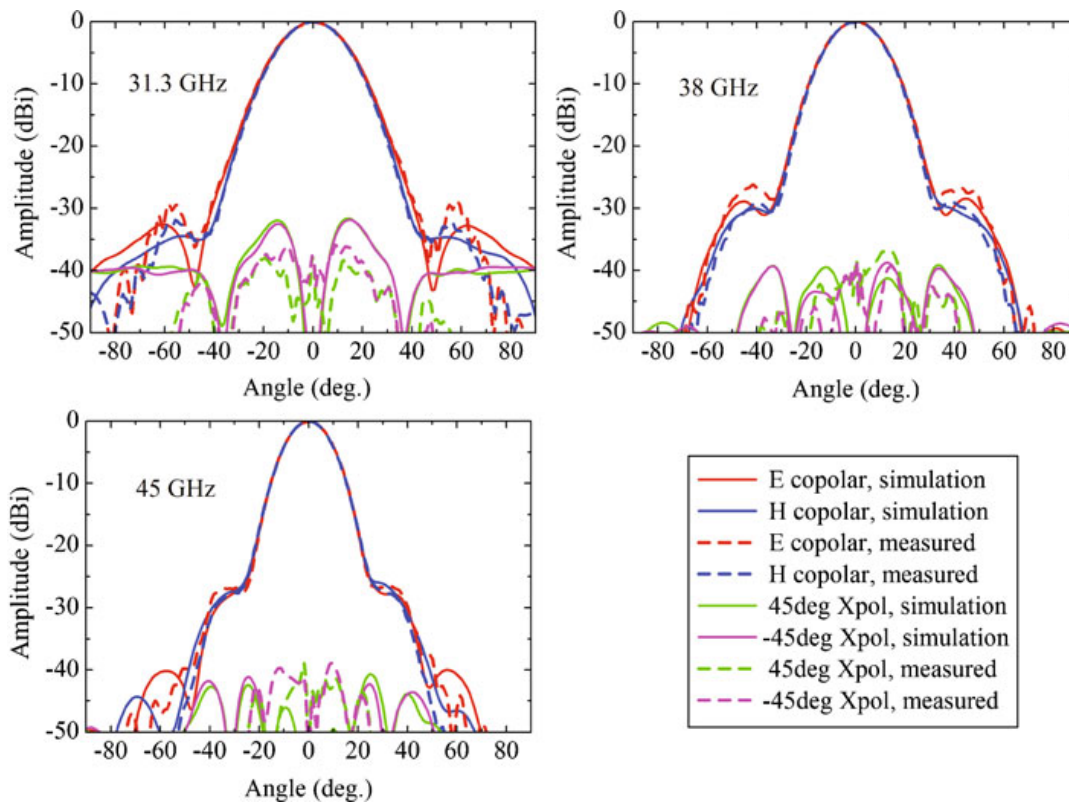


Fig. 4 Measured and simulated co-polar (E and H planes) and cross-polar (45 and -45 planes) radiation pattern comparison for 31.3, 38 and 45 GHz. *Dotted lines* correspond to the measurements results while the *straight lines* corresponds to the simulation results.

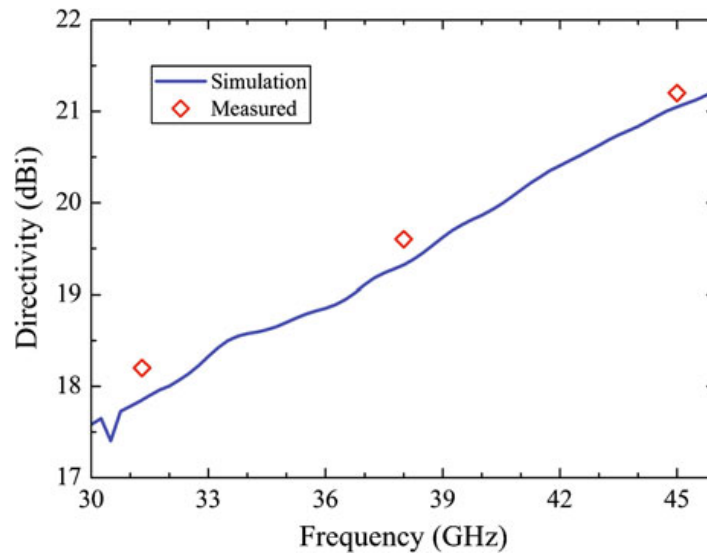
4.2 Co- and cross-polar patterns

The co-polar and cross-polar radiation patterns are shown in Fig. 4. The copolar measurements are identical to the simulated ones down to -25 dB at all frequencies. At lower amplitude values, especially around the first sidelobe levels, the measurements are always somewhat large with respect to the simulations. The difference in cross-polar amplitude between the simulations and measurements, especially at 38 and 45 GHz, are of about $+5$ dB. However, all the cross-polar and first sidelobe level measurements fulfill the horn-performance specifications.

4.3 Directivity and level of the first side-lobe

From the simulated and measured radiation patterns we have obtained the directivities and the levels of the first side-lobes. The results are summarized in Figs. 5 and 6. In both cases, the measured and simulated values show similar frequency dependence. In the case of the measured directivities, they are slightly overestimated in around 0.3 dB for each case. This is probably due to the uncertainty when predicting the total isotropic radiated power of our horn from the planar near-field measurement once the far-field transformation is

Fig. 5 Measured and predicted directivity of the constructed horn.

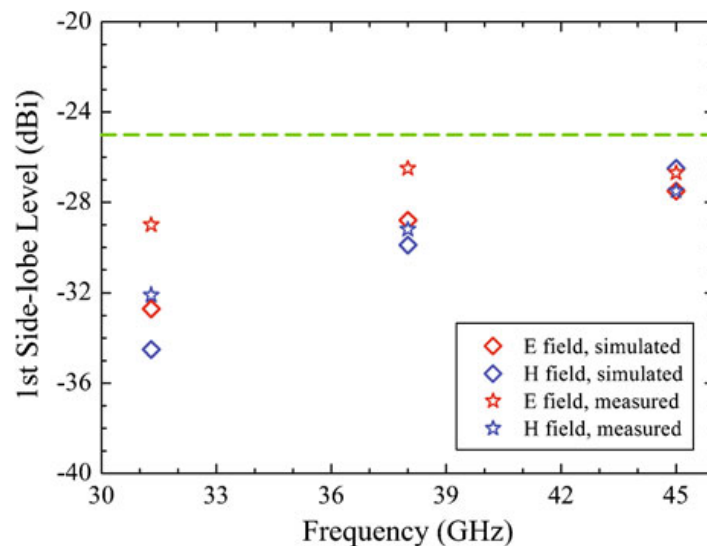


done using the FFT methods. Regarding the first side-lobe level, it is typically below -26 dB across the whole band, which implies that the specifications set for the horn are satisfied.

4.4 Phase plots and phase center location

The measured phase of the E and H fields and their corresponding simulated HFSS values at 31.3, 38 and 45 GHz are shown in Fig. 7. The measured results agree very well with the simulations since the phase diagrams are quite flat in the region where the amplitude radiation reaches its maximum. In Fig. 8 the phase center location (PCL) retrieved from the measured and simulated cases are presented. The measured PCLs coincide with the simulated cases

Fig. 6 Measured and simulated first side-lobe levels. The *green dotted line* denotes the maximal first side-lobe level specification of the horn.



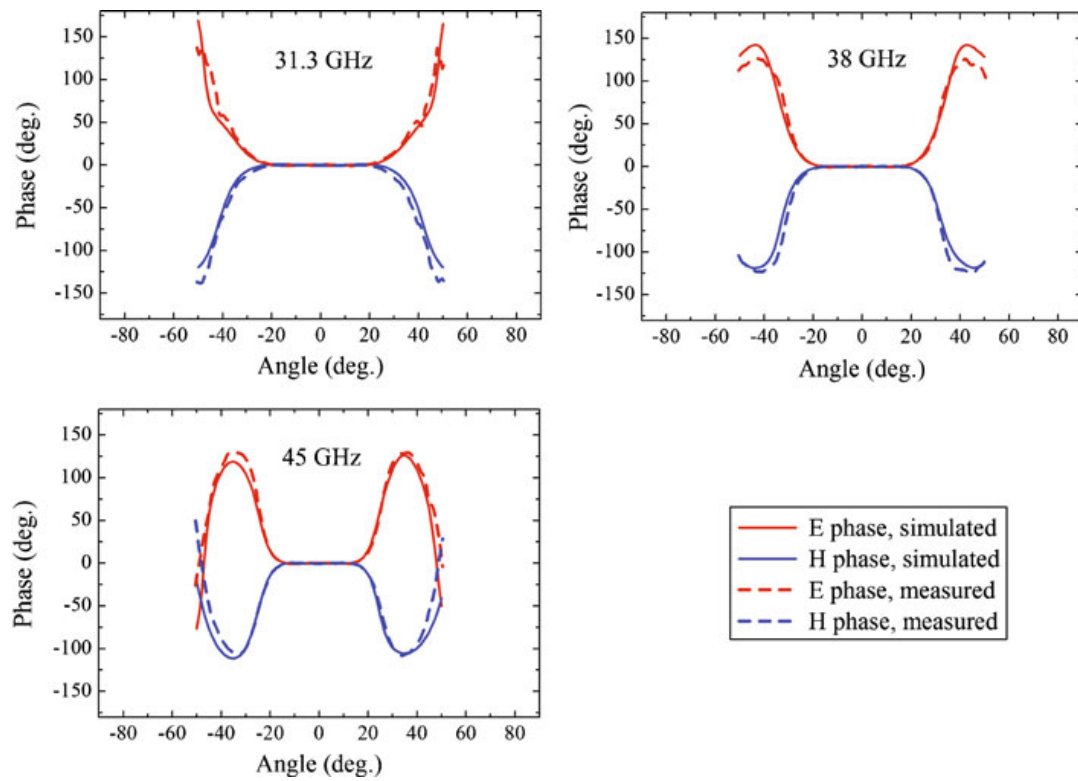
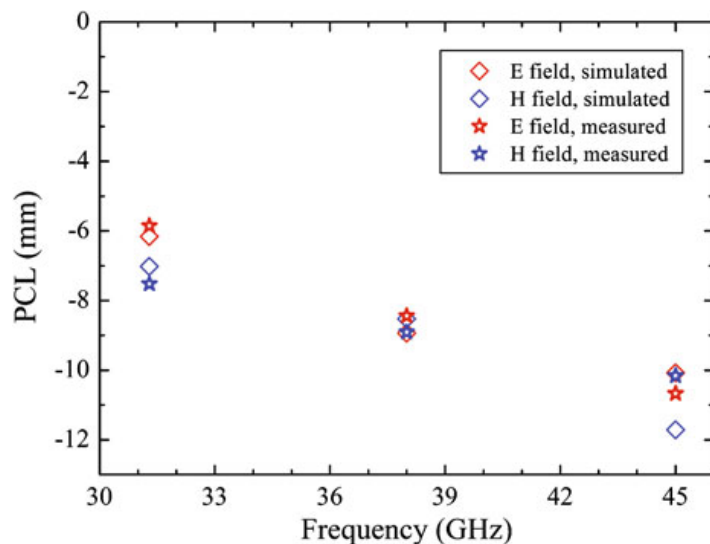


Fig. 7 Measured and simulated phase plots results for the E (red lines) and H planes (blue lines) at 31.3, 38 and 45 GHz.

within about 0.5 mm. The exception is the PCL of the H-field at 45 GHz, where the difference with its corresponding simulated value is of about 1.5 mm. This discrepancy may be attributed to small construction imperfections in the corrugation profile which is more sensitive at higher frequencies.

Fig. 8 Measured and simulated phase center locations for the E (red) and H fields (blue).



5 Conclusions

We have successfully constructed a spline-profile optimized corrugated horn using split-block techniques. The measurements of its return losses, directivity, first side-lobe levels, and its co- and cross-polar radiation pattern measurements agree very well with the HFSS simulation results and fulfill all the required specifications imposed by ALMA for its Band 1. The measured phase and phase-center location of the horn show similar deviations from the HFSS simulation. Furthermore, it was demonstrated that the construction discontinuities, due to the horn being split in two parts, were negligible and causes no detectable anomalies in the cross polar measured pattern. This construction technique is, therefore, suitable and could replace electroplating techniques. Another advantage of the horn design is that it has a similar or even better performance than a standard corrugated horn design but with almost half its size. This is an important mechanical achievement since the space in an ALMA receiver is limited.

Acknowledgements This work was supported by the Chilean Center of Excellence in Astrophysics and Associated Technologies (PBF 06), and by the ALMA-CONICYT Fund for the Development of Chilean Astronomy (Projects 31080003 and 31080004).

References

1. H. Rudolf, M. Carter, and A. Baryshev, "The ALMA Front End Optics-System Aspects and European Measurement Results," *IEEE Transactions on Antennas and Propagation*, Vol. 55, No. 11, November 2007.
2. C. Granet, G.L. James, R. Bolton, G. Moorey, "A smooth-walled spline-profile horn as an alternative to the corrugated horn for wide band millimeter-wave applications," *IEEE Transactions on Antennas and Propagation*, Vol. 52, No. 3, March 2004, pp. 848–854.
3. C. Granet, T.S. Bird, "Optimization of corrugated horn radiation patterns via a spline-profile," *ANTEM 2002, 9th International Symposium on Antenna Technology and Applied Electromagnetics*, Montreal, Canada, 2002, pp 307–310.
4. C. Granet, P. Mena, P. Zorzi, I.M. Davis, J.S. Kot, G. Pope, "Corrugated and Smooth-Walled Spline-Profile 31.3–45 GHz Horns for ALMA." *Proceedings of the 4th European Conference on Antennas and Propagation*, Barcelona, Spain, 12–16 April 2010.
5. C. Granet and G. L. James, "Design of corrugated horns: A primer," *IEEE Antennas & Propagation Magazine*, Vol. 47, No 2, April 2005, pp. 76–84. (Correction in *IEEE Antennas & Propagation Magazine*, Vol. 47, No 4, August 2005, p. 98).
6. ALMA Front-end Optics Design Report. Document: FEND-40.02.00.00-035-B-REP.
7. S. Gregson, J. McCormick and C. Parini, "Principles of Planar Near-Field Antenna Measurements." Institution of Engineering and Technology Press, 2007.
8. T. Brockett and Y. Rahmat-Samii, "A Novel Portable Bipolar Near-field Measurement System for Millimeter-wave Antennas: Construction, Development, and Verification," *IEEE Antennas and Propagation Magazine*, Vol. 50, No. 5. October 2008.
9. D. Janse van Rensbur, "Millimeter Wave Near-Field Antenna Testing." *Nearfield Systems Inc. Microwave Product Digest Article*, Aug 2010.
10. P.N. Betjes, "An algorithm for automated phase center determination and its implementation," *AMTA Conference*, 2007.

Bibliography

- [1] Baars J. editor, "ALMA project book", *Atacama Large Millimeter/Submillimeter Array*, Version 5.50, 2002. [Online]. Available: <http://www.alma.nrao.edu>. [Accessed: Oct 2008].
- [2] D. Johnstone et. al, "The science case for building a Band 1 receiver for ALMA", arXiv:0910.1609v2 [astro-ph.IM]
- [3] F.J. Lovas and R.A. Dragoset, "NIST Recommended Rest Frequencies for Observed Interstellar Molecular Microwave Transitions", *National Institute of Standards and Technology, Gaithersburg, MD.*, version 2.0.1, 2002 Revision. [Online]. Available: <http://physics.nist.gov/restfreq> [Accessed: Oct 2008].
- [4] W. D. Watson and H. W. Wyld, "The Relationship Between the Circular Polarization and the Magnetic Field for Astrophysical Masers with Weak Zeeman Splitting", *The Astrophysical Journal*, September 2001, Volume 558, Issue 1, pp. L55-L58.
- [5] Hideyuki Kobayashi et al. "The VERA project (VLBI Exploration of Radio Astrometry)", *Transits of Venus: New Views of the Solar System and Galaxy Proceedings IAU Colloquium No. 196*, 2004
- [6] Fabian Walter¹ et al., "Molecular gas in the host galaxy of a quasar at redshift $z = 6.42$ ", *Nature* 424, 406-408, 24 July 2003.
- [7] Douglas Scott, "ALMA and the Sunyaev-Zeldovich effect", Band 1 workshop presentation, Victoria, Canada October 2008.
- [8] K.Rohlfs and T.Wilson, "Tools for radio astronomy", Chapter 9.12, *A&A Library*, second edition 1990.
- [9] "EVLA project book". [pdf]. Available: <http://www.aoc.nrao.edu/evla/admin/projbook/chap5.pdf>. [Accessed: Nov 2008]
- [10] Tony Minter, "Observing with the Green Bank Telescope". [pdf]. Available: <http://www.gb.nrao.edu/gbtprops/obsman/GBTog.pdf>. [Accessed: Nov 2008]
- [11] S. Padin et al. "The Cosmic Background Imager Cosmic Background Imager", *Publications of the Astronomical Society of the Pacific*, Vol 114, 2002 January.
- [12] "QUIET", quiet.uchicago.edu/instrumentation/index.html, [Accessed: Sept 2008].
- [13] "Receivers for the Effelsberg 100-m Telescope". Available:

- <http://www.mpifr.de/div/effelsberg/receivers/receiver.html>. [Accessed: Nov 2008]
- [14] “Kashima 34m Antenna”, Available: www2.nict.go.jp/w/w114/stsi/34m/antenna-34m/index.html. [Accessed: Nov 2008].
- [15] “Information for MOPRA observers”, Available: <http://www.narrabri.atnf.csiro.au/mopra/obsinfo2.html>. [Accessed: Nov 2008].
- [16] “ATCA@7mm System Performance”, Available: <http://www.atnf.csiro.au/observers/docs/7mm/systemp.html> [Accessed: Nov 2008].
- [17] “Description of the Onsala 20 m telescope”. Available: <http://www.chalmers.se/rss/oso-en/observations/20-m-telescope/>, [Accessed: Nov 2008]
- [18] Larry D’Addario and Mark Holdaway, “Joint Distribution of Atmospheric Transparency and Phase Fluctuations at Chatnantor”, ALMA MEMO 521, November 2003
- [19] Otarola A. et al., “Atmospheric transparency at Chajnantor: 1973-2003” ALMA Memo 512, January 2005.
- [20] “Atacama Path-Finder Experiment”, Available: <http://www.apex-telescope.org/>, [Accessed: Oct 2008].
- [21] Juan R. Pardo, José Cernicharo, and Eugene Serabyn, “Atmospheric Transmission at Microwaves (ATM): An Improved Model for Millimeter/Submillimeter Applications”, IEEE Transactions on antennas and propagation, Vol. 49, No 12, December 2001
- [22] Robert E. Collin, “Foundations for Microwave Engineering”, John Wiley and Sons, second edition, 1992
- [23] K.Rohlf and T.Wilson, “Tools for radio astronomy”, Chapter 4, A&A Library, second edition 1990.
- [24] Pozar, “Microwave Engineering”, Chapter 11, John Wiley & Sons, Second edition 1998
- [25] Robert E. Collin, “Foundations for Microwave Engineering”, Chapter 10, John Wiley and Sons, second edition, 1992
- [26] Steve Marsh, “Practical MMIC Design”, Chapter 4 and 5, Artech House , 2006.
- [27] Guillermo Gonzalez, “Microwave transistor amplifiers analysis and design”, Prentice Hall, 1997.
- [28] Marian Pospieszalsky, “Modeling of Noise Parameters of MESFET’s and MODFET’s and Their Frequency and Temperature Dependence”, IEEE Transactions on microwave theory and techniques. Vol 37. No 9. September 1989
- [29] Agilent-ADS EEHEMT Model.
- [30] Gallego, J.D., “Experimental results of gain fluctuations and noise in microwave low noise cryogenic amplifiers”, SPIE international symposium on fluctuations and noise, 2004

- [31] N. Jiang et al “Stability of preamplifier in 84-116GHz receiver”, Joint 30th Intl. Conf. on Infrared and Millimeter Waves & 13th Intl. Conf. on Terahertz Electronics, 2005
- [32] S. Weinreb et al, “Cryogenic MMIC low noise amplifiers”, Galium Arsenide applications symposium, Paris, 2000
- [33] Larry r. D’Addario, “Gain stability: requirements and design consideration”, Alma Memo 466, May 2003
- [34] Takashi Mimura, “The Early History of the High Electron Mobility Transistor (HEMT)”, IEEE Transactions on microwave theory and techniques Vol. 50, No. 3, March 2002
- [35] Macgregor S. Reid, Editor, “Low-Noise Systems in the Deep Space Network”, Issued by the Deep Space Communications and Navigation Systems, Center of Excellence Jet Propulsion Laboratory and California Institute of Technology, 2008.
- [36] A. Tessmann, “220 -GHz metamorphic HEMT amplifier MMICs for high-resolution imaging applications”, IEEE Solid-State Circuits, vol. 40, pp. 2070 - 2076, Oct. 2005.
- [37] Arnulf Leuther et al, “50 nm MHEMT Technology for G- and H-Band MMICs” ,2007 International Conference on Indium Phosphide and Related Materials ,Conference Proceedings TuA2-4, 19th IPRM 14 - 18, May 2007 Matsue, Japan
- [38] M. Dammann et al, ”Reliability of 50nm low-noise metamorphic HEMTs and LNAs”, IEE Electron. Lett. 41, 699, (2005)
- [39] <http://www.ommic.com/>
- [40] <http://www.winfoundry.com/>
- [41] D. M. Fanning, et al. “25 W X-band GaN on Si MMIC”, GaAs MANTECH 2005 Conf. Proc., New Orleans, USA, April 11th-14th, 2005.
- [42] F. van Raay, et al., “A Microstrip X-Band AlGaN/GaN Power Amplifier MMIC on s.i. SiC Substrate”, IEEE microwave and wireless components letters, Vol. 15, No. 4, April 2005
- [43] William R. Deal et al.’ “A W-Band InAs/AlSb Low-Noise/Low-Power Amplifier”, IEEE Microwave and Wireless components letters, VOL. 15, No. 4, April 2005
- [44] X.B. Mei et al, “35-nm InP HEMT SMMIC Amplifier With 4.4-dB Gain at 308 GHz”, IEEE electron device letters, Vol. 28, No. 6, June 2007
- [45] Gilles Dambrine at al., “A new method for determining the FET Small-Signal Equivalent Circuit”, IEEE Transactions on microwave and techniques, Vol 36, No 7, July 1988
- [46] Shigeru Yanagawa, “Analytical method for determining equivalent circuit parameter of GaAs FET’s” , IEEE Transactions on microwave theory and techniques, vol 44, No 10, October 1996.
- [47] H. Fukui, “Design of Microwave GaAs MESFET’s for Broad-Band Low-Noise Amplifiers”, IEEE Transactions on Microwave Theory and Techniques, Vol. MTT-27, July 1979, pp. 643-650.

- [48] H. Fukui, Addendum to “Design of Microwave GaAs MESFET’s for Broad-Band Low-Noise Amplifiers”, IEEE Transactions on Microwave Theory and Techniques, Vol. MTT-29, October 1981.
- [49] Pospieszalsky M, “Extremely Low Noise amplification with cryogenic FETs and HFETs: 1970-2004”, IEEE microwave magazine, September 2005,
- [50] T. Gaier, M. Seiffert, C. R. Lawrence, “Millimeter-Wave MMIC Cameras and the QUIET Experiment”
- [51] Pekka Kangaslahti, et al., “Planar Polarimetry Receivers for Large Imaging Arrays at Q-band”
- [52] B. Aja, E. Artal, L. De La Fuente, J.P Pascual, A. Mediavilla, N. Roddis, D. Kettle, W.F. Winder, L. Pradell and P. de Paco, “Very low noise differential radiometer at 30 Ghz for the Planck LFI”, IEEE Transactions on microwave and techniques 53(6), 2050-2062 (2005).
- [53] J. Shell1, “The Cryogenic DC Behavior of Cryo3/AZ1 InP 0.1-by-80-Micrometer-Gate High Electron Mobility Transistor Devices”, IPN Progress Report 42-169 May 15, 2007
- [54] Marian W. Pospieszalski et al. , “Design and performance of wideband, low noise, millimeter-wave amplifiers for the microwave anisotropy probe radiometers”, Microwave Symposium Digest. 2000 IEEE MTT-S International.
- [55] Franck Robin et al., “InP HEMT-Based CPW Amplifiers for 94 and 110 GHz”, Conference on Indium Phosphide and Related Materials , 12-16 May 2003.
- [56] <http://www.ums-gaas.com/>
- [57] J.E.Fernandez, “A noise temperature measurement system using a cryogenic attenuator”. TMO Progress Report 42-135, November 1998.
- [58] Agilent application note 57-2, “Noise Figure Measurement Accuracy- The Y-Factor Method”.
- [59] Lorene Samoska, “Towards Terahertz MMIC Amplifiers: Present Status and Trends”, Microwave Symposium Digest, IEEE MTT-S International, 2006.
- [60] E. W. Bryerton, X. Mei, Y. Kim, W. Deal, W. Yoshida, M. Lange, J. Uyeda, M. Morgan, and R. Lai, “A W-Band Low-Noise Amplifier with 22K Noise Temperature”, Microwave Symposium Digest, 2009. MTT '09. IEEE MTT-S International.
- [61] Ciccognani W., Limiti E., Longhi P. and Renvoise M., “MMIC LNAs for radioastronomy applications using advanced industrial 70nm metamorphic technology” IEEE journal of solid state circuits, vol 45, N° 1, October 2010.
- [62] Yuh-Jing Hwang and Chau-Ching Chiong, “Development of MHEMT MMICs for Band-1 Receiver of Atacama Large Millimeter Array in Taiwan”, ALMA Band-1 Workshop in Hertzberg Institute of Astrophysics, Victoria, October 08-10, 2008
- [63] B. Aja, M. Seelmann-Eggebert, A. Leuther, H. Massler, M. Schlechtweg, J. D. Gallego, I. López-Fernández, C. Diez, I. Malo, E. Villa, E. Artal, “4-12 GHz and 25-34 GHz Cryogenic MHEMT MMIC Low Noise Amplifiers for Radio Astronomy”, Microwave Symposium Digest (MTT), 2012 IEEE MTT-S International, Canada 2012.

- [64] B. Aja, K. Schuster, F. Schäfer, J. D. Gallego, S. Chartier, M. Seelmann-Eggebert, I. Kallfass, A. Leuther, H. Massler, M. Schlechtweg, C. Diez, I. López-Fernandez, S. Lenz, and S. Türk, “Cryogenic Low-Noise mHEMT-Based MMIC Amplifiers for 4-12 GHz Band”, IEEE Microwave and Wireless Components Letters, Vol. 21, N 11, November 2011.
- [65] J. de Mingo, A. Moliner, and A. Comerbn, “Waveguide-to-Coupled Fin-Line Transition in Ka Band”, IEEE Microwave and guided wave letters, Vol. 6, No. IO, October, 1996.
- [66] J. Kooi et al., “A full-height waveguide to thin-film microstrip transition with exceptional RF bandwidth and coupling efficiency”, Int. J. Infrared Millimeter Waves, vol. 24, no. 3, pp. 261 - 284, Mar. 2003.
- [67] Yoke-Choy Leong, Weinreb, S., “Full Band Waveguide-to-Microstrip Probe Transition”, Microwave Symposium Digest, 1999 IEEE MTT-S International Volume 4, Page(s):1435 - 1438
- [68] C. Jarufe, “Diseño y fabricacion de un amplificador de microondas de bajo ruido para la banda de 31-45 GHz”, Engineering thesis, Universidad de Chile, 2008.
- [69] M. Carter et Al, “ALMA Front End Optics Design Report”, ALMA internal document FEND-40.02.00-035-B-REP.March 2007.
- [70] Paul F. Goldsmith , “Quasioptical system”, chapter5, IEEE press 1998
- [71] P. Zorzi, D. Henke, S. Claude, P. Mena., “Revisiting the ALMA Band 1 Optics Design,” Proceedings of the 21th International Symposium on Space Terahertz Technology, Oxford, March 23-25, 2010.
- [72] S. Asayama, M. Kamikura, “Development of Double-Ridged Waveguide Orthomode Transducer for the 2 MM Band”, Journal of Infrared Millimeter and Terahertz Waves, 17 March 2009
- [73] M. Kamikura, M. Naruse, S. Asayama, N. Satou, W. Shan, Y. Sekimoto, “Development of a Submillimeter Double-Ridged Waveguide Ortho-Mode Transducer (OMT)”, Journal of Infrared Millimeter and Terahertz Waves, 26 March 2010.
- [74] A. R. Kerr, “ Elements for E-plane split-blocks waveguide circuits” Nat. Radio Astronomy Observatory, ALMA Memo 381, Jul. 2001. [Online]. Available: <http://www.alma.nrao.edu/memos>
- [75] Hans Rudolf, Matthew Carter, and Andrey Baryshev, “ The ALMA Front End Optics - System Aspects and European Measurement Results ”, IEEE TRANSACTIONS ON ANTENNAS AND PROPAGATION, VOL. 55, NO. 11, NOVEMBER 2007
- [76] P. Zorzi, C. Granet, F. Colleoni, N. Reyes, J. Pizarro, P. Mena, L. Bronfman, “Construction and measurement of a 31.3-45 GHz Optimized Spline- profile horn with corrugations”, Journal of Infrared Millimeter wave and terahertz waves, October 2011.
- [77] P.J.B Clarricoats and A.D. Olver, “Corrugated horns for microwave antennas”, IEE electromagnetic Waves Series 18, Published by Peter Peregrinus, London, UK, 1984.
- [78] C. Granet et al. “ A smooth-Walled spline-profile horn as an alternative to the corrugated horn for wide band millimeter-wave applications”, IEEE Transactions on Antenna and Propagation Vol 52, N°3, March 2004.

- [79] Colleoni Franco, “Diseño e implementación de un sistema de medición de patrones de radiación de antenas en el campo cercano”, Engineering thesis, Universidad de Chile, To be submitted (2012).
- [80] A. M. Boifot, E. Lier, and T. Schaug-Pettersen, “Simple and broadband orthomode transducer”, *Proc. Inst. Elect. Eng.*, vol. 137, no. 6, pp. 396 - 400, 1990.
- [81] A. Navarrini and R. L. Plambeck, “A turnstile junction waveguide orthomode transducer”, *IEEE Trans. Microw. Theory Tech.*, vol. MTT-54, no. 1, pp. 272 - 277, Jan. 2006.
- [82] G. Pisano, L. Pietranera, K. Isaak, L. Piccirillo, B. Johnson, B. Maffei, and S. Melhuish., “A broadband WR10 turnstile junction orthomode transducer”, *IEEE microwave and wireless components letters*, vol. 17, no. 4, April. 2007.
- [83] A. Dunning, “Double Ridged Orthogonal Mode Transducer for the 16-26 GHz Microwave Band”, *Proc. of the Workshop on the Applications of Radio Science*, February 20-22, 2002.
- [84] A. Mediavilla, J.L. Cano, K. Cepero, “On the octave bandwidth properties of octagonal-shaped waveguide mode transformer”, *IEEE Transactions on Microwave Theory and Techniques*, Vol 59, No. 10, October 2011.
- [85] ALMA Band 5 Cartridge team, “ALMA Band 5 cartridge preliminary design report”, ALMA internal document FEND-40.02.05.00-010-A-REP, March 2008.
- [86] C. E. Barnes, “Broad-band isolators and variable attenuators for millimeter wavelengths”, *IRE Trans. Microwave Theory Tech.*, vol.MTT-9, pp. 519 - 523, Nov. 1961.
- [87] Russell Bolton, Russell Gough “Cryogenic Performance of Millitech Model FBI-22 Waveguide Isolator”, AT Technical Document Series, AT/39.3/127, May 2, 2006.
- [88] N. Erickson, R. Grosslein, R. Erickson, and S. Weinreb, “A cryogenic Focal Plane Array for 85-115 GHz Using MMIC preamplifiers”, *IEEE 1999 MTT-S Digest*, vol.1 pp 251-254
- [89] Pozar, “Microwave Engineering” John Wiley & Sons, Second edition 1998
- [90] Liu Affi-Shyi , WU Ruey-Beei and LB Yi-Cheng, “A compact design of W-band high-pass waveguide filter using genetic algorithms and full-wave finite element analysis”, *IEICE transactions on electronics* ISSN 0916-8524 ,2005, vol. 88, no8, pp. 1764-1771.
- [91] Soto M., “Estudio de la Dinámica de la Estructura del Receptor Radioastronómico para la Banda 1 de Alma”, Engineering thesis, Universidad de Chile, To be submitted (2012).
- [92] Y. Sekimoto et al. “Cartridge Test Cryostats for ALMA Front End ´´”, ALMA memo 455, April 18, 2003
- [93] Nicolas Reyes, Pablo Zorzi, Jose Pizarro, Ricardo Finger, F. Patricio Mena and Leonardo Bronfman, “A Dual Ridge Broadband Orthomode Transducer for the 7-mm Band”, *Journal of Infrared Millimeter wave and terahertz waves*, 2012, DOI: 10.1007/s10762-012-9942-6